

ELECTROCHEMICAL AND SURFACE ANALYSIS OF METAL IONS AND TDP-43 PROTEIN INTERACTIONS

A Thesis Submitted to the Committee of Graduate Studies

in Partial Fulfillment of the Requirements for the Degree of Master of Science in the Faculty of
Arts and Science

TRENT UNIVERSITY

Peterborough, Ontario, Canada

© Copyright by **Meaghan O. F. Tabobondung 2023**

Environmental and Life Sciences M.Sc. Graduate Program

May 2023

Abstract


Electrochemical and surface analysis of metal ions and TDP-43 protein interactions

Meaghan O. F. Tabobondung

Amyotrophic lateral sclerosis (ALS) is a neurodegenerative disorder characterized by progressive loss in function of motor neurons. Elevated levels of biologically important metal ions, such as copper (II) (Cu(II)), zinc (II) (Zn(II)) or iron (III) (Fe(III)), may contribute to the disease. Moreover, Cu(II) interactions with other proteins associated with ALS have been investigated; however, the effects of metallation on TAR DNA-binding protein of 43 kDa (TDP-43) are less known. The aim of the thesis was to evaluate interactions between full-length TDP-43 and metal ions, and gain insight into the mechanisms of these interactions. In Chapter 2, electrochemical methods were used to evaluate the coordination of Cu(II) ions to immobilized TDP-43. Cu(II)-TDP-43 binding was favourable at a neutral pH. Surface characterization confirmed protein immobilization and Cu(II)-TDP-43 coordination. Competitive Zn(II) ion binding studies revealed Zn(II) increases Cu(II) binding. In Chapter 3, Fe(III) ion binding studies revealed that Fe(III) reduces Cu(II) binding when co-exposed to the TDP-43-Au surface. Data shows significant uptake of Cu(II) by TDP-43 protein which may have important implications in normal and diseased states of TDP-43, indicating surface bioelectrochemistry is a viable tool for fundamental exploration of proteins and metals, and their interactions, as they inform disease mechanisms, disease detection and drug screening.

Keywords: amyotrophic lateral sclerosis, TDP-43, electrochemistry, x-ray photoelectron spectroscopy, ellipsometry, contact angle, metalation, metal ions, surface modifications, surface characterization, reactive oxidative species, metal dysregulation, neurotoxic, metal coordination, current signal, bioelectrochemistry, neurodegenerative disease.

AbbreviationsALS, amyotrophic lateral sclerosis;

 CV, cyclic voltammetry;

CTD, C-terminal domain;

DNA, deoxyribonucleic acid;

EIS, electrochemical impedance spectroscopy;

fALS, familial amyotrophic lateral sclerosis;

LCD, low-complexity domain

LLPS, liquid-liquid phase separation;

NES, nuclear export signal;

NLS, nuclear localization signal;

NTD, N-terminal domain;

PTM, post-translational modifications;


RNA, ribonucleic acid;

RRM1/2, RNA-recognition motif 1 & 2;

sALS, sporadic amyotrophic lateral sclerosis;

SWV, square wave voltammetry;

TDP-43, transactive response DNA binding protein 43 kDa;

 PTM, post-translational modification;

Acknowledgements

I am forever thankful to my supervisor, Dr. Martic, for her knowledge and guidance throughout every step of this research process and the expertise you have shared with me. I am grateful that I was able to experience a variety of research techniques thanks to Dr. Martic.

I would like to also extend my thanks and gratitude to Dr. Emery and Dr. Huber for their advice and encouraging words throughout the two years of my M.Sc.

I would also like to thank my friends, lab mates (Martic lab, old and new), and colleagues (Dr. Iraklii Ebralidze, Ontario Tech University), for working with me in and outside of the lab, allowing me to broaden my research, and develop a better understanding of the data collected.

I'd also like to thank my immediate family, as well as the Istvan family, for their unwavering encouragement and support over the last two years. Lastly, I am forever grateful for my boyfriend for his support through both the good and bad results during the experimental phases, and everything else he has helped me through during this time.

I'd also like to acknowledge that these experiments were conducted on traditional territory of the Mississauga Anishinaabeg. I am grateful to have learned so much on the beautiful lands that they have cared for.

Chi-miigwetch (a big thank you) to all of those who helped may this happen.

Preface

The following thesis is presented in manuscript format and based on four chapters – one of which (Chapter 2) will be submitted for publication. The first author is Meaghan Tabobondung who, with Dr. Martic, took the lead on the synthesis of the projects, experimental design, data analysis, and the writing of the manuscripts. A note on the format: Reference and citation styles of the journal where these chapters were published or accepted has been used. Other significant research contributions are detailed in Appendix 1. *Other Significant Research Contributions* These include peer-reviewed published papers, and manuscripts under review.

Table of Contents

Abstract	ii
Keywords	iii
Abbreviations	iii
Acknowledgements	iv
Preface	v
Table of Contents	vi
List of Figures	ix
Chapter 1 Introduction: TDP-43 and Metal Ion Interactions, an Insight into Amyotrophic Lateral Sclerosis Disease Pathogenesis	1
<i>1.1. Amyotrophic Lateral Sclerosis</i>	1
<i>1.2. Transactive Response DNA Binding Protein of 43kDa</i>	3
1.2.1. Biological Functions of TDP-43	6
1.2.2. TDP-43 Pathogenesis and Aggregation	8
<i>1.3. Metal Ions and TDP-43</i>	14
1.3.1. Zinc (Zn(II))	16
1.3.2. Mercury (Hg(II))	19
1.3.3. Lead (Pb (II))	20
1.3.4. Iron (Fe(III))	21
1.3.5. Copper (Cu(II))	22
<i>1.4. Analytical Methods for the Study of Metal Ion-TDP-43 Interactions</i>	24
1.4.1. Mass Spectrometry	24
1.4.2. Circular Dichroism	25
1.4.3. Isothermal Titration Calorimetry	27
1.4.4. Electrochemistry	29
<i>1.5. Thesis Research Rationale</i>	34
Chapter 2 : Electrochemical and Surface Analysis of Cu(II) and Zn(II) Metal Ions and TDP-43 Protein Interactions**	36
Abstract	37
<i>2.1 Introduction</i>	38
<i>2.2. Experimental</i>	41
2.2.1. Materials and Methods	41
2.2.2. TDP-43 Expression, Purification and Characterization	42

2.2.3. Electrochemical Measurements	43
2.2.4. Cleaning of Au Electrodes	44
2.2.5. Preparation of Protein Solution	44
2.2.6. Preparation of TDP-43 Films on Au Electrodes	44
2.2.7. Interactions with Metal Ions	45
2.2.8. Sample Preparation for Surface Characterization	45
2.2.9. Ellipsometry.....	46
2.2.10. Contact Angle Measurements	46
2.2.11. X-ray Photoelectron Spectroscopy.....	46
2.3. Results and Discussion	47
2.3.1. Biochemical Characterization of TDP-43	47
2.3.2. TDP-43-Au Film Fabrication	48
2.3.3. Interactions of Cu(II) with TDP-43-Au Surfaces	56
2.3.4. pH Affect on Cu(II)-TDP-43 Interactions.....	62
2.3.5. Cu(II)/Zn(II)-TDP-43 Studies.....	65
2.4 Conclusion	70
2.5 Author Information	72
2.6. Acknowledgements	72
Chapter 3 : Electrochemical Analysis of Fe(III) and Cu(II) Interactions with TDP-43	73
Abstract.....	73
3.1. Introduction.....	74
3.2. Experimental Section	78
3.2.1. Materials and Methods	78
3.2.2. Cleaning of Au Electrodes	78
3.2.3. Preparation of Protein Solution	79
3.2.4. Preparation of TDP-43 Films on Au Electrodes	79
3.2.5. Interactions with Metal Ions	79
3.3. Results and Discussion	80
3.4 Conclusions.....	85
Chapter 4 : Conclusions and Future Work.....	87
4.1 Conclusions.....	87
4.1.1. Cu(II) Binding to TDP-43.....	88
4.1.2. The Influence of Zn(II) Cu(II)-TDP-43 Binding	89

4.1.3. The Influence of Fe(III) on Cu(II)-TDP-43 Binding	91
<i>4.2. Future Research Directions</i>	92
4.2.2. TDP-43 Structure Post Metal Ion Binding	94
4.2.3. Metal Ion Binding to Aggregated TDP-43	95
4.2.4. Metal Ion Binding to ALS-Linked TDP-43 Mutations	96
References	98
Appendices	118
<i>Appendix 1. Other Significant Research Contributions</i>	118
<i>Appendix 2. Supplementary information (Chapter 2)</i>	121
<i>Appendix 3. Supplementary information (Chapter 3)</i>	161

List of Figures

Chapter 1

Figure 1.1. (A) Summary of N-terminal domain structure.	5
Figure 1.2. (A) Domain map showing the relative sizes of TDP-43 domains, N-terminal, RNA recognition, and C-terminal domains, respectively.....	7
Figure 1.3. Model proposed by Conicella et al. (2016), of C-terminal domain-driven liquid-liquid phase separation.....	10
Figure 1.4. Schematic by Hussain et al. (2022) demonstrating the impact of the loss of TDP-43 function in both the nucleus and cytoplasm.....	13
Figure 1.5. Schematic by Othman and Yabe (2015), showing reactive oxidative species (ROS) generation and neutralization in neuronal cells, and their role in neurodegenerative disease.	15
Figure 1.6. Hypothesized binding sights for Zn(II) coordination to TDP-43 RRM domains.....	18
Figure 1.7. Schematic of TDP-43 binding to electrode surface for electrochemical measurement.	30
Figure 1.8. (A) Cyclic voltammograms of 50 μM β -amyloid (dashed curve) and 50 μM β -amyloid spiked with 50 μM Cu(II) (solid curve) at a glassy carbon disk electrode surface, from Jiang et al. (2007).....	32

Chapter 2

Figure 2.1. Schematic illustration of TDP-43-Au film and subsequent Cu(II) binding to form the redox active Cu(II)/TDP-43 protein film on Au-surface.	40
Figure 2.2. Domain map showing the relative sizes of TDP-43 domains, N-terminal, RNA recognition, and C-terminal domains, respectively.....	48
Figure 2.3. Schematic illustration of the surface modifications of Bare Au: (i) Lipoic acid,	49
Figure 2.4. A) Cyclic voltammograms and B) Nyquist plots of stepwise surface modifications of bare Au surface for fabrication of TDP-43-Au film	52
Figure 2.5. XPS spectra of TDP-43-Au film showing A) S 2p peaks at 162.0, 163.5, and 165.1 eV;	55
Figure 2.6. A) CVs of TDP-43-Au film before (black dash line) and after (blue solid line) 350 μM Cu(II) binding;	58
Figure 2.7. XPS spectra of Cu and S for (A, C) TDP-43-Au and (B,D) Cu(II)-TDP-43-Au films.	61
Figure 2.8. A) Representative SWV measurements of 500 μM Cu(II)-TDP-43-Au surface at pH 3 (yellow) and pH 7.4 (green);.....	64
Figure 2.9. Schematic representation of competitive and displacive studies conducted to determine other metal ions, specifically Zn(II) (grey) effect on Cu(II)-TDP-43 binding.	66
Figure 2.10. XPS spectra of TDP-43 film exposed to Cu(II) and Zn(II) in varying successions.	69

Chapter 3

Figure 3.1. Schematic representation of competitive and displacive studies conducted to determine the effect of other metal ions, specifically Fe(III) (green) on Cu(II)-TDP-43 binding.	77
Figure 3.2. A) TDP-43-Au film exposed to 1 mM Fe (III) solution (green) and phosphate buffer (blue) in $[\text{Fe}(\text{CN})_6]^{-3/4}$ redox probe.	82
Figure 3.3. A) Representative SWV measurements of TDP-43-Au surface (grey), Cu(II)-TDP-43-Au surface (blue) and 350 μM Cu(II)-1 mM Fe(III) exposure surface (green), simultaneously;	84

Chapter 1 Introduction: TDP-43 and Metal Ion Interactions, an Insight into Amyotrophic Lateral Sclerosis Disease Pathogenesis

1.1. Amyotrophic Lateral Sclerosis

Neurodegenerative diseases affect the nervous system, often by targeting neurons and causing a progressive loss in their function, overall affecting the communication with the brain. These diseases cause disruptions in movement, cognition, and behaviour. Examples of common neurodegenerative disorders include Alzheimer's, Parkinson's, and Huntington's disease, as well as amyotrophic lateral sclerosis (ALS), frontotemporal dementia, and spinocerebellar ataxias. Most neurodegenerative disorders are amyloidoses, tauopathies, alpha-synucleinopathies, and TDP-43 (TAR DNA binding protein) proteinopathies.¹ Neurodegeneration is caused by abnormal protein folding, which leads to protein accumulation and contributes to the histopathologies, which are often used for diagnoses.¹ Although every neurodegenerative disease has distinct characteristics, there is often overlap.¹ Treatments available for neurodegenerative diseases are limited. Most aim to relieve the symptoms of the disease, and not to slow the progression or cure the disease itself.²

ALS is a well-known neurodegenerative disease that targets the motor system in humans. Ultimately, communication between the brain and muscles is lost, leading to paralysis. Clinically, individuals diagnosed with the disease can see a loss of neuron function at all levels of the motor system. After onset, it is not possible to slow or stop the progression of the disease, resulting in 50% of those diagnosed dying within three years.³ The symptoms experienced by the patients are considered in relation to the affected neurological regions. For instance, a lumbar onset would indicate degradation of the anterior horn cells, which would affect lower motor neuron function.³

Patients often have issues with mobility, specifically walking difficulties.³ As the disease progresses, mobility issues become more severe, and individuals often lose the ability to talk, walk, eat, or breathe. The reduced mobility is caused by a loss of neuromuscular connection, axonal retraction, and neuronal cell death. Movement is based on the contraction of muscles. Contraction occurs after chemical signals have been propagated, and electrical signals are responsible for this occurrence. In ALS, the essential electrical signal is disrupted by protein dysfunction.⁴ Thus, ALS symptoms manifest because of loss of function in the motor neurons.

Motor neurons can be split into two groups, upper and lower. Upper motor neurons extend from the brain stem to the spinal cord.⁵ In contrast, lower motor neurons extend from the spinal cord and connect the muscle groups.⁶ The motor neurons propagate chemical signals created by electrical impulses from the brain to specific muscles. The propagation of the electrical impulses to the muscles stimulates muscle contraction and, thus, movement. In patients with ALS, these electrical signals are interrupted due to misfolded proteins or genetic variations.⁶ There are two different forms of ALS an individual may be diagnosed with, either sporadic ALS (sALS) or familial ALS (fALS).⁷ fALS diagnosis is relevant if there is a familial history of ALS through generations and is the less common form of ALS,⁷ whereas, sALS is the most prevalent and has an average age of onset of 55-56 years of age.⁸ This form of ALS can affect any individual, regardless of family history.⁷ Regardless of the type of ALS the individual is diagnosed with, similar proteins are affected as the disease progresses.

Protein pathogenesis, specifically misfolding and aggregation, was discovered to be a significant contributor to ALS and other neurodegenerative diseases.⁹ Protein pathogenesis is defined as hyperaccumulation of protein leading to structural abnormalities of the proteins, causing disruption to normal functioning cells.¹⁰ Currently, there are several proteins associated with ALS,

one of which is the transactive response (TAR) DNA binding protein of 43 kDa (TDP-43) responsible for 97% of cases¹¹ Post-translation modifications (PTMs) such as ubiquitination, hyperphosphorylation, and fragmentation of TDP-43 are linked to ALS. TDP-43 is also classified as a prion-like protein, suggesting that it may influence other TDP-43 proteins to aggregate.¹² Overall, evidence suggests that TDP-43 plays a role in ALS pathogenesis, making it a protein of interest to study, to determine any mechanisms by which it contributes to ALS.

1.2. Transactive Response DNA Binding Protein of 43kDa

Many studies have been conducted to determine the different structural elements of TDP-43. TDP-43 is composed of four domains, the N-terminal domain with a nuclear export signal, two RNA recognition motifs (RRM) which can bind RNA molecules, and a glycine-rich C-terminal domain (CTD) (1.2 A and B) that allows for protein-protein interactions.¹³ TDP-43 is a ubiquitous protein encoded by the TARDBP gene on the short arm of chromosome 1.¹⁴ The protein belongs to the heterogeneous nuclear ribonucleoprotein (hnRNP) family.¹² The N-terminal of the protein contains a ubiquitin-like fold, one α -helix, and six β -sheets, promoting TDP-43 self-oligomerization¹⁵ (Fig. 1.1A). The two RRM domains comprise five β -sheets and two α -helices¹² (Fig. 1.1B and C). The RRM regions bind UG/TG-rich regions of single-stranded DNA/RNA to perform its various functions in transcription, translation, and mRNA processing.^{16,17} The CTD of TDP-43 allows for the cellular location of the proteins and regulates the protein-protein interactions¹⁸ (Fig. 1.3). The domain is rich in glycine, glutamine, and asparagine and resembles a similar sequence to prion-like domains¹² (Fig. 1.2 A and B). Overall, the secondary structure of the various TDP-43 domains is well understood. However, there are still gaps in understanding its

tertiary structure. Thus, potential binding or interaction sites of other molecules or proteins cannot be accurately determined without systematic studies.

1.2.1. Biological Functions of TDP-43

Healthy TDP-43 is shuttled between the nucleus and cytoplasm, primarily in neuronal cells. In the N-terminus, there is a nuclear localization signal (NLS), which mediates the transportation of TDP-43 into the nucleus. The N-terminal region also contains a nuclear export signal (NES) (Fig. 1.2 A and B) that allows for the transport of TDP-43 from the nucleus to the cytoplasm. The protein is normally concentrated in the nucleus, but the NES and NLS features enable the protein to shuttle back and forth between the cytoplasm and nucleus.²⁰ TDP-43 is an RNA-binding protein and contains two RNA recognition motifs capable of binding RNA (Fig 1.2 A and B). In the nucleus, TDP-43 is a regulator of transcription and is involved in RNA processing. Specifically, TDP-43 is involved in splicing, by mediating splicing repression, to protect from aberrant splicing.²¹ TDP-43 acts as a negative splicing regulator by binding to UG-repeated elements. However, its splicing inhibition is dependent on the interaction with other hnRNPs, such as A1/A2/B1/C with the C-terminal.²² TDP-43 can also play a positive role in the splicing process, specifically for exon inclusion.²² After binding to an exon, TDP-43 can recruit splicing complexes or antagonize negative splicing regulators. TDP-43 is also involved in stabilizing, transporting, and translating of RNA, by binding to UG-rich RNA sequences within the two RNA recognition motifs.²³ Additionally, TDP-43 is involved in microRNA maturation.²⁰ The TDP-43 protein interacts with numerous proteins and RNAs in multi-protein/RNA complexes which allows for the mRNA processes to occur, such as splicing, stability, transport, microRNA maturation, and translation.²⁰ The protein is involved in mRNA metabolism within the cytoplasm and is dependent on the ability of TDP-43 to bind the mRNA molecules.²⁴ Additionally, TDP-43 has a strong association with stress granules (SGs) and translational machinery.²⁴

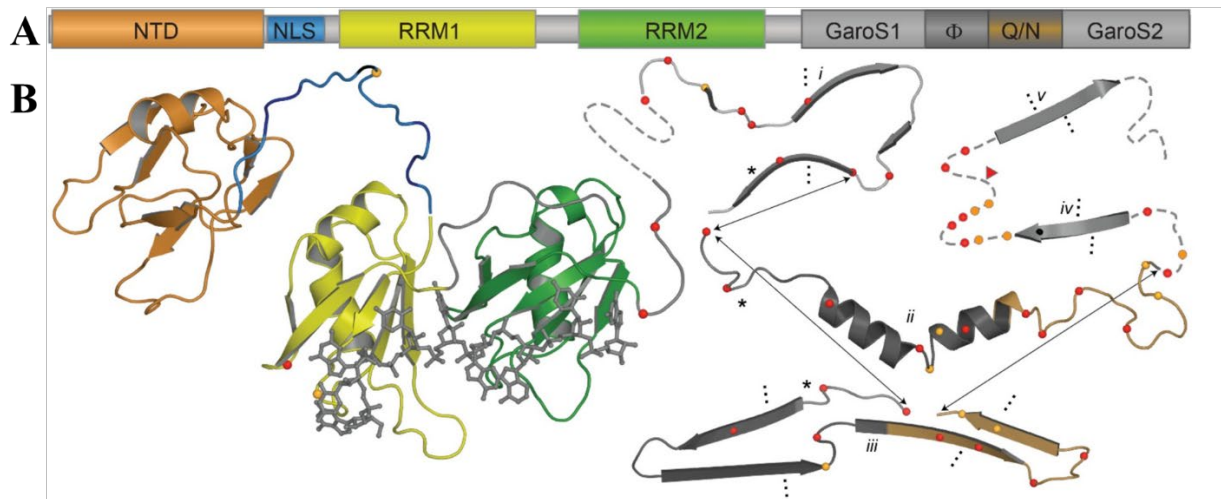


Figure 1.2. (A) Domain map showing the relative sizes of TDP-43 domains, N-terminal, RNA recognition, and C-terminal domains, respectively. Gly-aromatic-Set-rich regions (GaroS1/2), hydrophobic region (Φ), and Glu-Arg-rich region (Q/N) are highlighted in the C-terminal domain.²⁵ (B) Respective secondary structures of the TDP-43 domain, colour coded to the domain map above. RRM domains show representative secondary structures bound to an RNA molecule.²⁵

SGs form in response to cellular stress, such as oxidative stress, heat shock, or osmotic shock. These SGs protect essential mRNA and machinery from degradation in response to changes in the cellular environments.²³ TDP-43 plays an important role in SG dynamics, both formation and disassembly. Several studies have demonstrated that depletion of TDP-43 in cells experiencing stress results in an impaired SG pathway.^{26,13} Cytoplasmic TDP-43 aggregation is also linked to SG formation due to the autoregulation properties of the protein.

TDP-43 autoregulates its synthesis through an auto-feedback mechanism by binding to its own untranslated 3' untranslated region. Due to this feedback loop, overexpression of TDP-43 leads to the down-regulation of endogenous TDP-43.^{27,28} TDP-43 has many essential roles in transcription and regulation, as well as cell survival. This essential protein also has tight regulation

through its auto-feedback mechanism, indicating there is a crucial role of TDP-43 function within mRNA processing and other processes within neuronal cells. The biological processes and roles in health for TDP-43 protein have been well studied, for example, the aggregation and accumulation of the protein leads to neurotoxicity, leading to neurodegeneration in otherwise healthy individuals. However, the mechanisms by which the protein becomes pathogenic and leads to diseases, such as ALS, is not as well understood. Thus, it is of interest to build upon the understanding of how TDP-43 may lead to ALS and its progression.

1.2.2. TDP-43 Pathogenesis and Aggregation

The mechanisms regulating the aggregation of TDP-43 in neuronal cells have been well studied. For example, it is understood that in diseased cells, TDP-43 is hyperphosphorylated and aggregated, compromising TDP-43 function.²⁹⁻³¹ Additionally, in pathological conditions, cleavage and ubiquitination of TDP-43 can also occur.¹² Possible mutations that cause aggregation have also been investigated. For example, mutations in the NLS result in cytoplasmic localization and aggregation of TDP-43,³² indicating that TDP-43 access to the nucleus is important to avoid accumulation in the cytoplasm. Additionally, there are studies suggesting that TDP-43 mislocalization contributes to ALS.³³ The accumulation of TDP-43 aggregates within the central nervous system is common in neurodegenerative diseases such as Alzheimer's disease, frontotemporal dementia, limbic age-related TDP-43 encephalopathy, and ALS.¹² Thus, it is clear that the aggregation of TDP-43 plays a large role in the neurodegeneration observed within these diseases. However, the mechanisms by which the proteins can aggregate can be wide-ranging, and other possible mechanisms of aggregation should be explored. Investigating the impact of PTMs on TDP-43 is a logical first step since PTMs on proteins is well established.

Pathological conditions can cause cleavage, hyperphosphorylation and ubiquitination of TDP-43. These PTMs result in the accumulation of cytoplasmic TDP-43 and disrupt normal TDP-43 functions (Fig 1.2). PTMs or mutations to TDP-43 interrupt the proteins ability to undergo liquid-liquid phase separation (LLPS), which is influenced by hydrophilic and hydrophobic residues of the protein in the low-complexity domain.¹² LLPS allows for the formation of membrane-less organelles that are associated with RNA processing. TDP-43 is present in several of these organelles.³⁴ The NTD and CTD of TDP-43 allow the protein to undergo LLPS and complete its functions³⁴ (Fig. 1.3). Most mutations associated with ALS occur in the CTD, and promote aggregation.³⁵ Several studies have expressed different mutations within the CTD of TDP-43 to determine their effects on the aggregation of the protein. Since the structure of the CTD of TDP-43 is responsible for most protein-protein interactions and is involved in the LLPS of TDP-43, disruptions in the CTD have significant impacts on the overall functions of TDP-43. In addition to impacts on TDP-43 function, the CTD may also contribute to the spread of TDP-43 aggregation in cells.

WT TDP-43:

Multivalent interactions promote phase separation

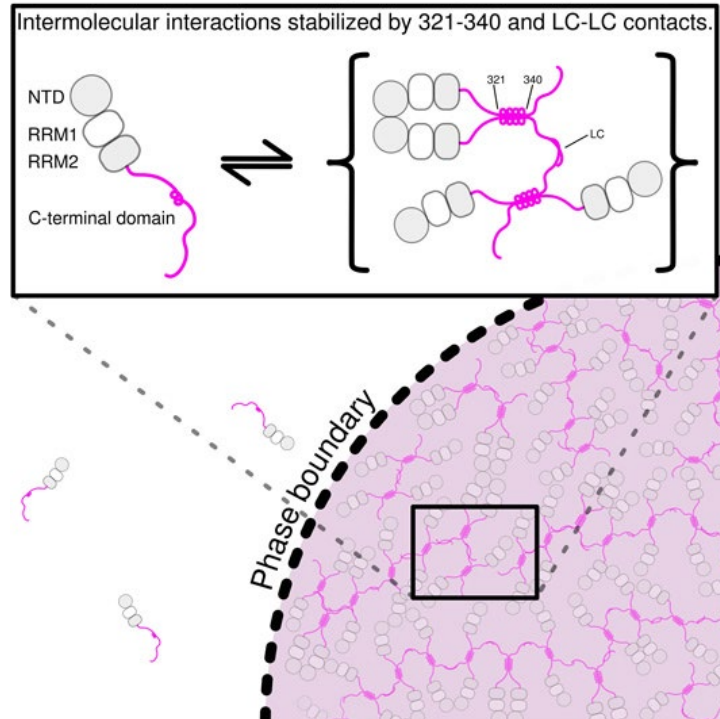


Figure 1.3. Model proposed by Conicella et al. (2016), of C-terminal domain-driven liquid-liquid phase separation. The prion-like CTD domain allows for protein-protein interactions with other TDP-43 or hnRNPs. The nature of the protein also allows for liquid-liquid phase separation to occur. TDP-43 has a CTD that mediated self-binding via contacts between the 321 to 340 residues in the α -helical structure. These interactions and the aromatic-rich prion-like LCD promote the liquid-liquid phase separation.

TDP-43 structure allows it to spread the aggregation to other TDP-43 proteins and cells. The aggregated TDP-43 is transferred from cell to cell in a mechanism similar to prion-like proteins.¹² Prion-like proteins have similar domains to that of the CTD of TDP-43, and play a key role in regulating the solubility and folding of the protein, but can also induce misfolding and self-aggregation.¹² Prion-like domains are low-complexity sequences, rich in uncharged polar amino acids and glycine.¹² The prion-like mechanism of aggregation in other proteins related to neurodegenerative diseases, such as amyloid- β , tau, and α -synuclein, are well studied.³⁷⁻³⁹ However, the mechanism by which TDP-43 induces cell-to-cell aggregation are less known.

Aggregated TDP-43 can be found in 97% of individuals affected by sALS.⁴⁰ Individuals affected by sALS have 52 missense mutations in *TARDBP* gene, encoding TDP-43. Of the 52 mutations, 49 affect residues within the CTD,⁴¹ indicating that TDP-43 aggregates due to CTD interactions within the cytosol.³⁶ Other factors influence TDP-43 aggregation, such as PTMs, cytoplasmic accumulation (Fig. 1.4), and abnormal binding of nucleic acids. Additionally, high electrolyte concentrations, such as imidazole and KCl, will reduce the stability of the protein and allow for easier induction of aggregation.⁴² Although TDP-43 aggregation related to PTMs and mutations has been well studied in literature, other factors that may influence the aggregation are not as well studied or understood.

However, the aggregation of TDP-43 appears to be motivated at large by the low-complexity domain (LCD) of the protein that undergoes LLPS.⁴³ The hydrophobic and hydrophilic residues in the LCD undergo mutations or modifications, affecting the ability for LLPS to occur.¹² The methionine-rich LCD is located in the CTD, where most ALS-linked mutations take place.⁴⁴ Johnson et al., introduced several ALS-linked TDP-43 mutations into the CTD, such as Q331K, M337V, Q343R, N345, R361S, and N390D. These mutations increased the number of TDP-43

aggregates, as well as accelerated aggregation of surrounding TDP-43.³⁵ The introduction of the mutations inhibits the protein's ability to undergo LLPS and cause aggregation. As previously stated, TDP-43 aggregation causes a feedback loop which increases the number of TDP-43 aggregates.

Thus, cytoplasmic TDP-43 aggregation occurs due to the negative-feedback loop mechanism of TDP-43, as well as cellular stress conditions¹² (Fig. 1.4). Cytoplasmic TDP-43 aggregation occurs because TDP-43 becomes upregulated in the nucleus when the nuclear TDP-43 is low, as part of its own regulatory auto-feedback system. However, due to dysfunction in TDP-43, the synthesized TDP-43 is shuttled to the cytoplasm, resulting in TDP-43 accumulation, and spreading of the aggregation in the cytoplasm.⁴⁵ TDP-43 will also relocate to the cytoplasm when the cell is under stress. Stress conditions, such as oxidative stress or heat shock, will increase the cytoplasmic transfer of nuclear TDP-43. The increased cytoplasmic TDP-43 forms SGs (Fig. 1.4), with other proteins and RNAs.⁴⁶⁻⁴⁹ SGs form to promote cell survival during unfavourable conditions, by protecting mRNA and mRNA-related proteins. Specifically, SGs will condense translationally stalled mRNAs, translation initiation factors, RNA-binding proteins, and ribosomal components.⁵⁰ When the stress dissipates, the SGs containing TDP-43 will disassemble, allowing for TDP-43 to relocate to the nucleus.⁵¹ However, chronic stress leads to the prolonged formation of the SGs, causing cytoplasmic TDP-43 inclusions.¹² Thus, once TDP-43 aggregation occurs within a cell, it is amplified by the auto-regulatory mechanisms of the protein. Overall, there are several different factors that have been well studied when investigating the causes of TDP-43 aggregation.

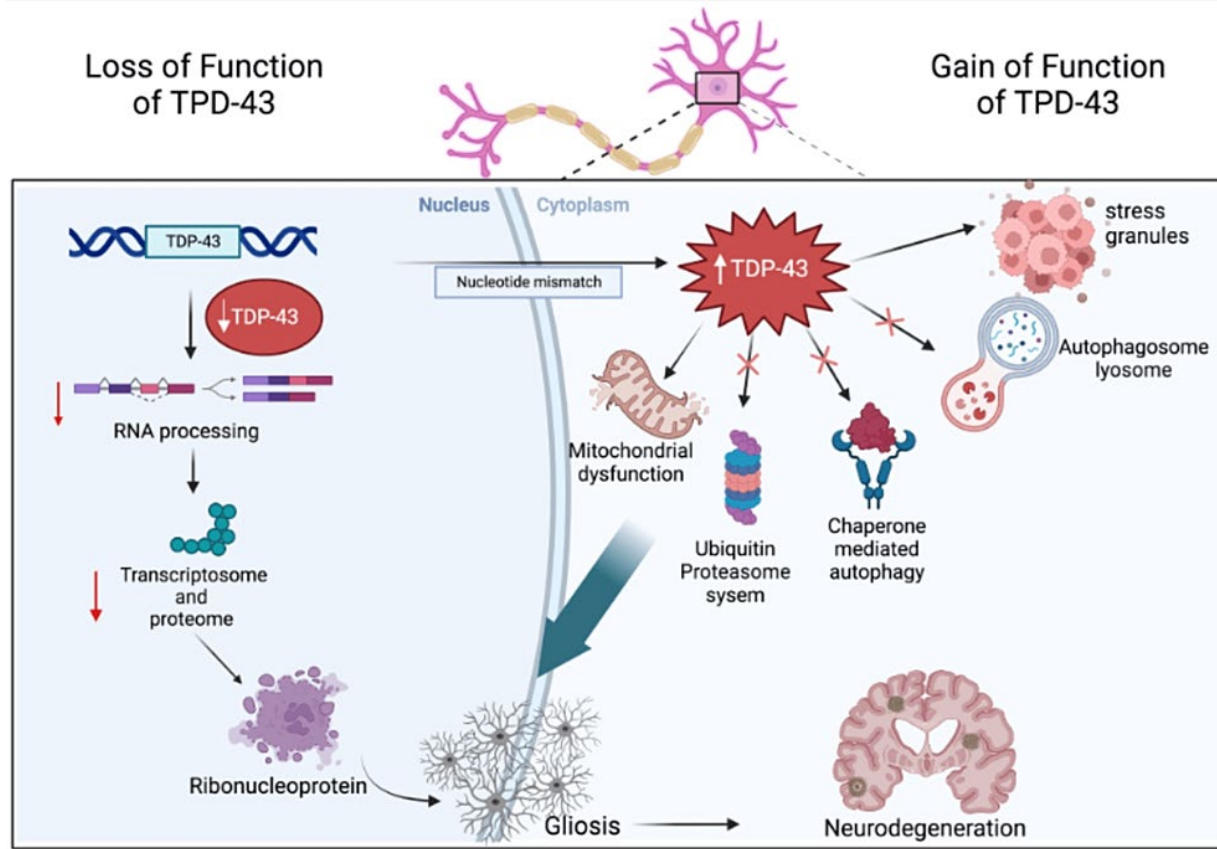


Figure 1.4. Schematic by Hussain et al. (2022) demonstrating the impact of the loss of TDP-43 function in both the nucleus and cytoplasm. In the nucleus, there is a decrease in nuclear TDP-43, thus reducing transcriptomes, proteasomes, and ribonucleoproteins, ultimately leading to gliosis and neurodegeneration. Additionally, cytoplasmic TDP-43 will increase, which impacts the normal functions of the ubiquitin-proteasome system, chaperone-mediated autophagy, autophagosome-lysosome degradation, stress granules, and mitochondrial dysfunction, also causing degeneration.

To summarize, the pathogenesis of TDP-43 has been well studied. It is well understood how and where the different types of posttranslational modifications occur, leading to TDP-43 dysfunction. The mechanism of TDP-43 aggregation is not as thoroughly studied, although there is an understanding of how aggregation affects the ability of the protein to function normally. However, more studies are required to provide a better understanding of factors, such as metal ions, that contribute to aggregation, and the mechanisms.

1.3. Metal Ions and TDP-43

Metal ions are essential for biochemical reactions to occur throughout the body. The specific roles vary, ranging from aiding in the structural integrity of proteins to acting as a cofactor in enzymes, aiding in the reaction process.⁵²⁻⁵⁴ Metal dyshomeostasis has been reported in many neurodegenerative diseases, and have been linked to the neurodegeneration process.^{55,56} Metal ions such as copper, zinc, and iron interact with different proteins throughout the body and play a role in many essential mechanisms. Additionally, it is common for ROS to form in diseases linked to metal dyshomeostasis, and these ROS cause damage to important cellular and nuclear components (Fig. 1.5). An abnormal metal ion concentration can influence disease onset or progression. Currently, it is not well understood how metal ions interact with TDP-43 and regulate its biochemistry, but recent publications suggest that metal ions do play a role.⁵⁷

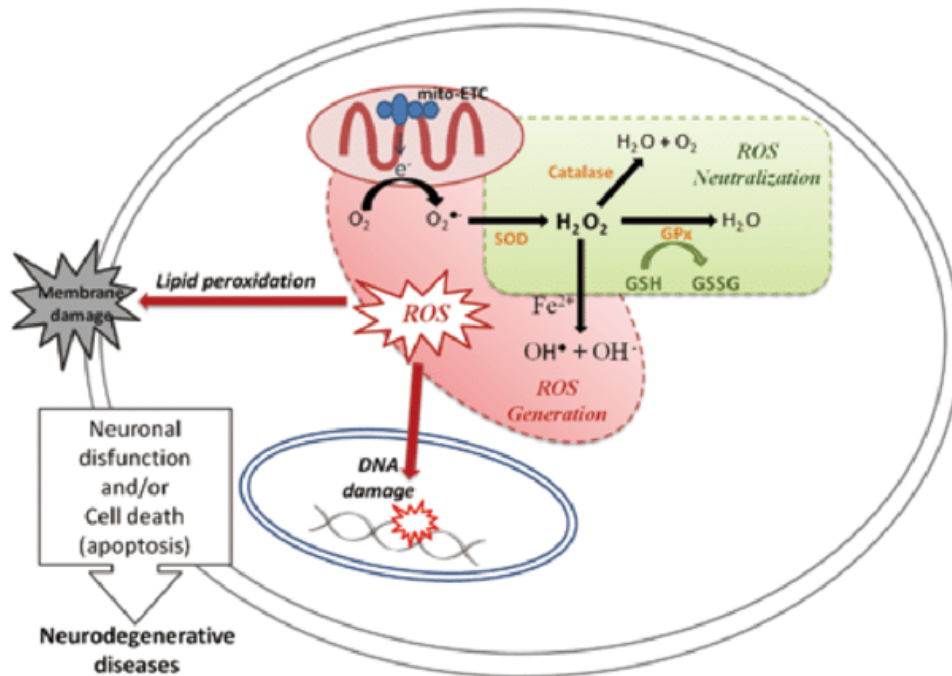



Figure 1.5. Schematic by Othman and Yabe (2015), showing reactive oxidative species (ROS) generation and neutralization in neuronal cells, and their role in neurodegenerative disease. Oxygen radicals are generated by oxygen metabolism, specifically the mitochondrial electron transport chain (mito-ETC). ROS neutralization occurs through the following pathways: oxygen radicals are converted to H_2O_2 via superoxide dismutase enzyme (SOD); H_2O_2 is converted to water through glutathione peroxidase (GPx) through the oxidation of glutathione (GSH) to oxidized glutathione (GSSG). Alternatively, ROS generation occurs when transition metals (such as Fe(II) or Cu(II)), interacts with H_2O_2 , which forms hydroxide radicals. Hydroxide radicals lead to DNA and membrane damage, ultimately causing neuronal cell dysfunction or death. 

Metal ion exposure and its link to ALS has been studied, specifically by looking at professions with neurotoxic metal exposure and the associated risk of ALS in the individuals within the profession.⁶⁰⁻⁶² For example, tool manufacturing, pottery, glass, and tile workers⁶³ are at increased risk of ALS, and these occupations involve neurotoxic metal exposure.^{64,65} Elevated metal ion concentrations have also been measured in ALS patients, such as aluminum, cadmium, cobalt, magnesium, lead, uranium, vanadium, selenium, zinc, iron, and copper.⁶⁶⁻⁷⁰ Studies suggest there is a link between metal ions and ALS, but the exact interplay between the two is poorly understood. Specifically, the pathophysiological mechanism of TDP-43 and the role of metal ions in causing ALS remains elusive.

1.3.1. Zinc (Zn(II))

Zn(II) is found in **the** blood, kidney, bones, liver, and brain. It plays important biological roles in cell division, DNA and RNA synthesis, and protein synthesis.⁷¹ Zinc also has effects on cognition, emotional stability, and memory.⁷² In neurons, zinc regulates postsynaptic excitability and protects against β -amyloid peptide neurotoxicity.⁷¹ However, at elevated concentrations, Zn(II) will translocate **into** neurons and inhibits various enzymes, influences mitochondrial respiration, and causes neuron depletion. Zinc readily forms stable coordination complexes within cells, thus, a majority of the intracellular zinc is bound to **proteins** and there is a low free zinc concentration.⁷³ However, since oxidative stress is associated with neurodegenerative diseases, Zn(II) may be released, causing an increase in free Zn(II).^{74,75} This increase in Zn(II) could prompt the denaturation of TDP-43, and aggregation.

Zn(II) has been shown to bind to TDP-43 in the RRM1/2 region.⁷³ Zn(II) binds to the RNA-binding domains of TDP-43 (residues 102-269), with an association constant of $2.8 \pm 0.2 \times 10^5 \text{ M}^{-1}$.⁷³ The binding of Zn(II) within this domain decreases the thermostability of the domains and

induce aggregation.⁷³ Garnier et al. (2017) analyzed the NMR structure of the RRM12 domains, with RNA bound to determine some potential Zn(II) binding sites, assuming binding sites for zinc would be to cysteine and histidine amino acids.⁷³ The potential binding site for Zn(II) in the RRM is hypothesized to be formed by Cys175, Cys173, and His116 in the β -strand of the RRM1 (Fig. 1.6). Whereas in the RRM2 domain, the hypothesized binding site was formed by His 256, Glu261, and Cys244.⁷³ The binding site within the RRM2 is located on the surface, in close proximity to the C-terminus. The CTD also contains several points for Zn(II) binding, such as His264.⁷³ Golovin et al. (2020) also investigated Zn(II) binding to TDP-43, specifically to the ²⁵⁶HISNAEPKH²⁶⁴ peptide form, which corresponds to the RRM2 domain of the protein.⁷⁶ It was determined that one Zn(II) can coordinate with the peptide by the His256, His264, Glu261, and the backbone of O from His 256.⁷⁶

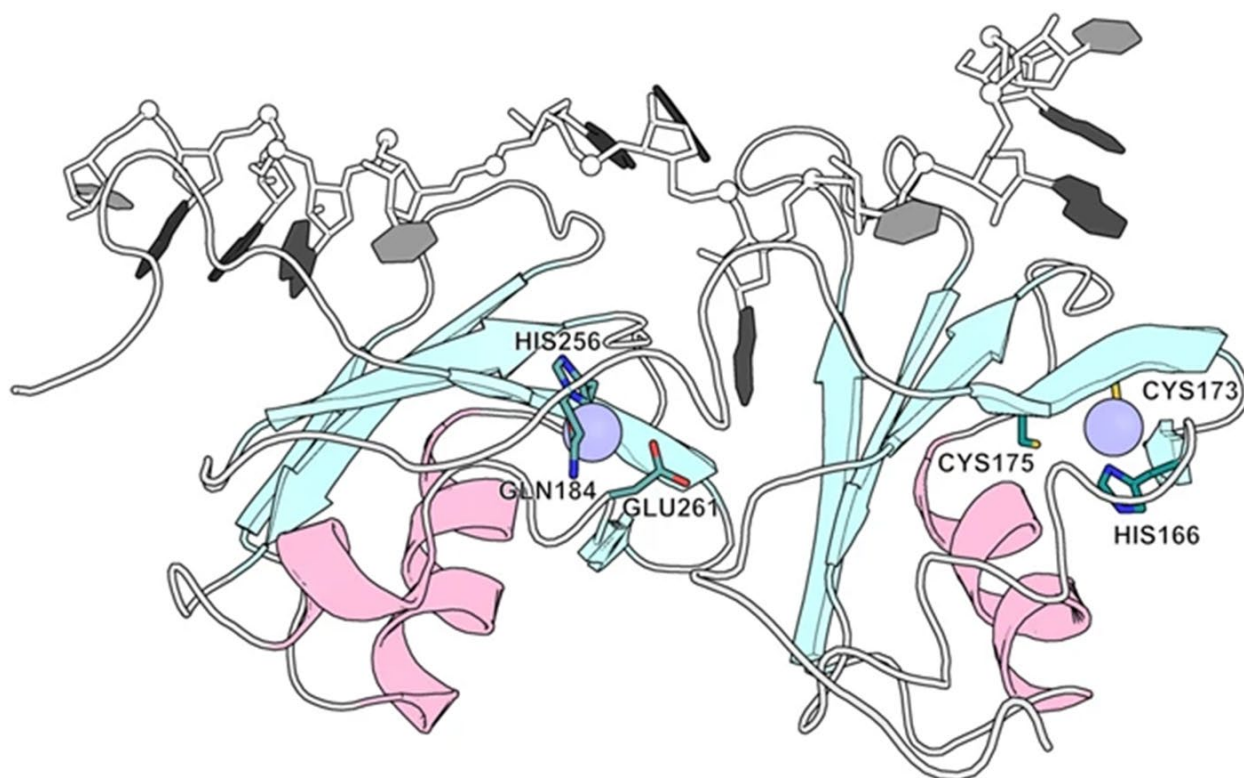


Figure 1.6. Hypothesized binding sights for Zn(II) coordination to TDP-43 RRM domains.⁷³ Two sites were identified for possible Zn(II) binding. In the last β -strand of the RRM1 domain, there is a site formed by Cys175, Cys173, and His166. The other is within the RRM2 domain, formed by His256, Glu261, and Cys244.

Although Garnier et al. (2017) and Golovin et al. (2020) provide evidence which suggested that there is binding between Zn(II) and the RRM domains of TDP-43, this interaction has not been studied in the biologically relevant context of full-length TDP-43.^{73,76} Full length TDP-43 and other disease variants of TDP-43 need to be investigated to determine if binding occurs. Following this, Zn(II) and its possible role in TDP-43 pathogenesis can be investigated further, and insight into ALS disease mechanisms can be gained.

1.3.2. Mercury (Hg(II))

Mercury (Hg) has no known functions within the body. However, people are often exposed to the toxic heavy metal. The most common exposure to Hg is through fish consumption or dental amalgam, which is a metal mixture used to fill cavities.⁷⁷ Methyl-Hg is absorbed through the gut and can deposit in many tissues, including the brain.⁷⁷ Although, elemental Hg crosses the blood-brain barrier more efficiently.⁷⁷ Inhalation of mercury vapour goes primarily to the brain.⁷⁸ There are two different types of Hg, organic and inorganic, both toxic to organisms. Methyl mercury and ethyl mercury are types of organic Hg and are more toxic forms compared to elemental Hg and salts. Hg exposure has been linked to ALS. Mercury intoxication has been reported to stimulate an ALS-resembling syndrome, which resolves in time with a reduction in Hg levels.⁷⁹⁻⁸¹ The effect of Hg on TDP-43 has been studied. Specifically, inorganic Hg was exposed to spinal cord tissue, and Hg and TDP-43 were simultaneously immunostained.⁸² Hg inclusions were observed in the tissue. However, TDP-43 aggregation was not observed. Additionally, no ALS-linked motor neuron symptoms were observed in the mice exposed to Hg.

Additionally, methyl-Hg and TDP-43 interactions were also studied. MethylHg was shown, with immunofluorescence, to increase nuclear TDP-43 aggregation and cell death.⁸³

MethylHg exposure, via drinking water, to mice also induced TDP-43 aggregation and mRNA splicing issues.⁸³ Data so far illustrate that environmental exposure to heavy and toxic metals may contribute to disease development. These environmental factors are exacerbated in remote regions where water monitoring is challenging.

1.3.3. Lead (Pb (II))

Lead (Pb), like Hg, has no known biological function in the body, and once it enters, it causes severe health effects.⁸⁴ Pb contains important properties, such as softness, malleability, ductility, resistance to corrosion, and poor conductivity, that make it useful in the industry, despite the toxic effects.⁸⁵ Additionally, Pb is non-biodegradable in nature, so continued use leads to accumulation in the environment.⁸⁵ Exposure to Pb often occurs from working in occupations that deal with leaded gasoline, smelting of Pb and its combustion, pottery, building boats, Pb-based paint, Pb-containing pipers, and battery recycling.⁸⁵ Pb has been thoroughly studied for its neurotoxic properties to gain a better understanding of how it contributes to neurodegenerative diseases.⁸⁵ Pb concentration was found to be elevated in both blood and cerebral spinal fluid (CSF) in ALS patients.⁶⁶⁻⁶⁸

TDP-43 aggregation is a known contributor to ALS; thus, Pb(II) was exposed to TDP-43 to determine if the metal ion can stimulate aggregation.⁸³ Different Pb(II) solutions were exposed to rat adrenal medulla cells, and the effect on TDP-43 was observed. Exposure of Pb(II) to these cells resulted in aggregation of TDP-43 and disruption in RNA metabolic functions, such as alternative splicing.⁸³ Environmental exposure to heavy and toxic metals may contribute to disease development, as indicated by these studies. However, the mechanism by which these metals

contribute to ALS needs to be further investigated. Further studies should be conducted to determine if the metal-induced aggregation is indirectly or directly caused by metal-binding.

1.3.4. Iron (Fe(III))

Iron (Fe) has important roles in intracellular redox reactions, and elevated levels of Fe are observed in the CSF of ALS patients.⁷⁰ Fe is a redox-active metal, circulating between Fe(II) and Fe(III) states. The homeostasis of the metal is maintained by iron-responsive/regulatory element proteins, which adjust the uptake or storage. Several receptors within the brain, such as the transferrin receptor, divalent metal transporter 1, amyloid precursor protein, ferroportin 1, ceruloplasmin, and ferritin, are involved in Fe trafficking.⁷⁰ Fe is a cofactor for various enzymes for normal brain metabolism, such as oxidative phosphorylation, transmitter formation, and myelination.⁷⁰ However, elevated Fe levels can be toxic, the free Fe catalyzes the formation of ROS, a key factor in ALS.⁷⁰ Fe(III) will react with H₂O₂ and form HO radicals. This Fenton reaction occurs naturally in biological systems,⁸⁶ and the formation of the radicals can be detrimental to cellular function and survival (Fig. 1.5).

Fe accumulates in the central nervous system of ALS patients.⁷⁰ However, exposure of Fe(II) to neuronal-like SY5Y cells did not increase aggregation or decrease TDP-43.⁸⁷ It is important to note that the SY5Y cells were previously treated with Zn(II), and then exposed to both Cu(II) and Fe(II), and this study did not directly monitor the impacts of Fe(II) on TDP-43.⁸⁷ Fe accumulations and TDP-43 aggregation have been observed in case studies of ALS patients presenting with speech apraxia and upper motor neuron symptoms.⁸⁸ However, whether the Fe accumulation causes TDP-43 aggregation is unknown. Although there is evidence of Fe(II)/(III) accumulation in ALS, further studies are required to determine if Fe(II)/(III) causes the

aggregation. Additionally, it would be of interest to determine how Fe(II) or Fe(III) interact with the protein in terms of binding sites.

1.3.5. Copper (Cu(II))

Copper (Cu) is essential to biological functions; it is required for growth, cardiovascular integrity, neuroendocrine function, and iron metabolism.⁸⁹ Cu is also an important factor for numerous enzymes in the nervous system and plays an important role in its development.⁹⁰ Dysregulation of Cu can lead to increased oxidative stress. There is a clear relationship between ROS and redox-active Cu(II).⁹¹ OH^- is one of the most abundant ROS species in nature, and it is generated by Fenton-type reactions between the reduced transition metal ion and H_2O_2 ,⁹¹ similar to Fe(III) (Fig. 1.5). A Fenton reaction is a process which converts hydrogen peroxide into a hydroxyl free radical.⁹² H_2O_2 is a by-product of oxygen metabolism in humans, which will complex with Cu(II) due to its highly reactive transition metal.⁹² Cu(II) can oxidize H_2O_2 to O_2 radicals and form Cu(I) in its place, which reacts with excess H_2O_2 to form HO radicals.⁹² Thus, when Cu(II) is not bound, it moves between its oxidized and reduced states, and this process can lead to the formation of ROS.⁹³ It has been reported that the coordination of Cu(II) to neurodegenerative peptides, such as amyloid, results in the formation of various ROS species.⁹¹ Neurons contain low concentrations of copper (II) ions, and elevated levels lead to toxic effects, including protein oxidation, neuronal membrane damage, and DNA damage.⁹³ The normal level of Cu(II) in neuronal cells is $40 \mu\text{M}$, while the elevated Cu(II) concentrations (related to diseases) are as high as $400 \mu\text{M}$.⁹¹

Although the prior treatment of neuronal-like SY5Y cells with Zn(II), followed by Cu(II) and Fe(II) did not increase aggregation or decrease the level of TDP-43.⁸⁷ Parker et al. (2012) demonstrated that treatment of SY5Y cells with Cu(II) bis-thiosemicarbazone complexes inhibited TDP-43 aggregation.⁹⁴ However, to our knowledge, this is the only piece of literature investigating the interactions between TDP-43 and Cu(II). The Cu(II)-TDP-43 interactions need to be further investigated to determine if the Cu(II) is an interactor for TDP-43, and if high Cu(II) concentration in the disease state contributes to TDP-43 pathogenesis.

Overall, there is evidence that metal ions interact with TDP-43. From previous studies, which investigated the effect of metal ion interactions on other neurodegenerative related proteins, it has been observed that metal ion interactions are capable of inducing aggregation in the proteins, suggesting that they may have a role in the pathogenesis of neurodegenerative diseases. Metal-protein interactions are a new field of interest, and thus literature examining these interactions can be limited; but this offers an exciting avenue of research. Investigating these metal interactions with TDP-43 can provide insight into how aggregation may occur. Furthermore, it can provide insight into the tertiary structure of protein, as coordination sites of metal ions are well reported in literature. Additionally, investigating this possible mechanism of pathogenesis may provide an avenue for new potential therapeutics for the disease, and perhaps blocking of disease progressions, as this is not possible with current treatment.

1.4. Analytical Methods for the Study of Metal Ion-TDP-43 Interactions

One of first steps in investigating metal ions and their possible involvement in TDP-43 pathogenesis is first establishing a correlation between the two. Many systematic studies have reported elevated metal ion concentrations in patients affected by ALS. The next step would be to investigate interactions between TDP-43 and metal ions. Metal ion interactions with TDP-43 were studied using immunofluorescence to detect TDP-43::GFP. Rat PC12 cells that were transfected with Tet-off-inducible wild-type TDP-43::GFP and grown.⁸³ The TDP-43::GFP was separated into two different types: diffuse nuclear (granule diameter of 3-11 μM , bias toward larger) and cellular puncta/aggregates (granule diameter of 1-5 μM , bias towards smaller),⁹⁵ to determine the effect of the metal ion on TDP-43. Larger granules indicated TDP-43 aggregation due to the presence of metal ions. Metal ion interactions with TDP-43 were also studied using immunostaining to detect TDP-43 in the spinal cord after metal exposure. TDP-43 was immunostained with both phosphorylation-dependent and independent antibodies to detect both types of TDP-43 and observe any possible aggregation.⁸² Although both Ash et al. and Boyd et al. observed aggregation of TDP-43 after metal ion exposure, there is no distinct evidence that TDP-43-metal ion binding causes the aggregation.⁸³ Thus, methods such as mass spectrometry (MS), circular dichroism (CD), isothermal titration calorimetry (ITC) and electrochemistry, provide a better understanding of TDP-43-metal ion interactions and binding.

1.4.1. Mass Spectrometry

Mass spectrometry (MS) is a common technique used in protein research and provides structural information about free protein and its complexes with metal ions. Golovin et al. utilized electrospray ionization (ESI)-MS to measure Zn(II) interactions with a TDP-43 RRM2 peptide.⁷⁶

To prevent dissociation of the Zn(II)-peptide complexes, soft ionization parameters were used. ESI-MS was utilized to allow for the detection of non-covalently bound multimeric peptide species.⁷⁶ Signals for the mono- (1032.5 m/z) and di-protonated (516.7 m/z) RRM2 peptide monomers were observed in the absence of Zn(II). When Zn(II) was exposed, signals at 547.8 and 578.7 m/z were detected, which corresponds to the RRM2 peptide complexed with one and two zinc ions.⁷⁶ Garnier et al. also used ESI-MS. In the absence of Zn(II), the RRM1/2 species had a calculated average mass of 19967.7 ± 1 Da, where the theoretical mass of the peptide is 19967.5.⁷³ However, after the exposure of Zn(II), the average mass was 20098 ± 1.4 Da, where the theoretical mass was 20099.5 Da, indicating the binding of two Zn(II) to the species.⁷³ Overall, Golovin et al. (2020) and Garnier et al. (2017) utilized mass spectrometry to investigate the interactions between TDP-43 and Zn(II).^{76,73} Both studies utilized peptides to investigate these interactions in the RRM domains of the protein specifically. Additionally, it was determined that two Zn(II) bind to the RRM peptide. While metallo-peptide studies have been reported, no MS data is available for the full-length protein and metal ion interactions and is required to determine the biological relevance of these interactions. Regardless, MS can be a suitable method for investigating TDP-43 interactions with metals and confirming coordination.

1.4.2. Circular Dichroism

Circular dichroism (CD) is a technique for the examination of protein structure in solution.⁹⁶ CD refers to the differential absorption of the two circularly polarized components of plane-polarized light. CD is used in protein studies because complementary structural information can be obtained from spectral regions.⁹⁶ Secondary structure information can be determined using

CD. The spectrum of peptide bands will depend on the content of α -helix, β -sheet, turns, and random coil.⁹⁷

Although there are no studies investigating interactions between metal ions and TDP-43, CD has been used to study the TDP-43 structure alone. Kuo et al. (2009) studied the structure of TDP-43 and utilized CD to monitor the thermal stability of an RRM2 dimer, rich in antiparallel β -sheets. The CD was monitored at 218 nm, to indicate the melting of the structure.¹⁶ Melting was indicated by changes in the difference between the absorbance of L and R components of the plane-polarized light, reported as ellipticity, in degrees.⁹⁶ Specifically, the absorbance of the R component of plane-polarized light increased because of the denaturation. The RRM2 domain was investigated to due to the presence of an atypical RRM fold, allowing self association of the RRM2 domains.⁹⁶ The discovery of this increased thermally stable RRM2 dimer can be used to provide a model for studying the TDP-43 aggregates, and seeing if the dimerization is a contributing factor to the protein pathology.

It would be of interest to use CD to monitor changes to the secondary structure induced by metal ion binding. However, metal-binding proteins may have charge transfer bands that are CD-active in the same region. Since the changes in CD are a sum of the secondary structure and charge transfer bands, no clear statement about the changes to the structure could be made.⁹⁷ This could be one explanation as to why TDP-43-metal interactions have not been explored using CD. Regardless, Kuo et al. did demonstrate that CD can be utilized to investigate the TDP-43 structure, and it is of interest to determine if the charge transfer bands from metal-protein binding interfere with CD results, as this method could provide insight into secondary structural changes in response to metal ion binding.

1.4.3. Isothermal Titration Calorimetry

Isothermal titration calorimetry (ITC) is a method used to determine the thermodynamic parameters of an interaction. For data collection, two cells are kept at the same temperature, then heat sensing devices detect the difference between the measurement and control cell and produce a signal. ITC measures the enthalpy of the reaction to provide a dissociation constant and a model-based binding stoichiometry.⁹⁷ The heat measured during analysis is a sum of all the reactions occurring, which include dilution, precipitation, oxidation, and degradation, during the titration of a metal ion to the protein.⁹⁷

Golovin et al. (2020) assessed zinc binding to a TDP-43 RRM2 peptide using ITC.⁷⁶ Zn(II) was injected into cells containing the peptide in solution. To gather more accurate results, the heat of dilution was measured by injecting Zn(II) into the buffer solution, and this value was subtracted from the heat of the reaction in the peptide solution. The association constant for Zn(II) binding to the RRM2 peptides was determined to be $1.6 \pm 0.3 \times 10^5 \text{ M}^{-1}$ ⁷⁶, which is similar to a Zn(II)-A β peptide association constant ($0.9 \pm 0.3 \times 10^5 \text{ M}^{-1}$,⁹⁸). The constant for Zn(II)-RRM2 binding is low; however, given that neuronal concentration of Zn(II) is increased due to the release of Zn from metalloproteins, it may be considered important in the role of aggregation.⁷⁶ The enthalpy of the interaction was also determined, -7.6 kcal/mol, showing the process is enthalpy driven, like A β ₆₋₁₄.⁹⁸ However, Zn(II)-RRM2 is an entropy unfavorable process, unlike A β ₆₋₁₄, indicating Zn(II) binding does cause the burying of hydrophobic residues.⁷⁶

Garnier et al. (2017) utilized ITC to examine the thermodynamics of Zn(II) binding to RRM 1 and 2.⁷³ Similar to Golovin et al. (2020), with the heat of dilution accounted for, the association constant for Zn(II)-RRM1/2 binding was $2.8 \pm 0.5 \times 10^5 \text{ M}^{-1}$.⁷⁶ The enthalpy of the

interaction was 15.2 ± 0.8 kcal/mol, showing that the interaction in enthalpy unfavourable. The Zn(II)-RRM1/2 was 73.6 cal/ K mol, indicating that there is an entropically driven.⁷³ Garnier et al. expected the ITC stoichiometry of Zn(II)-RRM1/2 binding to be around 2, but less than 0.4 ± 0.1 was measured.⁷³ this indicates that the ITC signal corresponds to one of the two Zn(II) binding sites, and the enthalpy of the second is undetectable.⁷³ The low stoichiometry indicates that the presence of Zn(II) binding reduces accessibility to other binding sites.⁷³ However, similar to MS methodology, only metallo-peptide studies have been reported, and further studies looking at full-length TDP-43 and metal ion interactions are required to determine the biological relevance of these interactions.

Overall, Golovin et al. (2020) utilized ITC to demonstrate Zn(II) binding to the RRM2 domain of TDP-43. The results also indicated that Zn(II) coordination to the domain may result in conformation changes.⁷⁶ Similarly, Garnier et al. (2017) investigated Zn(II) interactions with the RRM 1 and 2 domains of TDP-43 using ITC. ITC data indicated Zn(II) binding and also suggested that the binding of Zn(II) to the RRM 1 and 2 may block further Zn(II) binding. These results indicate that TDP-43 may be capable of binding metal ions, and given that metal ion concentrations increase in ALS, it is of interest to further study these interactions to determine if they play a role in TDP-43 pathogenesis. However, interrogating metalloproteins is challenging, and alternative approaches are needed to make fundamental discoveries in TDP-43 biochemistry. ITC allows for the investigation of metal ion binding to proteins but does not allow for further investigation of these interactions, such as conformational changes.



1.4.4. Electrochemistry

Studies of TDP-43 by electrochemistry are scarce, and metal ion interactions with the protein have not been investigated using electrochemistry. To our knowledge, there are only two studies investigating TDP-43 using electrochemistry at this time. Dia et al. developed an electrochemical biosensor for a human TDP-43 peptide.⁹⁹ Using ferri/ferrocyanide as a redox probe, differential pulse voltammetry (DPV), and electrochemical impedance spectroscopy (EIS), TDP-43 peptide was detected using Ab on Au surfaces in the presence of a ferri/ferrocyanide redox probe, using differential pulse voltammetry and electrochemical impedance spectroscopy (EIS) (Fig. 1.7A).⁹⁹ The sensor was a label-free method and allowed for a limit of detection (LOD) at 0.5 ng/mL. Full-length TDP-43 protein detection was also detected using TDP-43 Ab on Au.¹⁰⁰ However, this sensor was based on the immunosensor sandwich assay for protein detection and required the secondary molecules to indicate TDP-43 binding (Fig. 1.7B). The LOD achieved using the Ab-based assay was 12 pg/mL.¹⁰⁰

Although these studies do not use TDP-43 directly bound to the surface or provide detail about metal ion binding to the surface, they do provide measures of TDP-43 protein in solution. In both cases, electrochemical signals were not associated with TDP-43. Dia et al., needed to use the ferri/ferrocyanide redox probe to indicate TDP-43 presence on the surface. The signal measure was based on the redox probes' accessibility to the electrode surface. Serafin et al., required the secondary horseradish peroxidase (HRP)-labelled Ab and 3,3',5,5'-tetramethylbenzidine (TMB) substrate as an indicator, which provided the signal measured. Regardless, these two studies provide a fundamental understanding of TDP-43 behaviours in electrochemical settings and indicate that electrochemical methods can be utilized to investigate this protein.

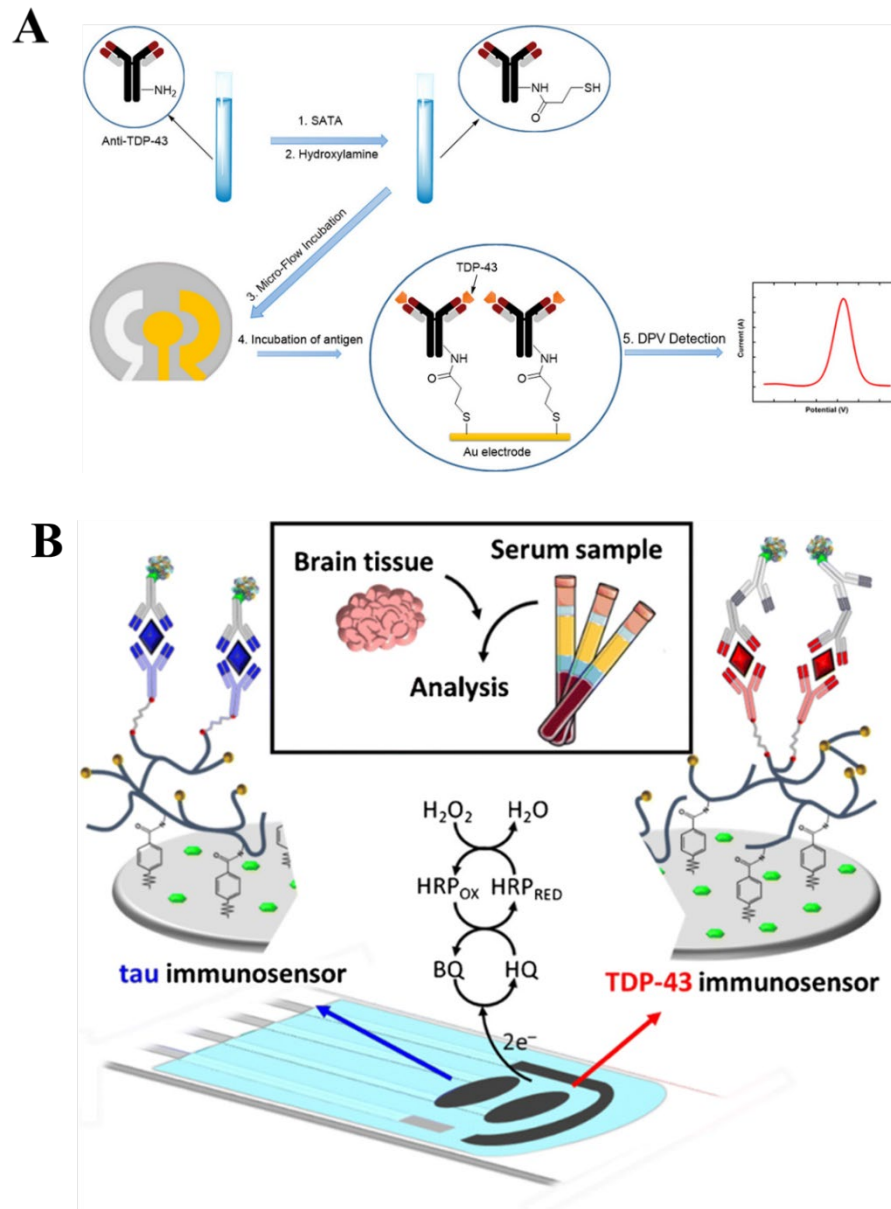


Figure 1.7. Schematic of TDP-43 binding to electrode surface for electrochemical measurement. **(A)** Dia et al. (2018) prepared a thiol-linked TDP-43 antibody to allow for easy immobilization onto the gold sensing surface, and allow for electrochemical detection of TDP-43 binding to the immobilized antibody using differential pulse voltammetry.⁹⁹ **(B)** Serafin et al. (2021) prepared a sandwich-type immunosensor for the detection of TDP-43, along with the neurodegenerative-related protein tau. A TDP-43 antibody was immobilized to an Au surface, and after TDP-43 was bound, the surface was exposed to horseradish peroxidase-labelled antibodies to allow for amperometric detection.¹⁰⁰

Electrochemical methods have been employed to study metal ion interactions and neurodegenerative disease biomarkers. Jiang et al. (2007) investigated the interactions between β -amyloid and Cu(II) using several methods, including solution electrochemistry. The glassy carbon working electrode was placed in a cell containing a β -amyloid solution, spiked with Cu(II), to monitor the interaction. The redox chemistry of the complex was investigated using cyclic voltammetry, the redox potential for the reduction of the bound Cu(II) was 0.08 V (Fig. 1.8A).¹⁰¹ Whereas Peng et al. 2010, utilized voltammetric experiments to determine the oxidation potential of α -synuclein binding to Fe(II).¹⁰² In the absence of Fe(II), a small irreversible oxidation peak at 0.73 V was observed (Fig.1.8B),¹⁰² which is attributed to the oxidation of tyrosine residues.¹⁰¹ However, this peak disappeared after Fe(II) exposure. Peng et al. postulated that this occurs because the α -synuclein-Fe(II) complex causes alterations in the secondary structure, reducing the number of tyrosine residues available for electrooxidation. Additionally, an oxidation (0.143 V) and reduction (-0.093 V) peaks appeared after Fe(II) exposure, corresponding to the oxidation of α -synuclein-Fe(II) and reduction of α -synuclein-Fe(III) (Fig. 1.8B).¹⁰²

Overall, Jiang et al. (2007) and Peng et al. (2010) demonstrated that metal-protein interactions can be monitored utilizing solution electrochemistry. The resulting data from the experiments provide a fundamental understanding of the metal-protein binding and can be utilized to confirm these interactions before moving to more time consuming or expensive methods.

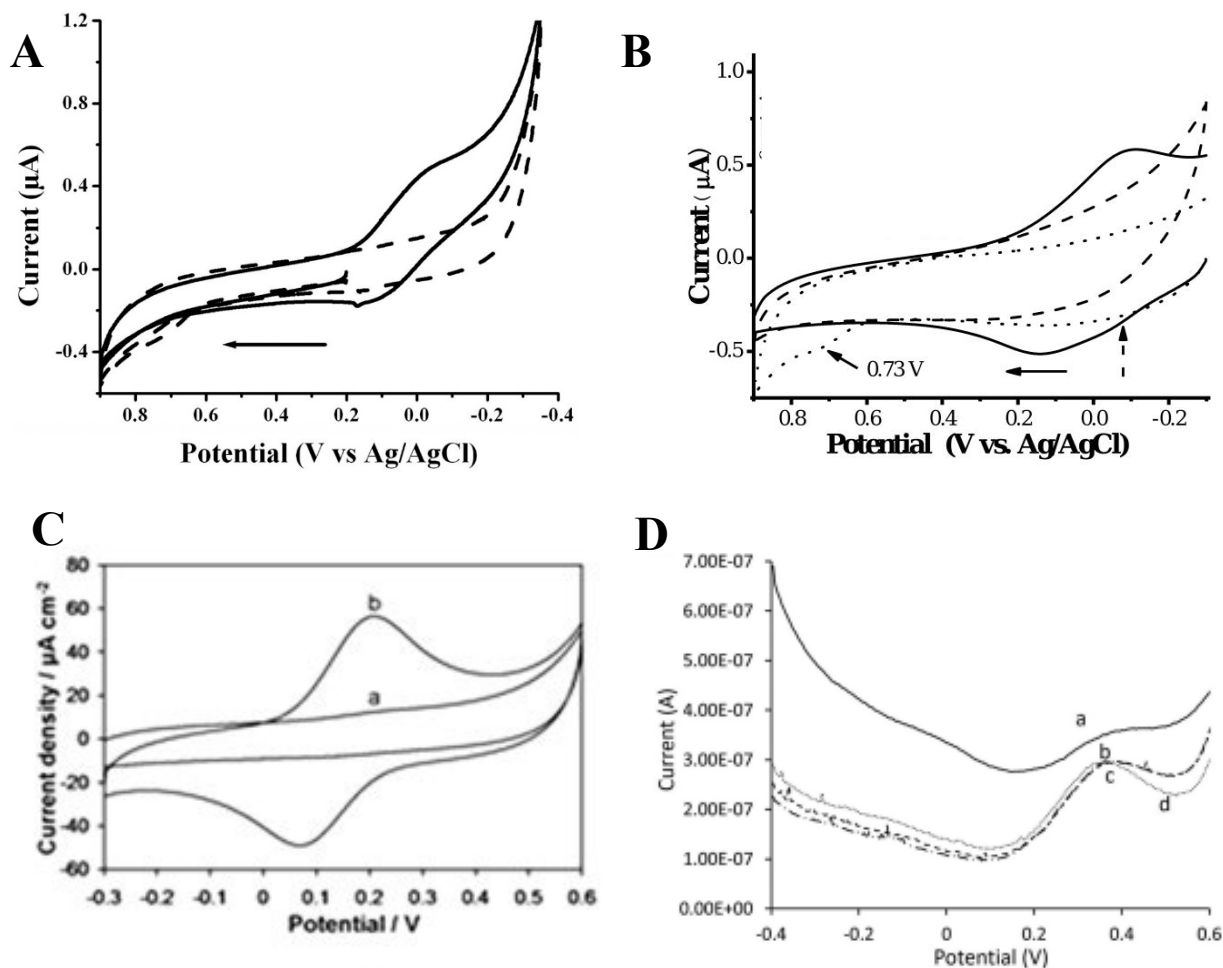


Figure 1.8. (A) Cyclic voltammograms of 50 μM β-amyloid (dashed curve) and 50 μM β-amyloid spiked with 50 μM Cu(II) (solid curve) at a glassy carbon disk electrode surface, from Jiang et al. (2007). Cu(II) redox potential was observed at 0.08V.¹⁰¹ (B) Cyclic voltammogram of 200 μM α-syn (dotted curve) and 200 μM Fe(II) spiked (solid curve) solution initially, and after 2 hours (dashed curve) from Peng et al. (2009). The oxidation curve for Fe(II) was observed at 0.143 V, and the reduction peak for Fe(III) was observed at -0.093 V.¹⁰² (C) Cyclic voltammogram of Tau films on the gold surface before (a) and after (b) incubation with Cu(II) solution, from Martic et al. (2013). The Cu(I) reduction peak was observed at 60 mV, and the Cu(II) oxidation peak to observed at 210 mV.¹⁰³ (D) Various mixtures of other peptides with R3 variant a) R3 mixed with R1, b) with R2, c) or with R4, from Golec et al. (2021). When the tau R3 peptide was mixed with other R peptides, similar SWV measurements were obtained, all resembling the Cu(II)/R3 peptide SWV profile. Indicating that R3 binds to Cu(II) with the strongest affinity compared to other peptides.¹⁰⁴

Martić et al. (2013) utilized surface electrochemistry to monitor the binding of Cu(II) to full-length tau-410 protein.¹⁰³ Tau was immobilized on gold surfaces, and the electrochemical signal measured before and after Cu(II) exposure was compared to verify the metal-protein interaction (Fig. 1.8C). Cu(II) exposed tau surfaces resulted in a signal at 140 ± 5 mV, which was due to the Cu(II)/Cu(I) redox couple.¹⁰³ Additionally, Cu(II) binding to the tau film was strong, as there was no reduction in signal intensity with repeated cycling.¹⁰³ Whereas, Golec et al. (2021) investigated Cu(II) binding to four tau R peptides using cyclic voltammetry, square-wave voltammetry, and differential pulse voltammetry.¹⁰⁴ A decrease in the current signal was observed, which was attributed to free Cu(II) binding to the R peptides in the solution.¹⁰⁴ This was the case for each peptide studied. Along with the reduced free Cu(II) signal, a new signal was observed, which was attributed to the Cu(II)-tau peptide complex. The R3 peptide had the strongest binding affinity, demonstrated using competition binding studies (Fig. 1.8D).¹⁰⁴ While electrochemical studies have been performed on other neurodegenerative disease-related proteins and metal ions, no such work has been reported to date for TDP-43.¹⁰⁵⁻¹⁰⁸

Overall, Martić et al. (2013) and Golec et al. (2021) demonstrated Cu(II) binding to tau protein, and provided evidence that these interactions can be monitored utilizing electrochemistry. The resulting data from the experiments provide a fundamental understanding of the Cu(II) interactions with protein. Specifically, signal observed at 140 mV after Cu(II) exposure to tau protein binding, provides an indication for where Cu(II) signals can be observed when immobilized to non-redox proteins, similar to TDP-43.¹⁰³ Additionally, free Cu(II) in the solution would provide a different potential for the Cu(II) signal, compared to the Cu(II) signal produced when it is bound to the protein surface.¹⁰⁴ Once more, demonstrating that metal-protein interactions can be monitored utilizing electrochemistry. In addition to providing a fundamental

understanding of the metal-protein binding, surface electrochemistry allows for the evaluation of these interactions utilizing minimal protein concentrations, allowing for cost effective investigations.

Overall, there are several different methods that can be utilized to investigate TDP-43 and metal ion interactions. Each method provides particular information regarding the possible interaction between the two, however, these methods are often required to be used in conjunction with one another to verify metal ion-TDP-43 interactions and or investigate the impact of the interactions on the protein structure. Utilizing these types of methods to investigate the metal-TDP-43 interactions will ultimately lead to a better understanding of the role of TDP-43 pathogenesis in ALS.

1.5. Thesis Research Rationale

Neurodegenerative diseases remain without a cure and early diagnosis. The lack of therapeutic and diagnostic tools is due to the poor understanding of disease pathogenesis. Specifically, the role of metal ions on protein pathogenesis is not fully understood, but when identified could lead to major discoveries in the field of metalloproteins and their role in aging and diseases. In this thesis, my objective was to determine if biologically relevant metal ions, such as Cu(II), Zn(II), Fe(III) interact with TDP-43. The biophysical studies were conducted by using electrochemical methods, which allow for direct monitoring of metal ion binding to the protein. The TDP-43 and metal exposed surfaces were also followed up by surface characterization. Due to the many benefits of electrochemistry, the unique properties of the protein were determined, such as redox potentials, reduction/oxidation reactions, metal ion competition and binding between

redox active metal ions and proteins, all of which are integral for a greater understanding of metalloproteins, especially in neurodegenerative diseases.

Chapter 2 describes Cu(II)-TDP-43 interactions using surface electrochemistry. The experimental surface was characterized using x-ray photoelectron spectroscopy (XPS), contact angle, and ellipsometry. Surface characterization was conducted to characterize Cu(II)-TDP-43 films, Cu(II)-free TDP-43 films, and verified other critical steps in surface modification. The effects of other biologically relevant metal ions, such as Zn(II) were evaluated in Chapter 2. Chapter 3 focused on the interplay between Cu(II) and Fe(III) and their interactions with TDP-43 protein film on Au surface. Using the bioelectrochemical approach, I provided a more fundamental understanding of the metallopathic relationship between TDP-43 and copper, and the effects other metal ions have on this interaction, by providing primary evidence that copper bound TDP-43. However, more research on the interaction could enhance the understanding of TDP-43 pathogenesis in ALS.

Chapter 2 : Electrochemical and Surface Analysis of Cu(II) and Zn(II) Metal Ions and TDP-43 Protein Interactions**

Meaghan Tabobondung¹, Chloe Connelly², Josephine Esposto¹, Iraklii Ebralidze³, Colin G. Wu,²
Sanela Martic^{1,4*}

¹ *Environmental and Life Sciences, Trent University, Peterborough, Ontario K9L 0G2, Canada*

² *Department of Chemistry, Oakland University, Rochester, Michigan 48309, USA*

³ *Faculty of Science, University of Ontario Institute of Technology, Oshawa, Ontario L1H 7K4, Canada*

⁴ *Department of Forensic Science, Trent University, Peterborough, Ontario K9L 0G2, Canada*

Keywords

Transactive response DNA-binding protein of 43 kDa (TDP-43); Amylotrophic lateral sclerosis (ALS); metalloprotein; reactive oxidative species (ROS); metal coordination; copper II (Cu(II)); surface electrochemistry; current signal; surface electrochemistry; metal displacement; metal competition

*** the following work will be submitted with a tentative submission deadline of April 2023*

M.T. performed all electrochemical experiments. M.T prepared surface analysis samples, samples were measured by M.T. with assistance from I.E. C.C. and C.W. contributed purified TDP-43 and text about the process.

Abstract

Amyotrophic lateral sclerosis (ALS) is a neurodegenerative disorder characterized by progressive loss in function of motor neurons. Both genetic and environmental factors contribute to ALS. Elevated copper (II) (Cu(II)) levels have been reported in ALS cases. Cu(II) interactions with other proteins associated with ALS have been investigated, however, the effects of metallation on transactive response (TAR) DNA-binding protein of 43 kDa (TDP-43) are less known. Normal TDP-43 has functions in alternative splicing and transcriptional regulation in the nucleus and, in the cytoplasm, it is responsible for stabilizing and transporting mRNA. However, in diseased cells, TDP-43 is hyperphosphorylated and aggregated, compromising TDP-43 function. There is increasing evidence that Cu(II) ions play a role in TDP-43 biochemistry. Here, I present an electrochemical and surface study of the interactions between full-length TDP-43 and Cu(II) ions. Compared to a Ag/AgCl reference electrode, the coordination of Cu(II) to the immobilized TDP-43-Au surface induced an electrochemical signal at approximately 0.18 V, due to the Cu(II)/Cu(I) redox couple. The binding of Cu(II) was also favourable at physiological pH. A competitive zinc(II) (Zn(II)) ion binding studies revealed TDP-43-Au films preferentially bind Cu(II), which may have biological significance.

2.1 Introduction

Metal ions can be essential for biochemical reactions to occur throughout the body. The specific roles vary, ranging from aiding in the structural integrity of proteins to acting as a catalytic point in enzymes.⁵²⁻⁵⁴ The impact of metal ions is also evident in certain diseases. Metal dyshomeostasis has been reported in many neurodegenerative diseases (NDD).^{55,56} Copper (II) (Cu(II)) ions promote the aggregation of several NDD-related proteins, including α -synuclein, tau, and β -amyloid, by directly binding to these targets.¹⁰⁹⁻¹¹¹ Dysregulation of metal ions, particularly copper, moves between its oxidized and reduced states, forming reactive oxidative species (ROS). Neurons contain low concentrations of Cu(II) ions, and elevated levels lead to toxic effects, including protein oxidation, neuronal membrane damage, and DNA damage.⁹³

Amyotrophic lateral sclerosis (ALS) is an NDD that is characterized by protein misfolding and aggregation, and recently, there is evidence that metal ions, such as Cu(II) and zinc(II) (Zn(II)), also play a role.⁵⁷ In particular, transactive response (TAR) DNA-binding protein of 43 kDa (TDP-43), found inside neuronal cells, contributes to the degeneration of motor neurons. Normal TDP-43 has functions in alternative splicing and transcriptional regulation in the nucleus and, in the cytoplasm, it is responsible for stabilizing and transporting mRNA.¹³ However, in diseased cells, TDP-43 is hyperphosphorylated and aggregated, compromising TDP-43 function.²⁹⁻³¹ Additionally, there have been recent studies suggesting that TDP-43 mislocalization also contributes to ALS.³³ Even though metal ion toxicity and the effect it has on other NDD-related proteins has been studied,¹¹²⁻¹¹⁴ the effects of metalation on TDP-43 are less known.⁵⁷ However, there is evidence that metal ions contribute to TDP-43 pathologies.^{115,57} There is increasing evidence that Cu(II) ion levels may play an important role in TDP-43 biochemistry. The binding of Cu(II) to cysteine (Cys) within the RRM1 domain causes Cys oxidation, and the oxidation leads

to loss of function in TDP-43 and aggregation.¹¹⁶ However, the neuronal-like cells (SY5Y) exposure to Cu(II) inhibited phosphorylation, and prevented aggregation (Parker et al., 2012). The binding of Cu(II) to cysteine within the RRM1 domain causes cysteine oxidation, and the oxidation leads to loss of function in TDP-43 and aggregation.¹¹⁶ Currently, it is not well understood how metal ions interact with TDP-43 and regulate its biochemistry. The redox chemistry of Cu(II) and Cu(II)/TDP-43 protein complex has not yet been identified, but is critical for understanding metal-catalyzed ROS formation and its role in ALS.

Electrochemical methods have been used to study NDD-related protein (peptides) interactions with Cu(II),¹⁰¹⁻¹⁰⁸ but Cu(II)/TDP-43 protein interactions have not been previously explored by electrochemical means. Due to the many benefits of electrochemistry, the unique properties of protein may be discovered, such as redox potentials, reduction/oxidation reactions, and binding between redox active metal ions and proteins. All of these facets are integral for greater understanding of metalloproteins, especially in NDD. Surface electrochemistry can also be used to measure conformation changes of proteins because of metal ion interactions.

Here, I employed the electrochemical technique square-wave (SWV) and cyclic voltammetry (CV) to monitor the interactions of the full-length TDP-43 protein with Cu(II) ions. The TDP-43 films were fabricated on the Au surface, and their interactions with Cu(II) were measured. The interactions of TDP-43 protein with Cu(II) ions were measured using surface electrochemistry, as depicted in Fig. 1. I hypothesized that, in the absence of Cu(II) ions, TDP-43 films on gold surfaces would be redox silent in the potential range of interest. However, upon binding to Cu(II) ions, an electrochemical signal is expected. Specifically, two peaks should be observed, which are associated with Cu(II) reduction and Cu(I) oxidation. The appearance of the peaks would indicate the formation of redox-active films, which can be detected using

electrochemical methods. Chapter 2 includes the evaluation of the concentration-dependent and pH-dependent binding of Cu(II) to the full-length TDP-43 protein films. The competitive and displacement metal ion binding of Zn(II) with Cu(II)/TDP-43 films was also explored. All metal ion-containing and free TDP-43 films were characterized by X-ray photoelectron spectroscopy, electrochemical impedance spectroscopy, and ellipsometry.

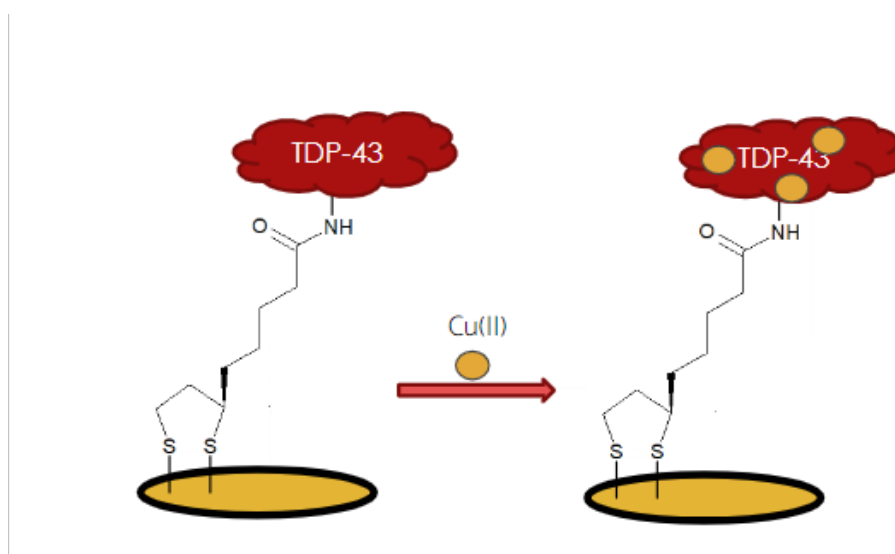


Figure 2.1. Schematic illustration of TDP-43-Au film and subsequent Cu(II) binding to form the redox active Cu(II)/TDP-43 protein film on Au-surface. The schematic diagram and coordination of Cu(II) to TDP-43 films are not to scale.

2.2. Experimental

2.2.1. Materials and Methods

The monobasic and dibasic potassium phosphate, 1-butylamine, hexanethiol, and reagent alcohol (EtOH) were purchased from Fisher Scientific. Potassium hydroxide (KOH) was purchased from Caledon Laboratory Chemicals. Ethanol was purchased from Commercial Alcohols by Greenfield Global. Potassium chloride was purchased from EMD. N-(3-dimethylamino-propyl)-N'-ethyl carbodiimide hydrochloride (EDC), N-hydroxysuccinimide (NHS), and DL α -lipoic acid were purchased from Sigma Aldrich (MO, USA). Alumina was purchased from Fisher Chemicals. Copper(II) nitrate 2.5 hydrate, was purchased from J. T. Baker. Zinc(II) perchlorate was purchased from Alfa Aesar (MA, USA). Potassium ferricyanide and potassium ferrocyanide was purchased from Acros Organics. Concentrated sulfuric acid was purchased from VWR Chemicals. The P-ladder was the Precision Plus Dual Colour Molecular Weight Marker (Bio-Rad, CA, USA). Primary antibodies used in this study were PA5-29949 ([antibody] = 1.59 mg/mL, rabbit polyclonal anti-TDP-43 1-289 [NTD-CTD], Invitrogen, MA, USA); anti-pTDP-43 (pSer410) antibody produced in rabbit ([antibody] = 1.0 mg/mL). Secondary antibodies (goat anti-rabbit IgG [H+L]-HRP [horseradish peroxidase] conjugate) were purchased from Bio-Rad (CA, USA). Alpha beta gamma buffer ($\alpha\beta\gamma$, pH 7.5) was prepared using sodium acetate (Sigma Aldrich Fine Chemicals, MO, USA), monosodium phosphate (VWR Chemicals, PA, USA), glycine (Invitrogen, MA, USA), and sodium chloride (Bio-Shop, CA). 1 M sodium hydroxide was used to adjust the pH of the buffer (Fisher Scientific, NY, USA). Sodium dodecyl sulfate (SDS) was purchased from Bio-Rad (CA, USA). All reagents were used without further purification.

2.2.2. TDP-43 Expression, Purification and Characterization

Full-length TDP-43 protein was expressed using a pET plasmid in E.coli Nico21. Bacterial cultures were grown in lysogeny broth media at 37 °C until an optical density of 0.4 - 0.6 was reached. This was measured using a UV-visible spectrophotometer at 600 nm (Nanodrop). Once the target optical density was reached, the cells were induced with 1mM IPTG and incubated at 16 °C overnight. After overnight incubation, cell lysis was carried out using lysis binding buffer containing 20 mM NaPi, 300 mM NaCl, 30 mM imidazole, 1 mM DTT, and 5% glycerol and PMSF. Then, the cells were sonicated for 10s on and 50s off for a total of 30 minutes at 40% amplitude. The lysate was centrifuged for 1.5 h at 18,500 rpm. The resulting supernatant was collected and syringe filtered using a 0.22 µm filter. The filtered supernatant was combined with 15 mL nickel resin that was equilibrated with the lysis/binding buffer and allowed to stir in a cold room for 1 hour. The supernatant/resin mixture was applied to a gravity flow column (BioRad) and washed using a series of buffers: a lysis/binding buffer and a wash buffer. The column was eluted with a buffer containing high concentration of imidazole. The elution was dialyzed against 20 mM HEPES pH 7.5, 150 mM KCl, 1 mM DTT, and 40% Glycerol three times for a minimum duration of 4 h between each buffer exchange. The elute was passed through a heparin FPLC column (AKTA Systems). The purest fractions were combined and concentrated to a final concentration of 9µM which was determined by UV spectroscopy (Nanodrop). The final protein sample was aliquoted and stored at -80 °C.

TDP-43 protein solution was spotted onto the nitrocellulose membrane and incubated overnight at 4 °C with primary anti-TDP-43 rabbit antibody (PA5-27221; 1:2000 in TBST; 3% BSA solution in TBST). The blots were incubated with secondary HRP-labeled goat anti-rabbit antibody (IgG; 1:1000 in TBST) for 45 min at RT; ~25°C. Dot blots were exposed to enhanced

chemiluminescence (ECL) reagent (1-2 min) and imaged using the ChemiDoc XRS Imaging system. The dot-blot analysis was carried out in duplicate to ensure accuracy.

2.2.3. Electrochemical Measurements

Electrochemical experiments were carried out using an Autolab PGSTAT302N by Metrohm AG. The gold disk electrodes (0.314 cm² surface area) were purchased from CH Instruments Inc. (TX, USA). A conventional three-electrode system using a working gold electrode, an auxiliary platinum wire electrode, and a reference Ag/AgCl/1.0 KCl electrode were used for all experiments. All surface characterization electrochemical experiments were performed in 10 mM potassium phosphate buffer (PB), pH 7.4, and 10 mM [Fe(CN)₆]^{3-/4-} unless otherwise specified. All measurements with Cu(II) were performed in a 10 mM potassium phosphate buffer (PB), pH 7.4. Cyclic voltammetry (CV) was performed at a scan rate of 100 mV/s and in the potential range between -0.4 and 0.7 V, for [Fe(CN)₆]^{3-/4-} or -0.6 to 0.6 for Cu(II) studies, unless otherwise stated. Square-wave voltammetry (SWV) was obtained by scanning the potential in the range -0.6 to 0.8 V at a frequency of 25 Hz and amplitude of 0.02 V. At a step height of 0.005 V, the effective scan rate was 0.12589 V/s unless otherwise stated. Electrochemical impedance spectroscopy (EIS) was applied at a frequency range of 1 – 100,000 Hz with an amplitude of 0.01 V. Fitted and experimental data were presented as Nyquist plots. The charge transfer resistance, R_{ct}, was determined by fitting the impedance data to the equivalent circuit. All experiments were performed in triplicates, and the corresponding error bars represent the standard deviations.

2.2.4. Cleaning of Au Electrodes

The Au disk electrodes were cleaned chemically in piranha solution (3:1 H₂SO₄:H₂O₂) for 5 min, then rinsed with deionized (DI) H₂O and polished on alumina slurry (80-200 mesh) for 3 min. After polishing, electrodes were sonicated in DI H₂O for 3 min to remove excess alumina and were cleaned electrochemically. Electrochemical cleaning was performed by running the CV in 0.5 M KOH solution at 0.5 V/s in the -2 - 0 V range. Followed by 0.5 M H₂SO₄ solution in the 0 - 1.5 V range at a scan rate of 0.5 V/s. The electrodes were then sonicated again for 5 min and cleaned electrochemically in 0.5 M H₂SO₄ once again. Clean Au electrodes were rinsed with DI water, then rinsed with ethanol.

2.2.5. Preparation of Protein Solution

10 mM PB was prepared by dissolving solid monobasic and dibasic potassium phosphate in reverse osmosis H₂O, and pH was adjusted to 7.4, using KOH solution. 500 μM Cu(II) was prepared by dissolving solid Cu(NO₃)₂ in PB, pH 7.4. 50, 100, 250, and 350 μM Cu(II) solutions were prepared by diluting 500 μM Cu(II) solution with PB, pH 7.4. 250 μM Zn(II) was prepared by dissolving solid Zn(II) perchlorate in PB, pH 7.4. 1 μM TDP-43 aliquots were diluted to 50 nM using PB, pH 7.4.

2.2.6. Preparation of TDP-43 Films on Au Electrodes

The clean Au electrodes were immersed in 4 mM DLα-lipoic (ethanol) at 4 °C overnight. After rinsing with ethanol, the electrodes were incubated in a mixture of 10 mM NHS (ethanol) and 8 mM EDC (ethanol) solution for 1 h at room temperature and rinsed with ethanol. After the surface was air dried, the electrodes were incubated in 50 nM TDP-43 (PB, pH 7.4) at 4 °C

overnight. After rinsing with PB followed by ethanol, the electrodes were immersed in 10 mM 1-butylamine (ethanol) for 1 h at room temperature. Electrodes were rinsed with ethanol and incubated in 10 mM hexanethiol (ethanol) for 30 min at room temperature. Subsequently, the electrodes were rinsed with ethanol followed by 10 mM PB, pH 7.4, prior to electrochemical measurements.

2.2.7. Interactions with Metal Ions

TDP-43-Au film was incubated in 5 μ L of various Cu(II) solutions in PB (pH 7.4) for 30 min at room temperature unless otherwise mentioned. The electrodes were rinsed with PB, prior to the measurements. The Cu(II) concentrations tested were 50, 100, 250, 350, and 500 μ M. The pH-dependent Cu(II) studies were performed at pH 3, 7.4, and 10.

The competition and displacement studies were carried out by incubating TDP-43-Au with 5 μ L of 350 μ M Cu(II) or 2 mM Zn(II) solutions for 30 min at room temperature, in succession or at the same time. The TDP-43 free surface was prepared as described above without the TDP-43 immobilization step. Next, the TDP-43-free surface was incubated in Cu(II) solution as described above.

2.2.8. Sample Preparation for Surface Characterization

The samples for surface characterization were prepared using 140 nm Au sputtered on 6 nm titanium wafer (Surface Science Western University, Canada). The Au wafers were sliced into substrates, which were cleaned by etching with piranha solution for 5 min and rinsing with DI water. Next, the substrates were rinsed with water, followed by ethanol, and preparation of the stepwise modification steps were performed as described above. Metal ion binding was carried out

at 250 μM Cu(II) and or 2 mM Zn(II) for 1 h at room temperature. Finally, the substrates were rinsed with 10 mM phosphate buffer, pH 7.4, and measured by ellipsometry, XPS, and contact angle measurements.

2.2.9. Ellipsometry

Multiwavelength ellipsometry was performed on a Film Sense FS-1 (NE, USA) Ellipsometer. The four LED light sources operated at 465 nm (blue), 525 nm (green), 590 nm (yellow), and 635 nm (red). The azimuthal orientation P of the internal polarizer set the polarization state of the incident beam to be $+45^\circ$. The reflected beam polarization state was automatically analyzed by the software based on the method proposed by Azzam.¹¹⁷ Each sample was tested in duplicate measurements.

2.2.10. Contact Angle Measurements

Contact angle (θ) was measured using the method based on the diameter of 3 μL droplet of deionized water to determine the surface wettability of various steps in surface modification on an Au surface. Each sample was tested in duplicate measurements.

2.2.11. X-ray Photoelectron Spectroscopy

X-ray photoelectron spectroscopy (XPS) measurements were carried out at the Materials Characterization Facility, Ontario Tech University, using a ThermoFisher Scientific Nexsa Surface Analysis System. The monochromated Al K α (1486.6 eV) X-ray source was at 12 kV, 6 mA emission current, and 400- μm spot size. The charge compensation was achieved using a flood gun. The chamber pressure was 7×10^{-8} mbar, and the survey spectra were at low energy axis point

density (1.0 eV point spacing) and low energy resolution (E-pass = 200 eV). The regional spectra was 0.1 eV point spacing and higher energy resolution E-pass = 50 eV. The XPS data was analyzed using Avantage software. A Shirley background function was used to approximate the experimental background. Scofield Al κ - α sensitivity factors were used to calculate relative atomic percentages. Each sample was tested in duplicate measurements.

2.3. Results and Discussion

2.3.1. Biochemical Characterization of TDP-43

TAR DNA-binding protein of 43 kDa (TDP-43) is composed of 414 amino acids and its primary sequence consists of an N-terminal domain (NTD), two RNA recognition motifs (RRM1 and RRM2) and an C-terminal domain (CTD) (Fig. 2.2). Importantly, TPD-43 has 6 Cys residues, 4 of which are located in the RRM domains. The full-length TDP-43 protein was expressed using a pET plasmid in E.coli, and purified. The growth of the TDP-43 construct produced high expression levels as evidenced by a high intensity band at ~50 kDa on SDS-PAGE (Fig S1A). To confirm that TDP-43 was not phosphorylated, dot blots were carried out and showed no phosphorylation at the S410 site (Fig. S1B). This purified full-length TDP-43 protein was used for electrochemical studies with metal ions. Non-phosphorylated TDP-43 was used to aid in the development of a fundamental understanding of Cu(II) and other metal ion interactions with TDP-43. If Cu(II) binding to TDP-43 was observed using the electrochemical methods, further studies could be done to determine if these interactions still occur with disease related types of TDP-43, such as mutants and forms of TDP-43 that are post-translationally modified incorrectly.

Additionally, the discovery of metal ion binding to normal TDP-43 may provide some insight into TDP-43 pathogenesis.



Figure 2.2. Domain map showing the relative sizes of TDP-43 domains, N-terminal, RNA recognition, and C-terminal domains, respectively. Adapted from François-Moutal et al. (2019).²⁵

2.3.2. TDP-43-Au Film Fabrication

To monitor Cu(II) binding to TDP-43, electrochemical methods were utilized. To investigate the interactions, TDP-43 must be immobilized to an electrode surface. Similar to other studies investigating metal interactions with proteins, a gold surface disc electrode was used to monitor binding to the surface.^{118,103} TDP-43 was immobilized to the surface through a reactive Lip-NHS ester. After TDP-43 immobilization, the surface was exposed to more solutions to remove other possible interaction sites for metal ions, and ensure metal ions were integrating with the TDP-43 surface.

In more detail, the fabrication of the TDP-43-Au surface is depicted in Fig. 2.3. Briefly, the lipoic acid (Lip) was immobilized on the Au surface (i), followed by EDC/NHS functionalization (ii) to generate a reactive Lip-NHS active ester on the Au surface. Next, the conjugation of the TDP-43 protein was achieved preferentially *via* a terminal amino group of protein with the active ester on the surface (iii). Subsequently, the unreacted NHS sites were blocked with n-butylamine (iv) and Au surface backfilled with diluent, hexanethiol (v). To verify

the surface modification steps, electrochemistry, contact angle, ellipsometry, and X-ray photoelectron spectroscopy were completed.

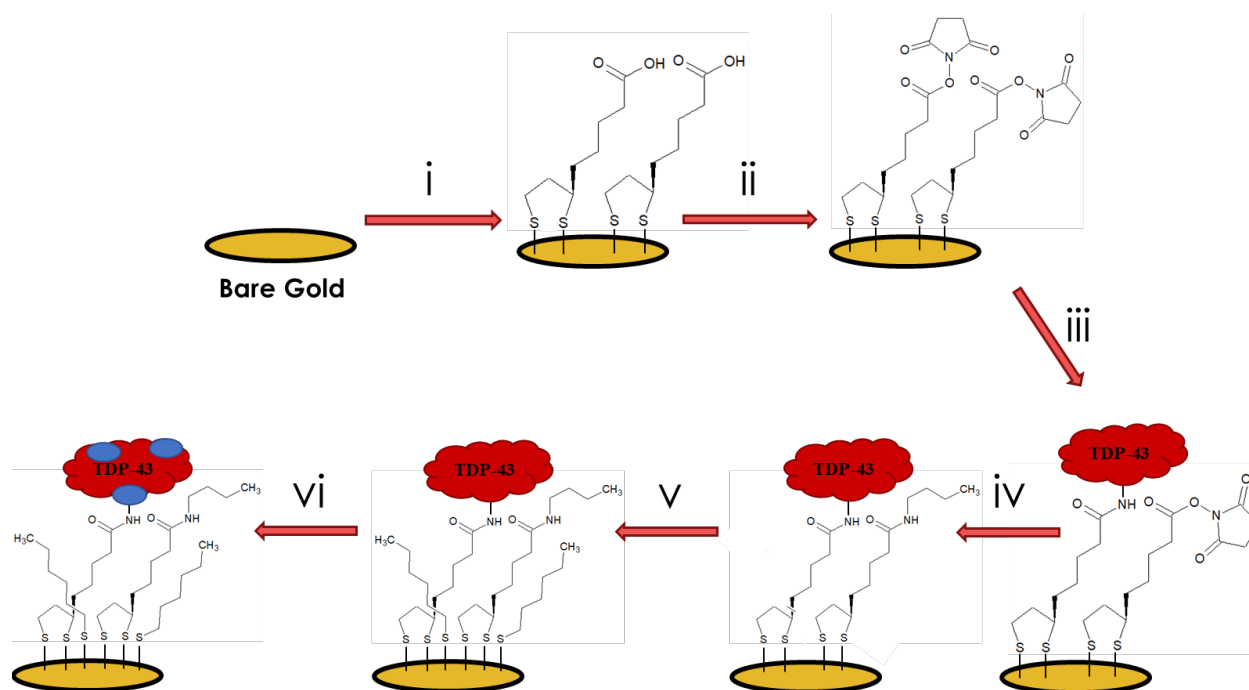


Figure 2.3. Schematic illustration of the surface modifications of Bare Au: (i) Lipoic acid, (ii) EDC and NHS, (iii) full-length TDP-43 protein, (iv) n-butylamine, (v) hexanethiol, and (vi) Cu (II) exposure.

The stepwise fabrication of the TDP-43–Au surface was characterized by CV as in Figure 2.2 in the presence of the redox couple $[\text{Fe}(\text{CN})_6]^{3-/4-}$. The bare-Au (a) electrode exhibited reversible oxidation/reduction peaks ($I_{\text{pa}} = -0.088 \text{ mA}$, $I_{\text{pc}} = 0.095 \text{ mA}$, $\Delta E = 0.17 \text{ V}$) (Fig. 2.4A). At this point in fabrication, the redox probe could interact with the surface readily. However, after the fabrication of active Lip-NHS ester and TDP-43 immobilization caused a reduction in the current and an increase in the peak difference ($\Delta E = 0.20 \text{ V}$). The reduced current and increased peak separation indicated that the accessibility of the redox probe to the Au surface was reduced, which verified that the Au surface is no longer bare and suggested that TDP-43 has been immobilized to the electrode surface. Blocking with 1-butylamine ($\Delta E = 0.43 \text{ V}$) and subsequent backfilling with hexanethiol caused more significant signal changes when compared to bare Au peaks ($\Delta E = 0.17 \text{ V}$). The blocking and backfilling steps were expected to increase the resistance of the film to the redox probe, as it introduced more steric hinderance and reduced the free gold surface to the redox probe. The increased peak separation indicated that the blocking and backfilling steps were successful, and thus the only possible binding site for Cu(II) would have been to the protein.

The stepwise fabrication of the TDP-43–Au surface was also monitored by EIS. The bare-Au (a) electrode was characterized by the diffusion-controlled process, Warburg parameter, W (Fig. 2.3B). Data were fitted using the equivalent circuit (inset Fig. 2.4B). In the event that data did not exhibit an obvious W component, data was fitted to the equivalent circuit composed of solution resistance (R_S), charge transfer resistance (R_{ct}), and constant phase element (CPE).^{119,120} The R_S value was dependent on the distance between the Au electrode surface, reference electrode, and the solution, and was likely to remain unchanged for the duration of the measurements. The R_{ct} was associated with the access that the redox probe had to the electrode and was related to the

resistance of electron transfer at the electrode surface. The R_{ct} corresponded to the diameter of the semi-circle observed in Nyquist Plots, where the larger diameter indicated an increased resistance.¹²¹ The bare Au was characterized by a low R_{ct} value (149 Ω) compared to the Lip-NHS film (R_{ct} = 1870 Ω). Again, further indication of successful immobilization of the TDP-43 to the bare gold surface. The blocking with 1-butylamine resulted in an increase in resistance due to successful blocking of unreacted NHS sites. The final TDP-43–Au surface was characterized by the R_{ct} of 1090 Ω . The increased R_{ct} from 149 to 1090 Ω indicated that the redox probe had a decreased accessibility to the gold surface after the final TDP-43-Au film was fabricated, which indicated changes occurred to the surface. It was assumed that these changes were correlated with successful surface modification, however, further studies were conducted to verify TDP-43-Au film fabrication.

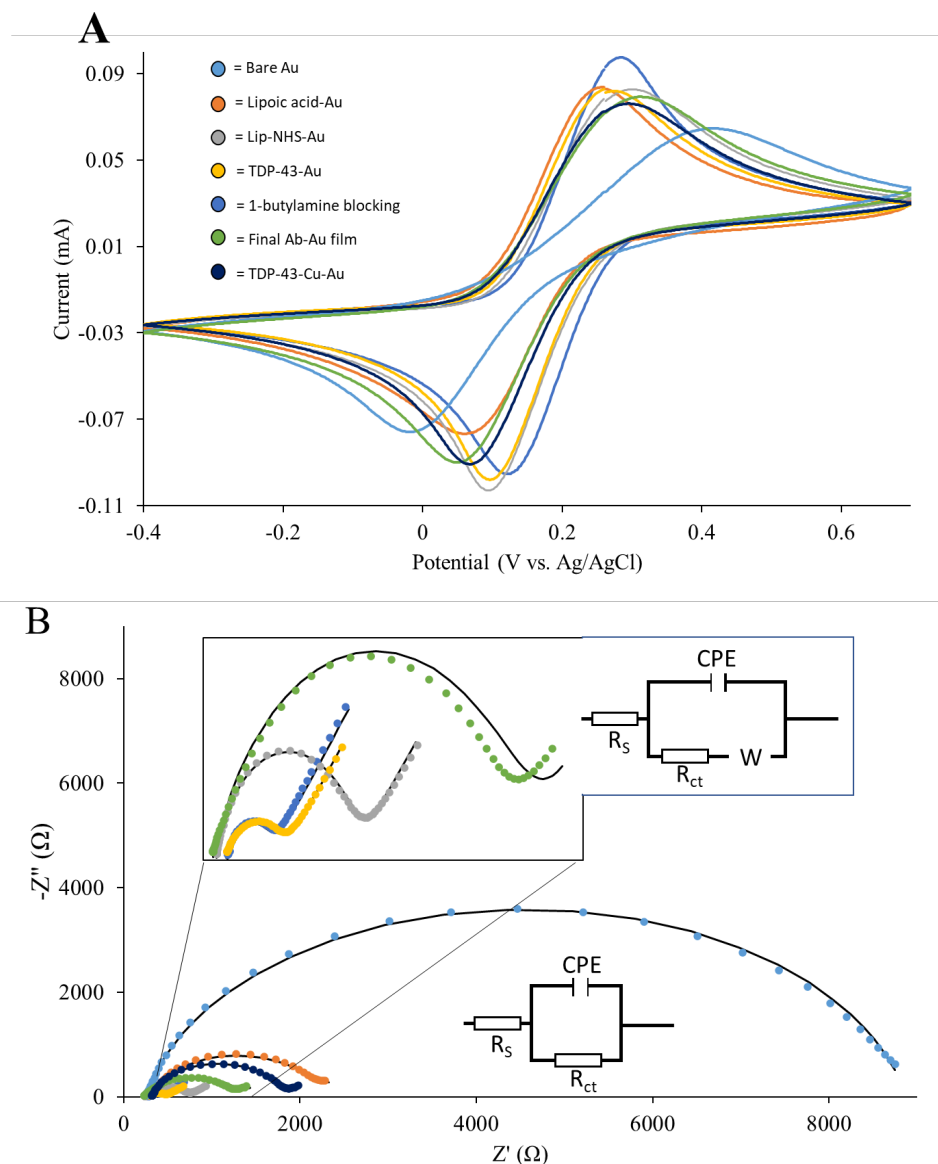


Figure 2.4. A) Cyclic voltammograms and **B)** Nyquist plots of stepwise surface modifications of bare Au surface for fabrication of TDP-43-Au film (Inset: the equivalent circuit used for fitting experimental data with W . Data without W were fitted with an exact circuit and W omitted; experimental data - symbols, fitted data - solid line). *Data collected by M.T.*

In addition to electrochemical surface characterization, surface modification was also evaluated using non-electrochemical methods. Ellipsometry was used to determine the relative film thickness of the TDP-43-Au film (3.1 ± 0.3 nm). The surface wettability was determined by measuring the contact angle. Typically, a hydrophobic surface would produce a larger contact angle,¹²² such as a bare Au at $67.1 \pm 1.1^\circ$. The contact angle of the TDP-43-Au film was $51.5 \pm 2.0^\circ$, which suggested that the surface was more hydrophilic after the addition of the protein to the surface. Finally, the surface modifications were also characterized by XPS. XPS analysis of the Lip-Au film showed O, C, and S content, with an 8.8:1.9:1.7 ratio, respectively, which was close to the expected values based on the Lip stoichiometry. The O 1s peak at 532.0 eV was observed, alongside the carbon C 1s peaks at 284.8 eV and 289.0 eV, which corresponded to the aliphatic and carbonyl carbon, respectively. The Lip-Au film was also confirmed by the characteristic two doublets at the S 2p binding energy (163.3 and 164.6 eV), which indicated the successful attachment of the Lip to the Au surface.¹²³ Pure monolayers would have exhibited two main doublets with an approximate ratio of 2:1, and a 1.2 eV splitting.¹²³ Unbound thiols have an S 2p_{1/2} binding energy of around 165 eV,¹²³ thus, the binding energy observed for the sample may have indicated the presence of some bound and some unbound Lip. The TDP-43-Au film was characterized by Au, S, C, N, O binding energies (Fig. 2.5). The S 2p binding energies at 162.0, 163.5, and 165.1 eV were observed (Fig. 2.5A). The bound thiol was associated with 162.0 eV peak, while unbound thiol or disulfide was assigned to the 163.5 eV.¹²⁴ The binding energy of the S 2p_{3/2} at 162.0 eV was consistent with the sulfur atoms bound to the Au surface as a thiolate species. The large difference in binding energy (1.3 eV) indicated the presence of bound thiolate. Additionally, the intensity of the S 2p peak at 163.5 eV increased compared to Lip-Au surface, which indicated the presence of additional unbound thiols, and the peak at 165.1 eV was attributed

to unbound disulfides of protein. In general, S-S and S-H bonding is located in the 163.5 - 165.0 eV range. The N 1s spectrum of the TDP-43-Au films was characterized by three major peaks at 401.9 eV, 400.4 eV and 399.09 eV (Fig. 2.5B). Amide nitrogen appeared at 400 eV, which indicated the presence of a protein on the surface. The blocking reagent may have also contributed to the signal. The peak at 401 eV indicated an ammonium group (sp^2), whereas the peak at 399 eV indicated pyridinic N due to His residues of protein (sp^2). The O 1s peak was centered at 532.2 eV, which was the expected binding energy for C–O bonds (Fig. 2.5C). The C 1s area can be deconvoluted into two peaks at 285.4 and 288.0 eV (Fig. 2.5D). The peak at 285 eV was characteristic of a C–C bond, whereas the 288 eV peak was representative of a carbonyl carbon.

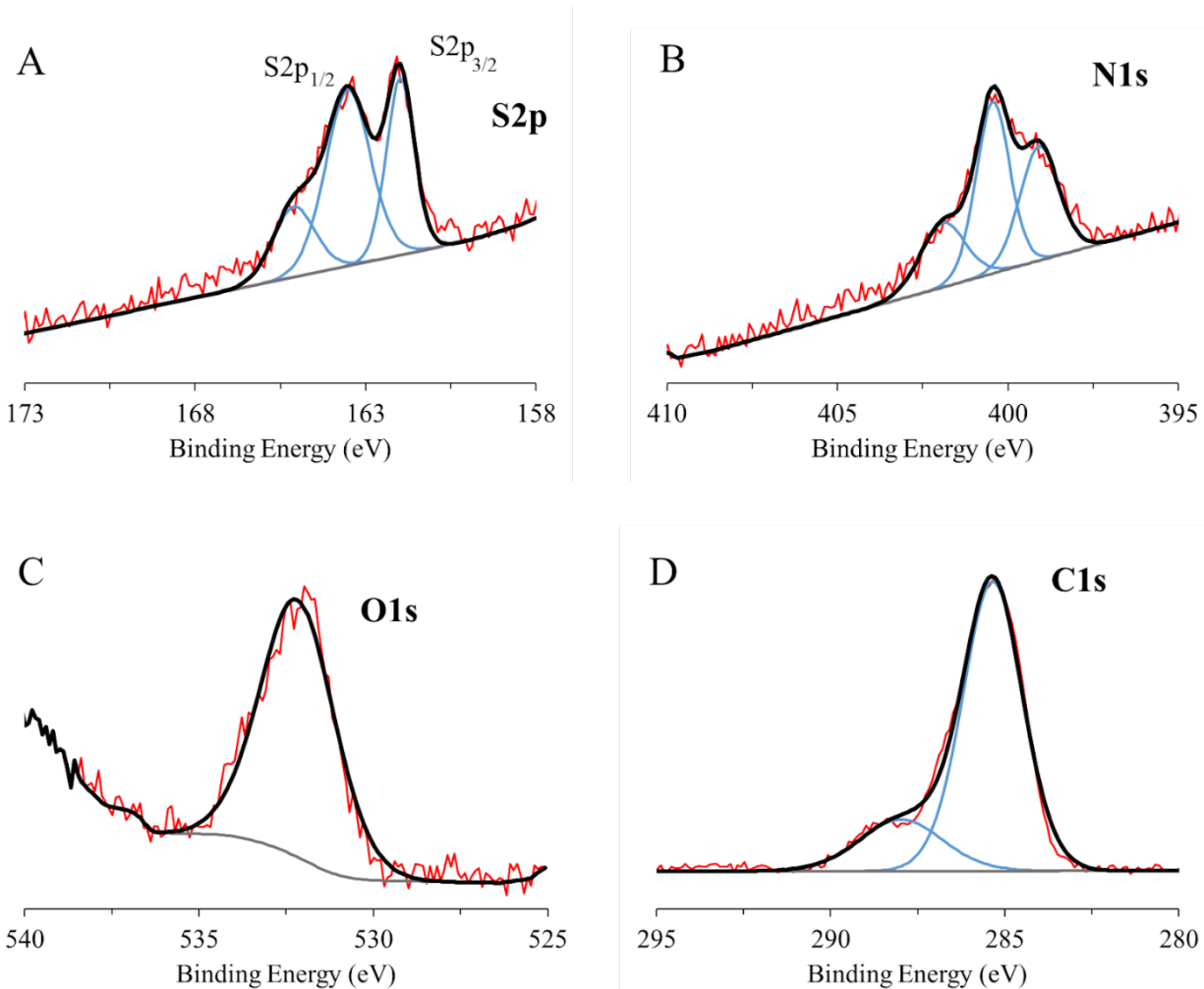


Figure 2.5. XPS spectra of TDP-43-Au film showing A) S 2p peaks at 162.0, 163.5, and 165.1 eV; B) N 1s peaks at 399.09, 400.44, and 401.91 eV; C) O 1s peak at 532.2 eV; and D) C 1s peaks at 285.35 and 287.98 eV. *Data collected by M.T. with assistance from I.E.*

Overall, the successful surface modification of the Au surface was verified using ellipsometry, contact angle, and XPS. Ellipsometry provided data showed that the thickness of the final film on the gold surface increased, compared to the unmodified gold surface, indicating changes occurred. The contact angle data provided information regarding the hydrophilic and hydrophobic properties of the surface after various steps in modification. The changes in these properties were consistent with the elemental composition of the surface at the various steps in modification. For example, the bare Au surface had a contact angle $67.1 \pm 1.1^\circ$, however, after Lip immobilization, and the introduction of more the strongly hydrophilic carboxyl groups, the contact angle was reduced to $51.6 \pm 1.9^\circ$. Finally, XPS provided the elemental composition of the final film and various steps in modification. Presence of the sulfur S 2p peaks indicated the successful immobilization of the Lip-NHS ester to the Au surface, which was required for the TDP-43 immobilization. Additionally, the ratio observed for the carbon C 1s, oxygen O 1s and nitrogen N 1s peaks were characteristic and similar to those observed in other studies looking at protein-immobilization.¹⁰³ Thus, data suggested that the procedure utilized for TDP-43 immobilization to the Au surface to allow for electrochemical measurements was adequate.

2.3.3. Interactions of Cu(II) with TDP-43-Au Surfaces

While the amyloidogenic CTD region of TDP-43 does not have amino acids which are able to chelate metal ions, the NTD and RRM domains contain 32 potential chelating sites (Cys, His and Glu residues). Hence, these amino acids are potential coordination sites for Cu(II). Once the TDP-43-Au film was fabricated, the film was exposed to Cu(II). Various concentrations of Cu(II) were tested with TDP-43-Au film (Fig. 2.6). The physiological level of Cu(II) in neuronal cells is $40 \mu\text{M}$, while the elevated Cu(II) concentrations (related to diseases) are as high as $400 \mu\text{M}$.⁹⁷

Upon Cu(II) binding to TDP-43-Au film, the cyclic voltammogram (Fig. 2.6A) shows a characteristic Cu(II)/Cu(I) redox couple at 160 mV. Notably, TDP-43-Au film was not redox active in the potential range measured (-0.6 - 0.6 V). The square-wave voltammograms (Fig. 2.6B) showed an increase in Cu-related signal with increasing metal ion concentrations. The relationship between electrochemical signal and the Cu(II) concentration (Fig. 2.6C) was linear with an R^2 value of 0.91 (Fig. S18). Thus, the electrochemical data suggests that Cu(II) binds to the TDP-43-Au surface when exposed. The concentration dependent studies also indicate that the Cu(II) electrochemical signal observed is directly correlated to the concentration of Cu(II) exposed to the surface. Additionally, from the concentration dependent studies, I observed that disease-related concentrations will bind to the fabricated TDP-43-Au surface, allowing us to monitor relevant concentrations in the metal ion interaction studies. It was assumed that the appearance of the reversible peaks was due to Cu(II) presence, however, further studies were conducted to verify TDP-43-Au film fabrication.

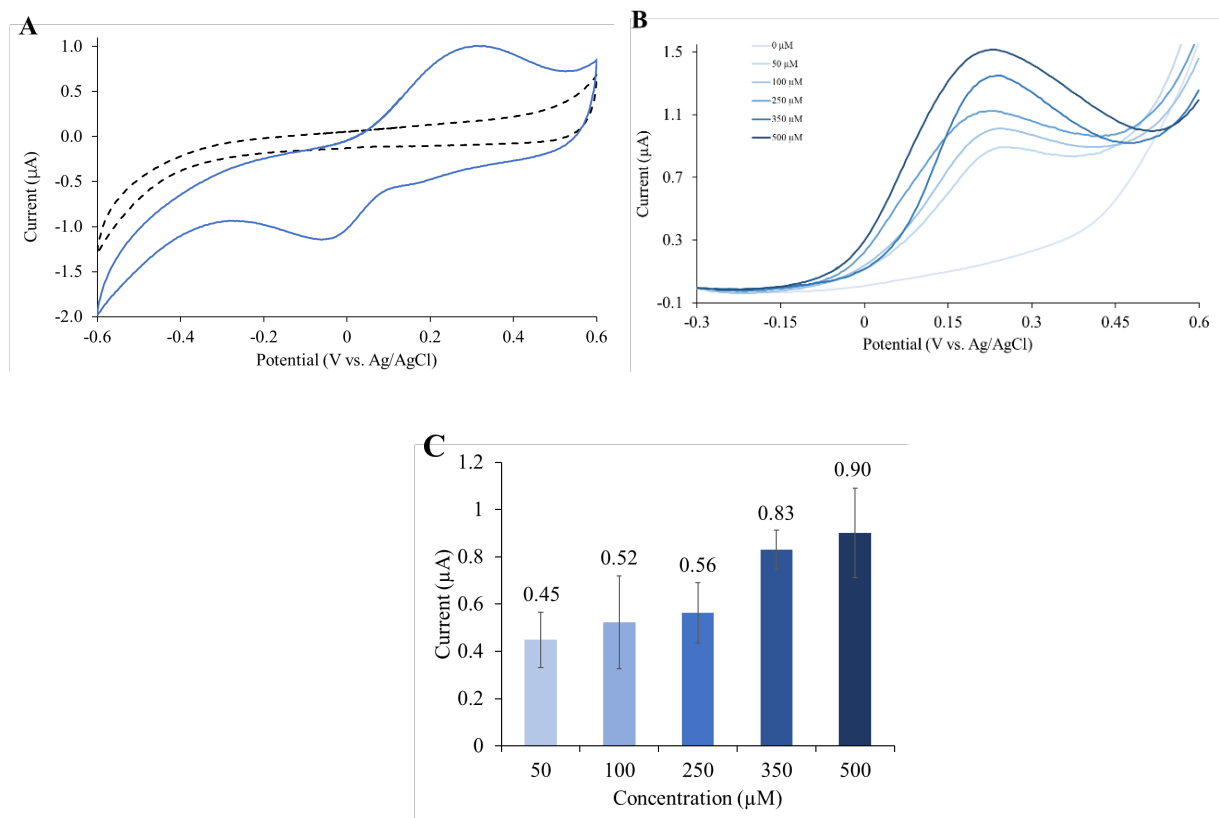


Figure 2.6. A) CVs of TDP-43-Au film before (black dash line) and after (blue solid line) 350 μM Cu(II) binding; **B)** Square wave voltammetry for TDP-43-Au film and varying concentrations of Cu(II); **C)** Plot of current as a function of Cu(II) concentrations (taken from B). *Data collected by M.T.*

The TDP-43–Au surface was characterized prior and post Cu(II) binding also using ellipsometry, contact angle, and XPS, to verify Cu(II) binding to the TDP-43 surface. Ellipsometry was used to determine the relative thickness of the TDP-43-Au surface prior to and post Cu(II) exposure. The thickness of the film remained relatively similar after Cu(II) exposure (3.8 ± 0.2 nm after, and 3.10 ± 0.3 nm before). Slight increase in film thickness may indicate that Cu(II) binding to TDP-43 induced a conformational change and change in overall thickness of the protein layer. The surface wettability post and prior Cu(II) exposure was also measured. After Cu(II) exposure, the contact angle for TDP-43-Au film increased to $47.6 \pm 2.4^\circ$, indicating a more hydrophilic surface. XPS analysis revealed the presence of O, C, S, N and Cu in the Cu(II)-TDP-43-Au film, as expected. No Cu(II) signal was observed for TDP-43-Au film (Fig. 2.7A). Well-defined Cu 2p binding energy contained a doublet at 933 (Cu 2p_{3/2}) and 952 (Cu 2p_{1/2}) eV¹²⁵ for Cu(II)-TDP-43-Au surface (Fig. 2.7B). The difference in binding energy was 19 eV. No satellite peaks were observed at the high energy side of the main lines, which is typical for Cu(I). Cu(II) would produce the satellite peaks. In addition, Cu(II) complexes are characterized by binding energy ~ 935 eV, while Cu(I) complexes were observed at ~ 933 eV.¹²⁶ It is possible that under X-ray radiation and vacuum, Cu(II) was reduced to Cu(I).¹²⁷ The other possibility is that Cu(II) coordinated to Cys residues leading to their oxidation and Cu(II) reduction. Of note is that XPS provides information from the surface and subsurface layers (2 - 5 nm), rather than from the bulk. If the chemical composition of bulk is different from that on the surface, then the XPS may not be fully representative of the whole system. The TDP-43-Au film had a S 2p_{3/2} binding energy at 162.0 eV (Fig. 2.7C) indicative of bound S on the surface, and this component dramatically decreased in the Cu(II)-TDP-43-Au surface (Fig. 2.7D). Notably, thiols of protein may preferentially bind to Cu(II)

rather than Au surface resulting in a decreased amount of bound thiols. Notably, minimal changes in N 1s spectra were observed for metalloprotein and protein films.

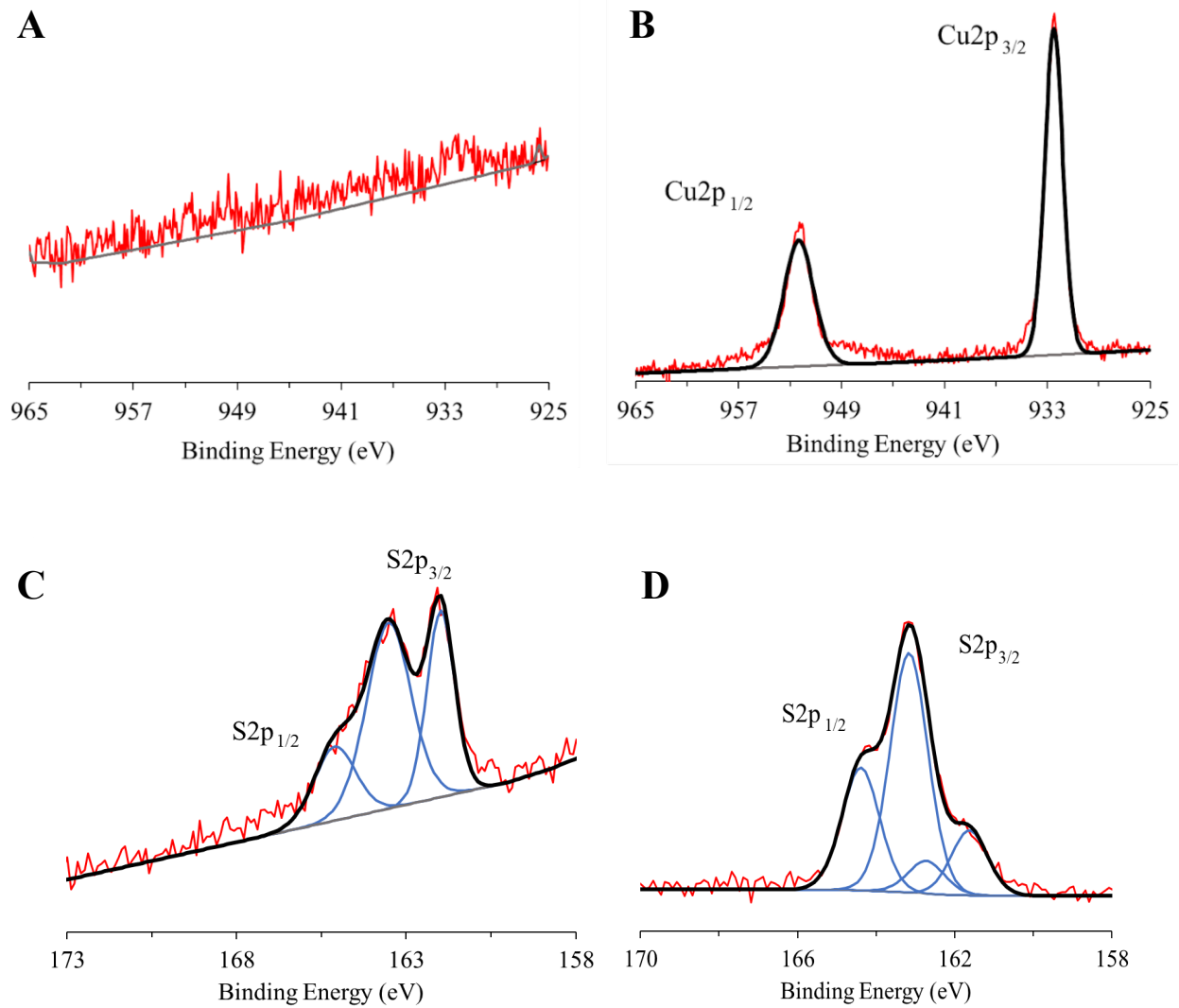


Figure 2.7. XPS spectra of Cu and S for (A, C) TDP-43-Au and (B,D) Cu(II)-TDP-43-Au films. **A)** No peaks within the Cu 2p spectra; **B)** Cu 2p spectra with peaks at 932.5 and 952.33 eV. **C)** S 2p peaks at 162.03, 163.64, and 165.34 eV; **D)** S 2p peaks at 162.04, 163.54, and 164.82 eV. Data collected by M.T. with assistance from I.E.

Overall, Cu(II)-TDP-43 binding at the Au surface was verified using ellipsometry, contact angle, and XPS. Most importantly, XPS provided the elemental composition of the final and Cu(II) exposed final films. The presence of the copper Cu 2p peaks with the Cu(II)-TDP-43-Au sample indicates Cu(II) presence. Since the samples were thoroughly rinsed, it is assumed that the Cu(II) present on the surface is bound to TDP-43. However, the Cu 2p spectra resemble the presence of Cu(I) instead of Cu(II) which may suggest that Cu(II) coordinated to Cys residues. Additionally, XPS shows a decrease in the S 2p_{3/2} after Cu(II) binding. This may be due to thiols preferentially binding to Cu(II), resulting in a decrease of bound thiols to the Au surface. Overall, these results indicate that Cu(II) was present at the TDP-43-Au surface, possibly coordinating with Cys residues in TDP-43. However, the XPS data indicated the method of exposure to the fabricated TDP-43-Au surface results in Cu(II) interactions, indicating that the electrochemical measurements used are adequate for investigating Cu(II)-TDP-43 interactions.

2.3.4. pH Affect on Cu(II)-TDP-43 Interactions

Cu(II)-TDP-43 interactions were further investigated to provide more context of the interaction in a biological setting. The effect of pH on Cu(II) binding to TDP-43-Au was also evaluated given the slightly acidic environment in neuronal cells as well as considering the pI value of the protein. Since the pI of TDP-43 is 5.8¹²⁸ the positively charged protein surface exists at pH=3 and negatively charged surface predominates at pH=7.4. A reduction in signal was observed when the TDP-43-Au film was exposed to Cu(II) under acidic conditions (pH = 3, 0.52 ± 0.023 μA), compared to a biologically relevant pH (pH = 7.4, 0.90 ± 0.19 μA) (Fig. 2.8A and B). Changes in the environmental pH may have caused a disruption in the protein's tertiary and

secondary structures and misfolding of TDP-43.¹²⁹ At pH 3, an asparagine (D105), and two histidines (H166, and H256), within the binding motif became protonated, likely inducing a conformational change.¹²⁹ The protonation of the His and Cys residues may have resulted in a loss of binding for Cu(II), causing the reduction in current signal. While this kind of conformational change was reported in solution, it may also partially appear when protein was immobilized onto the surface despite its limited freedom to move, by being bound to a surface. Hence, the lower current observed may have been due to lower Cu(II) binding to protein film. Data indicated that the Cu(II)-TDP-43 interactions were influenced by the environmental pH, showing a preference for Cu(II) binding at the biological pH of 7.4. Additionally, the pH studies provided insight into possible binding sites of Cu(II), His and Cys residues, as the protonation of these residues disrupted and minimized Cu(II) binding to the film. However, since the Cu(II) signal was still observed, Cu(II) binding is not completely lost, suggesting Cu(II) may have other binding sites.

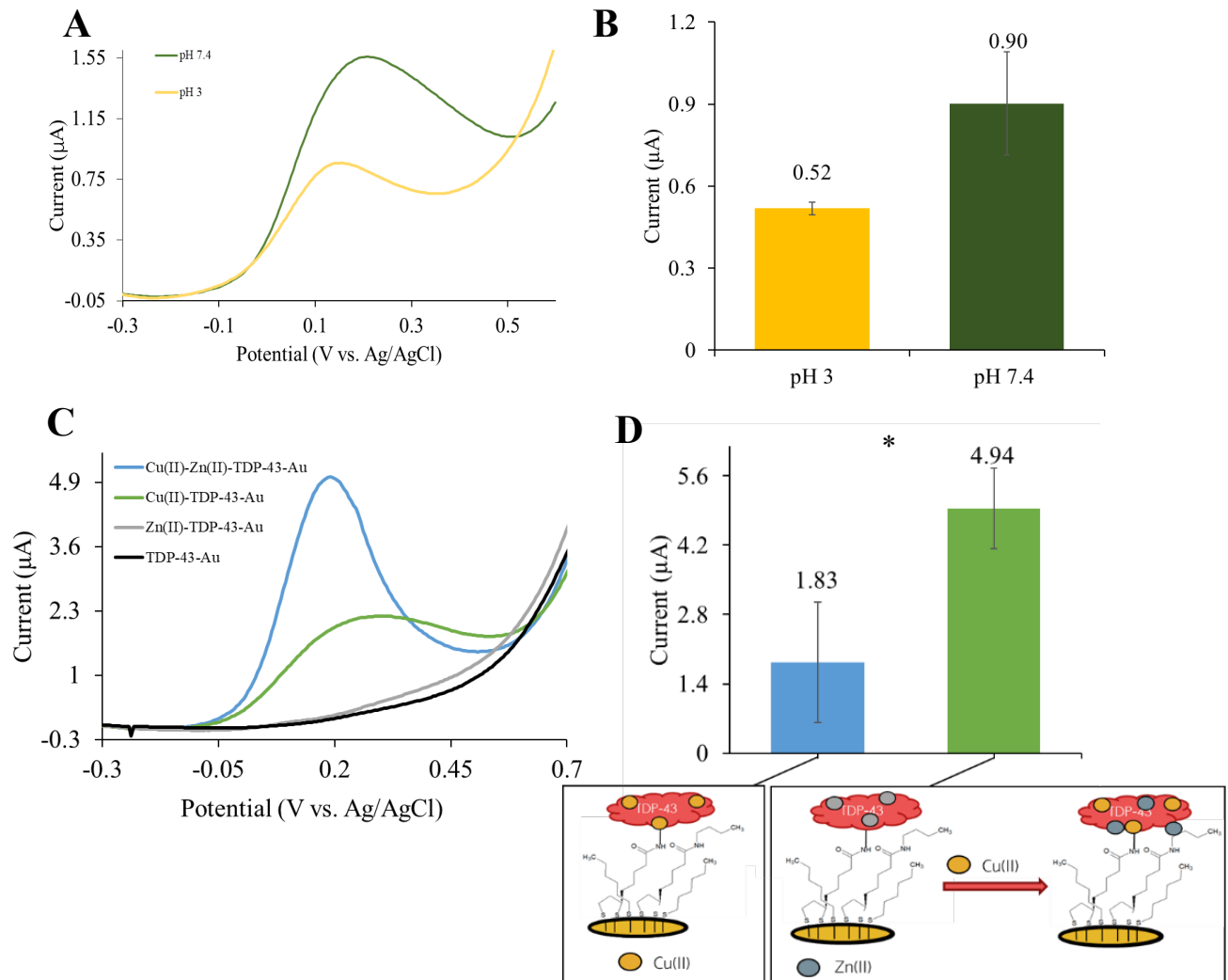


Figure 2.8. A) Representative SWV measurements of 500 μM Cu(II)-TDP-43-Au surface at pH 3 (yellow) and pH 7.4 (green); B) Plot of current for TDP-43-Au and Cu(II) at various pH values ($I = 0.52 \pm 0.023 \mu\text{A}$ for pH 3 and $I = 0.90 \pm 0.19 \mu\text{A}$ for pH 7.4); C) Representative SWV measurements of TDP-43-Au surface (black), 2 mM Zn(II)-TDP-43-Au surface (grey), 2 mM Zn(II)-TDP-43-Au surface followed by 350 μM Cu(II) exposure (blue), and Cu(II)-TDP-43-Au surface (green); D) Plot of current for 350 μM Cu(II)-TDP-43-Au (green, $I = 1.83 \pm 1.22 \mu\text{A}$) and 2 mM Zn(II)-TDP-43-Au, followed by 350 μM Cu(II) exposure (blue, $I = 4.94 \pm 0.127 \mu\text{A}$). Statistical data performed for all data ($n=3$) (Table S9), statistical significance is indicated by ‘*’, non statistically significant data is indicated by ‘ns’. *Data collected by M.T.*

2.3.5. Cu(II)/Zn(II)-TDP-43 Studies

In addition to Cu(II), Zn(II) has many biological roles in the body. In the brain, Zn(II) is stored within synaptic vesicles where it modulates brain excitability, and contributes to normal cognitive and emotional functioning.^{130,131} Given the biological roles of Zn(II), it is considered a potent neurotoxin, and its homeostasis plays a critical role in normal functioning. It has been demonstrated that Zn(II) binds to the RRM domain as well as the His residues within the 256-HISNAEPKH-264 TDP-43 peptide sequence.⁷⁶ Notably, two Zn(II) metal ions were found to bind to the RRM2 (102-269) fragment with a binding constant of $0.1 - 1 \times 10^6 \text{ M}^{-1}$ fragment resulting in protein aggregation.⁷³ The potential Zn(II) binding sites were determined to be Cys173, Cys175 and His166 in RRM1 domain and Cys244, His256, and Glu261. Additionally, both Cu(II) and Zn(II) may coordinate to similar His and Cys residues. Thus, it was of interest to evaluate how TDP-43 protein interacted with these metal ions. Several systematic studies were performed (Fig. 2.9) and included: a) Cu(II) binding and subsequent Zn(II) coordination to determine the ability of Zn(II) to displace Cu(II), b) Zn(II) binding and subsequent Cu(II) coordination to determine the ability of Cu(II) to displace Zn(II), and c) direct competition with co-mixed Cu(II) and Zn(II) to determine preferential binding. Overall, it was hypothesized that Zn(II) will prevent some Cu(II) binding when exposed to the surface first, due to their similar properties and binding sites reported.

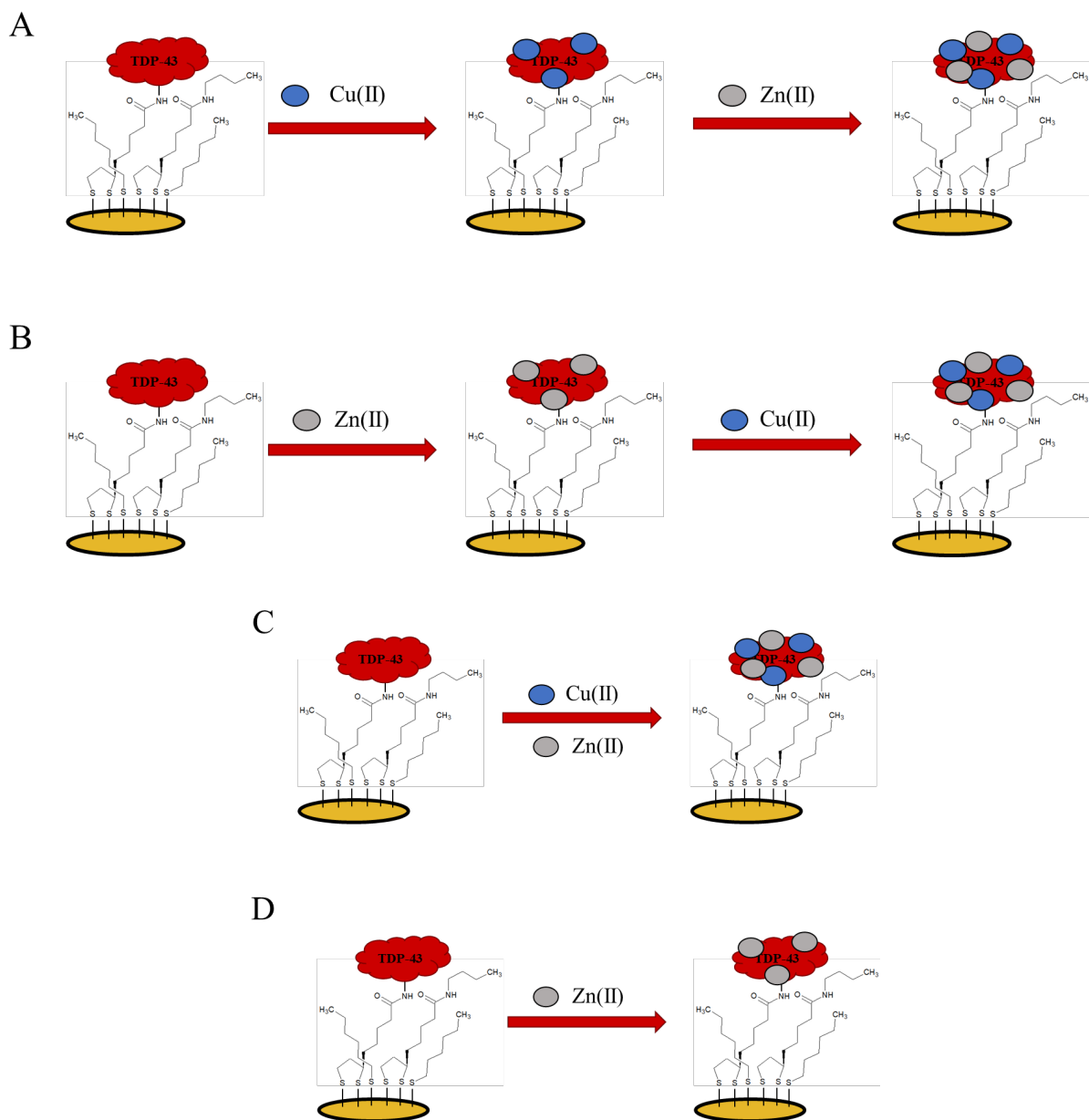


Figure 2.9. Schematic representation of competitive and displacive studies conducted to determine other metal ions, specifically Zn(II) (grey) effect on Cu(II)-TDP-43 binding. **A)** Cu(II) (blue) binding and subsequent Zn(II) coordination to determine the ability of Zn(II) to displace Cu(II); **B)** Zn(II) binding and subsequent Cu(II) coordination to determine ability of Cu(II) to displace Zn(II); **C)** Direct competition with co-mixed Cu(II) and Fe(III) to determine preferential binding; **D)** Zn(II) coordination to TDP-43 surface, to determine metal ion binding. The schematic diagram and coordination of Cu(II)/Zn(II) to TDP-43 films are not to scale.

Since Zn(II) is redox silent, no signal was observed after its binding to TDP-43-Au film (Fig. S21). XPS was performed to verify Zn(II) binding to the TDP-43-Au surface. Following the Zn(II)-TDP-43-Au formation, the subsequent exposure to Cu(II) produced the characteristic Cu(II)/(I) redox couple indicative of Cu(II) ability to bind to such film. However, current for Cu(II)-Zn(II)-TDP-43-Au film was statistically significantly higher ($I = 4.94 \pm 0.81 \mu\text{A}$) than for Cu(II)-TDP-43-Au film ($I = 1.83 \pm 1.22 \mu\text{A}$) (Fig. 2.8C and D), indicating that the initial Zn(II) exposure had an impact on Cu(II) binding, presumably causing conformational changes that increased Cu(II) binding to TDP-43. Similarly, when the Cu(II)-TDP-43-Au was exposed to Zn(II), no statistical differences were observed in current (Fig. S22A), indicating the inability of Zn(II) to displace Cu(II). Finally, when a co-mixture of Cu(II) and Zn(II) was exposed to the TDP-43-Au surface the current was similar to Cu(II)-TDP-43-Au (Fig. S22D), again indicating that TDP-43 had preferential binding to Cu(II), compared to Zn(II). Interestingly, I did not see that Zn(II) prevented Cu(II) binding as hypothesized. Instead, I observed that prior exposure to Zn(II) lead to an increase in Cu(II) binding. The hypothesized mechanism for this interaction was that Zn(II) interacts with the TDP-43 film and caused conformational changes which increased Cu(II) binding. Curtain et al (2001) reported that Cu(II) binding to amyloid- β peptides was cooperative in nature.¹³² Additionally, it was determined that Zn(II) competed with Cu(II) for binding to the same sites, however, the cooperative Cu(II) binding to amyloid- β was still observed. Thus, I hypothesis that a similar mechanism occurred at the TDP-43 surface, where Zn(II) increases the cooperative Cu(II) binding mechanism. However, since Zn(II) is redox silent, the presence of Zn(II) needed to be verified using XPS.

XPS was performed to determine if Zn(II) coordinated to TDP-43-Au. The Zn 2p 3/2 and 2p 1/2 binding energies expected at 1021 and 1044 eV were not observed for any of the TDP-43-Au films. Typical Zn 2p binding energies for Zn-peptide films were reported to be in the 1021 - 1028 eV range.¹³³ Specifically, the binding energy at 1028 eV is expected when the local chemical environment for Zn atoms in the mononuclear complex, such as Zn(His)₂. Analogously, zinc acetate had reportedly similar binding energy at 1027 eV due to the tetrahedral Zn atom surrounded by O atoms from carbonyl groups. Notably 1027 eV band was not observed in this study (Fig. 2.10B, D, and F). The absence of Zn(II) in XPS may have been due to weak binding of Zn(II) to TDP-43 as well as weak transitions associated with Zn(II) in XPS measurements. Notably, when Zn(II)-TDP-43-Au film was exposed to Cu(II), the Cu 2p was observed in XPS, indicating Cu(II) binding (Fig. 2.10C). The Cu 2p was also observed when Cu(II)-TDP-43-Au film was exposed to the Zn(II), indicating lack of Cu(II) displacement (Fig. 2.10A). Similarly, a co-mixture of Cu(II) and Zn(II) resulted in the Cu(II) signal as well (Fig. 2.10E), pointing to the ability of Cu(II) to bind to TDP-43-Au despite the presence of Zn(II). This was also observed in the electrochemical measurements. Overall, Cu(II) binding to TDP-43 was observed in each of the cases both displacive and the competition studies, indicated by the presence of the 2 Cu 2p spectra peaks. Zn(II) binding to TDP-43 was less clear based on the XPS results. Similar to the Cu 2p spectra, two Zn 2p peaks were expected, however that was not the case. The absence of the peaks may be due to weak binding, or issues with the XPS method itself. Thus, additional studies, such as mass spectrometry are required to determine if Zn(II) binds to TDP-43.

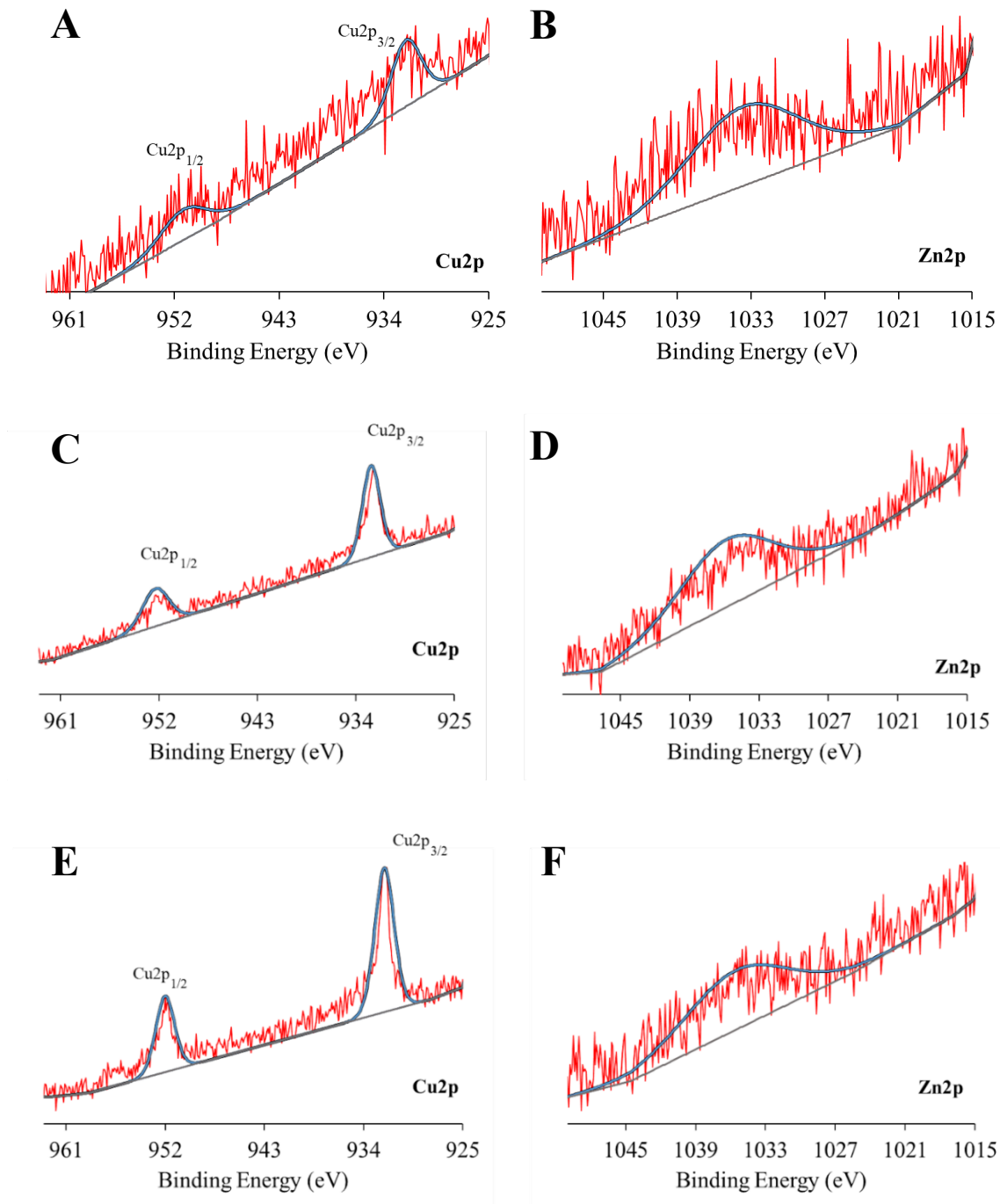


Figure 2.10. XPS spectra of TDP-43 film exposed to Cu(II) and Zn(II) in varying successions. A) Cu(II) exposure to TDP-43, followed by Zn(II) exposure. Shows Cu 2p and B) Zn 2p XPS spectra. C) Zn(II) exposure to TDP-43, followed by Cu(II) exposure, showing Cu 2p and D) Zn 2p XPS spectra. E) Co-mixture of Zn(II) and Cu(II) exposed to TDP-43, simultaneously. Shows Cu 2p and F) Zn 2p XPS spectra. *Data collected by M.T. with assistance from I.E.*

The data suggested that Zn(II) may have influenced Cu(II)-TDP-43 binding. However, Zn(II) was only shown to have a statistically significant impact on Cu(II)-TDP-43 binding when it was exposed to the surface before Cu(II), which increased the Cu(II) signal. A hypothesis for this impact on Cu(II) binding to TDP-43 when exposed to Zn(II) prior, was that Zn(II) interactions with TDP-43 caused structural changes which increased available Cu(II) binding sites. However, further studies, such as circular dichroism (CD), should be conducted to investigate and verify changes to the structure upon metal exposure. Additionally, data indicated that Cu(II) may bind to Zn(II) more readily, as co-exposure of the two metal ions to the surface has no statistically significant impact on Cu(II) binding (Table S9). Thus, in biological context, the elevated Zn(II) levels may influence the Cu(II)-TDP-43 binding. However, Zn(II) did not seem to have a negative impact on Cu(II) binding. It was hypothesized that uncoordinated TDP-43 interacts with Zn(II) and causes structural changes which increased Cu(II) binding.

2.4 Conclusion

In this chapter, I set out to evaluate metal ion binding to TDP-43 for the first time, using electrochemical methods. Additionally, this was the first study, to our knowledge, which investigates the direct interactions between Cu(II) and TDP-43. Electrochemistry was utilized because Cu(II) binding to the protein produced a distinct electrochemical signal which could be quantified. The distinct signal allowed for Cu(II)-TDP-43 interaction evaluation in different biological contexts. Additionally, it allowed for the evaluation of the impact of other metal ions on the Cu(II)-TDP-43 interaction.

In this chapter, I demonstrated successful immobilization of TDP-43 films on Au surfaces, which were further characterized by (non)electrochemical methods. The direct binding of Cu(II)

ions to the TDP-43-Au film was detected and quantified using electrochemical methods. Cu(II)-TDP-43 binding was influenced by the environmental pH, and was favourable at a neutral pH value. In this chapter, I also set out to determine the Cu(II) interactions with TDP-43 in biological conditions. The data obtained from the studies investigating the impact of pH on these interactions supported the importance of considering environmental pH when studying metal ion/protein interactions. Neutral pH interactions were strong, which may contribute to the pathology of TDP-43. In relation to biologically relevant studies, Cu(II)-TDP-43 interactions were investigated in the context of other biologically metal ions, Zn(II) and later Fe(III) (Chapter 3). The displacive metal ion studies revealed that Zn(II) did not outcompete or displace Cu(II) from the TDP-43-Au surface. However, the data collected did indicate that exposing the TDP-43-Au film to Zn(II) prior to Cu(II) increased the Cu(II) signal, suggesting that Zn(II) may have interacted with the surface and caused changes that increased Cu(II) coordination. All the different metal coordination to TDP-43 were also confirmed by surface characterization measurements. Cu(II)-TDP-43 samples indicate successful Cu(II) binding to TDP-43. However, XPS data with regards to Zn(II) interactions with TDP-43 and Cu(II)-TDP-43 was less clear. Thus I am suggesting additional work to verify Zn(II) coordination to TDP-43. Additionally, CD should be conducted to see if the increase in Cu(II) signal is due to Zn(II) induced structural changes. Overall data suggest that, in the disease state of ALS, with elevated metal ion concentrations, Cu(II) will likely coordinate to TDP-43. The metalloprotein formation has a biological significance, and the protein bioelectrochemistry is well suited for monitoring metal ion binding, which is the critical step in understanding the role of metalloproteins in normal and diseased states.

2.5 Author Information

Corresponding Author

*Department of Forensic Science, Environmental and Life Sciences, Trent University, 1600

West Bank Drive, Peterborough, Ontario K9L 0G2, Canada

Email: sanelamartic@trentu.ca

Author Contributions

M.T. and S.M. conceived and designed the experiments collaboratively. S.M. provided the fundamental idea and direction. M.T. performed the experiments. M.T. and S.M. analyzed the data. M.T. and S.M. wrote the main text. C.C. and C.W. contributed purified TDP-43 and text about the process. I.E. provided expertise on surface characterization and contributed to some analysis.

Funding Sources

The authors thank Trent University for support, and the University Grant Research Program.

Notes

The authors declare no competing financial or intellectual interests.

2.6. Acknowledgements

The authors, M.T. and S.M., thank the Environmental and Life Sciences at Trent University. M.T. and S.M. sincerely thank Dr. Iraklii Ebralidze at the Materials Characterization Facility for their time and use of the contact angle equipment, and ellipsometry and XPS instrumentation.

Chapter 3 : Electrochemical Analysis of Fe(III) and Cu(II) Interactions with TDP-43

Abstract

In addition to elevated copper (II) (Cu(II)) levels reported in ALS cases, elevated iron (Fe) has also been reported. Iron has neurotoxic properties, and may lead to an increase in oxidative stress, related to neurodegenerative diseases. However, the exact iron interactions with TDP-43 have not been studied. There has been a link between TDP-43 pathogenesis in ALS and iron, but it is unclear if Fe directly binds TDP-43. Fe(III) binding sites identified in other proteins are known to include two Tyr, one Asp, and one His residue, but this has not been demonstrated for TDP-43. Thus, I am interested in determining whether Fe(III) binds to TDP-43, and affects the Cu(II). Electrochemical methods were used to monitor Cu(II) binding to TDP-43 under displacement and competition conditions with Fe(III). Herein, I observed that the exposure of the Fe(III) to TDP-43 resulted in the production of a more conductive film, due to incorporation of Fe(III) into the protein. Additionally, I observed that exposing TDP-43 to Cu(II) and Fe(III) simultaneously resulted in a statistically significant increase in current signal, compared to Cu(II) only. Data indicate that Fe(III) metal ions may influence Cu(II) binding to TDP-43, which may have biological consequences.

3.1. Introduction

As discussed in Chapter 2, metal ions are required for several biochemical reactions to occur. In addition to Cu(II) and Zn(II), Iron (Fe) is of interest. This metal ion has important biological roles in the body, similar to Cu(II) and Zn(II). However, some of the unique roles of iron include its requirement for the synthesis of oxygen transport proteins, specifically hemoglobin and myoglobin.¹³⁴ Iron is also required for the formation of heme enzymes, or other iron-containing enzymes, involved in electron transfer and oxidation reduction reactions.¹³⁴ Moreover, in the brain, Fe is involved in DNA synthesis, oxygen transport and respiration, myelin synthesis, and neurotransmitter synthesis and metabolism.¹³⁵ However, in excess, Fe has neurotoxic properties. Excess Fe can oversaturate storage molecules, and lead to the formation of iron pools, which can lead to oxidative damage and cell death. Some Fe accumulation is observed in healthy aging individuals.⁷⁰ However, Fe accumulation in particular regions within the brain has been observed in neurodegenerative diseases, and is associated with oxidative stress.¹³⁵ It is unclear whether Fe accumulation is a primary event, or a secondary effect, of neurodegeneration.¹³⁵ Elevated levels of Fe, based on Fe serum-status indicators, have also been reported in ALS patients.¹³⁶⁻¹³⁷ Additionally, elevated levels are observed in the CSF.⁷⁰ Two preliminary studies have been conducted to look at Fe and TDP-43 interactions or binding.^{87,88} Caragounis et al. (2010) investigated the impact of metal ions on the decreased amount or aggregation of TDP-43 in neuronal-like cells. The metal ions investigated in these studies were Zn(II), Fe(II), and Cu(II), with an emphasis on Zn(II). Fe(I) and Cu(II) were exposed after Zn(II) exposure to TDP-43, to investigate the impact these metal ions had Zn(II)-TDP-43 interactions.⁸⁷ Mitani et al. (2021) reported both Fe accumulation and TDP-43 aggregation in a systematic review of ALS case studies.⁸⁸ However, neither of these Fe related studies directly monitor Fe interactions with TDP-

43, and to our knowledge, there are no other studies looking at these possible interactions. Thus, more research looking directly at Fe impacts on TDP-43 are required. The general concern with Fe accumulation is the production of ROS. Specifically, Fe(III) will react with H₂O₂ and form HO radicals, within biological systems.⁸⁶ The formation of these radicals will negatively impact cellular function and survival and, although there is evidence of Fe(II)/(III) accumulation in ALS, the role it plays in the pathogenesis is unknown.

Due to the biological roles of Fe, many binding sites of the metal ion in different proteins have been investigated. For example, transferrin, which is a protein that mediates the transport of iron through blood plasma, binds Fe(III). Fe(III) will coordinate with two Tyr, one Asp and one His residue, as well as a bidentate ion in a nearby pocket.¹³⁸ A carboxylate oxygen, two phenolate oxygens, and one imidazole nitrogen, from the side chains of the aforementioned residues, are ideal for binding Fe(III).¹³⁸ However, there have been no studies to determine if similar binding sites exist in TDP-43. Although possible Fe binding sites to TDP-43 have not been studied, other similar neurodegenerative related proteins and Fe interactions have been investigated. There are studies investigating the binding of both Fe(II) and Fe(III), and their impact on Cu(II) binding to the neurodegenerative related proteins, such as tau and amyloid- β . However, in these studies, Fe(III) was shown to have different binding sites, and impact the conformation of the proteins, indirectly impacting Cu(II) binding.¹¹⁸ Since the impact of a similar metal ion, Zn(II), on Cu(II)-TDP-43 interactions was investigated in Chapter 2, it was of more interest to investigate the impacts of Fe(III) on the interactions, because it shares dissimilar binding sites with Cu(II).

Investigating the impact of Fe ions on the Cu(II)-TDP-43 interaction is of interest, particularly Fe(III), as these metal ions are often found together and have similar properties and

biological roles. Determining if metal ions bind to TDP-43 and if the binding is metal ion-dependent is of importance in relation to ROS production and oxidative stress. I investigated Fe(III) interaction with TDP-43, and the impact this may have on Cu(II) binding to the protein, using electrochemistry. Several systematic studies (Fig. 3.1) were performed and include: a) Cu(II) binding and subsequent Fe(III) coordination to determine ability of Fe(III) to displace Cu(II), b) Fe (III) binding and subsequent Cu(II) coordination to determine ability of Cu(II) to displace Fe(III), and c) direct competition with co-mixed Cu(II) and Fe(III) to determine preferential binding. Based on the data from previous studies looking at Fe(III)-protein binding, I hypothesized that Fe(III) will bind to TDP-43, due to the presence of several binding sites. Additionally, I expect a reduction in Cu(II) signal when Fe(III) binds to competing protein sites. By contrast, if Fe(III) binds to unrelated and dissimilar sites to Cu(II), then no change in Cu(II) signal will be observed.

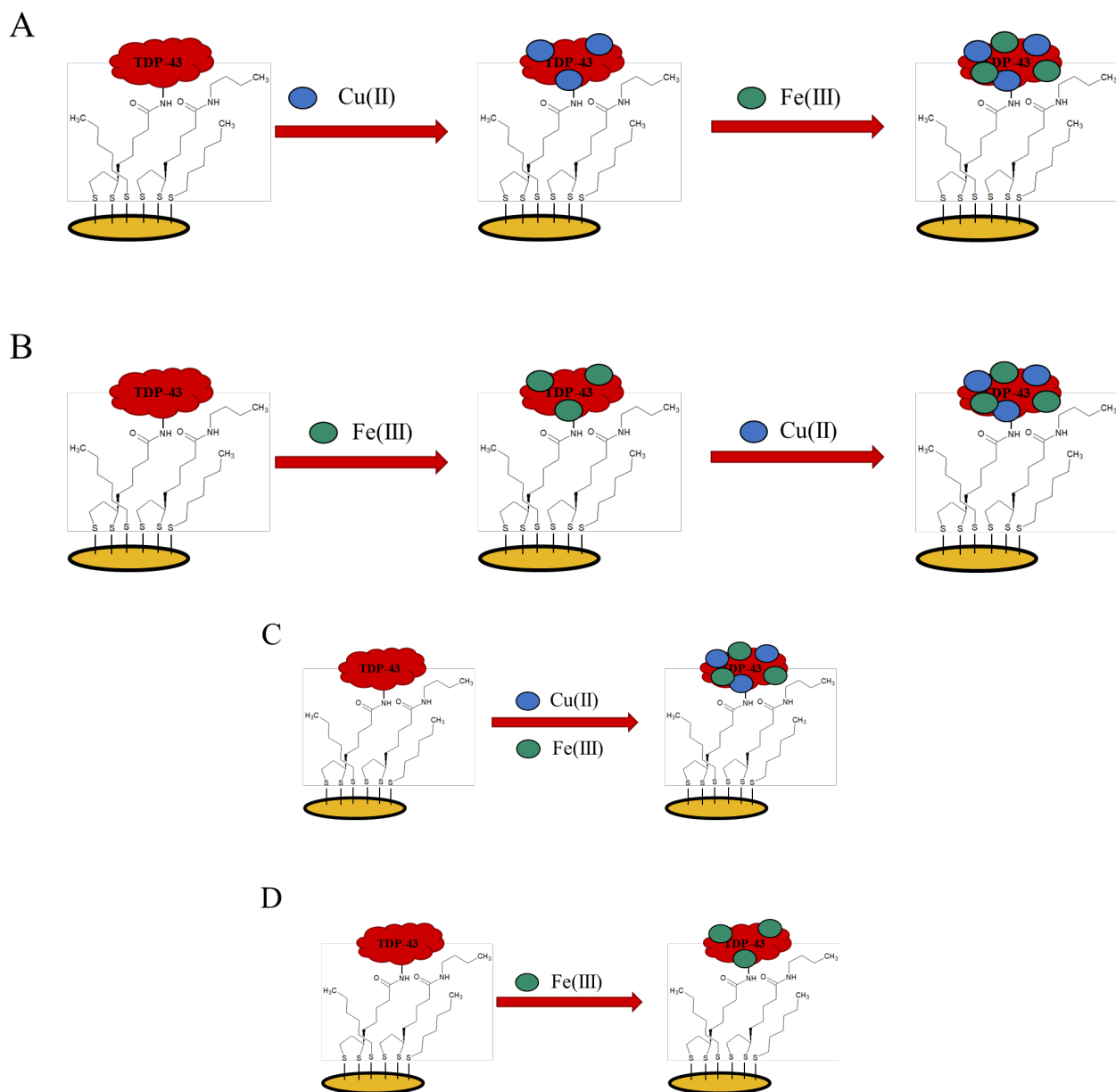


Figure 3.1. Schematic representation of competitive and displacive studies conducted to determine the effect of other metal ions, specifically Fe(III) (green) on Cu(II)-TDP-43 binding. **A)** Cu(II) (blue) binding and subsequent Fe(III) coordination to determine the ability of Fe(III) to displace Cu(II); **B)** Fe(III) binding and subsequent Cu(II) coordination to determine ability of Cu(II) to displace Fe(III); **C)** Direct competition with co-mixed Cu(II) and Fe(III) to determine preferential binding; **D)** Fe(III) coordination to TDP-43 surface, to determine metal ion binding. The schematic diagram and coordination of Cu(II)/Fe(III) to TDP-43 films are not to scale.

3.2. Experimental Section

3.2.1. Materials and Methods

The monobasic and dibasic potassium phosphate, 1-butylamine, hexanethiol, and reagent alcohol (EtOH) were purchased from Fisher Scientific. Potassium hydroxide (KOH) was purchased from Caledon Laboratory Chemicals (ON, CAN). Ethanol was purchased from Commercial Alcohols by Greenfield Global (ON, CAN). Potassium chloride was purchased from EMD. N-(3 dimethylamino- propyl)-N'-ethyl carbodiimide hydrochloride (EDC), N-hydroxysuccinimide (NHS), and DL α -lipoic acid were purchased from Sigma Aldrich (MO, USA). Alumina was purchased from Fisher Chemicals (PA, USA). Copper(II) nitrate 2.5 hydrate, was purchased from J. T. Baker (NJ, USA). Iron(III) perchlorate was purchased from Alfa Aesar (MA, USA). Potassium ferricyanide and potassium ferrocyanide was purchased from Acros Organics (Belgium). Concentrated sulfuric acid was purchased from VWR Chemicals (PA, USA).

3.2.2. Cleaning of Au Electrodes

The Au disk electrodes were cleaned chemically in piranha solution (3:1 H₂SO₄:H₂O₂) for 5 min, then rinsed with deionized (DI) H₂O and polished on alumina slurry (80-200 mesh) for 3 min. After polishing, electrodes were sonicated in DI H₂O for 3 min to remove excess alumina and were cleaned electrochemically. Electrochemical cleaning was performed by running the CV in 0.5 M KOH solution at 0.5 V/s in the -2 - 0 V range. Followed by 0.5 M H₂SO₄ solution in the 0 - 1.5 V range at a scan rate of 0.5 V/s. The electrodes were then sonicated again for 5 min and cleaned electrochemically in 0.5 M H₂SO₄ once again. Clean Au electrodes were rinsed with DI water, then rinsed with ethanol.

3.2.3. Preparation of Protein Solution

10 mM PB was prepared by dissolving solid monobasic and dibasic potassium phosphate in reverse osmosis H₂O, and the pH was adjusted to 7.4, using KOH solution. 500 μ M Cu(II) was prepared by dissolving solid Cu(NO₃)₂ in PB, pH 7.4. 50, 100, 250, and 350 μ M Cu(II) solutions were prepared by diluting 500 μ M Cu(II) solution with PB, pH 7.4. 1 mM Fe(III) was prepared by dissolving solid Fe(III) perchlorate in PB, pH 7.4. 1 μ M TDP-43 aliquots were diluted to 50 nM using PB, pH 7.4.

3.2.4. Preparation of TDP-43 Films on Au Electrodes

The clean Au electrodes were immersed in 4 mM DL α -lipoic (ethanol) at 4 °C overnight. After rinsing with ethanol, the electrodes were incubated in a mixture of 10 mM NHS (ethanol) and 8 mM EDC (ethanol) solution for 1 h at room temperature and rinsed with ethanol. After the surface was air dried, the electrodes were incubated in 50 nM TDP-43 (PB, pH 7.4) at 4 °C overnight. After rinsing with PB followed by ethanol, the electrodes were immersed in 10 mM 1-butylamine (ethanol) for 1 h at room temperature. Electrodes were rinsed with ethanol and incubated in 10 mM hexanethiol (ethanol) for 30 min at room temperature. Subsequently, the electrodes were rinsed with ethanol, followed by 10 mM PB, pH 7.4, prior to electrochemical measurements.

3.2.5. Interactions with Metal Ions

For Fe(III) displacement studies, the TDP-43-Au film was incubated in 5 μ L of 350 μ M Cu(II) solution in PB (pH 7.4) for 30 min at room temperature. The electrodes were rinsed with PB, prior to and post the measurements, and air dried. Then the Cu(II)-TDP-43-Au film was

incubated in 5 μL of 1 mM Fe(III) solution in PB (pH 7.4) for 30 min at room temperature. The electrodes were rinsed with PB, prior to the measurements. This was repeated for the second displacement study, however, 1 mM Fe(III) was incubated first, then 350 μM Cu(II) was incubated onto the Zn(II)-TDP-43-Au film.

For the Fe(III) competition studies, the TDP-43-Au film was incubated in 5 μL of a 350 μM Cu(II)-1 mM Fe(III) solution and in PB (pH 7.4) for 30 min at room temperature. The electrodes were rinsed with PB, prior to the measurements.

3.3. *Results and Discussion*

From the fabrication of the TDP-43-Au film, I hoped to determine metal ion binding properties of the protein. In Chapter 2, I demonstrated that Cu(II) ions bind to the TDP-43-Au surface through electrochemical methods, based on the appearance of the characteristic oxidation and reduction peaks of Cu. Then, I further investigated this interaction by exposing the TDP-43 surface to Zn(II) and Cu(II), in several systematic studies, to determine if Zn(II) ions have an effect on Cu(II) binding. Similarly, the aim of Chapter 3 is to investigate the effects of Fe(III) binding on the Cu(II) interactions with TDP-43.

The first step in the study was to determine if Fe(III) binds to the TDP-43-Au film in the absence of Cu(II). This was done by fabricating the TDP-43-Au surface and exposing it to disease relevant concentration of Fe. However, it should be specified that no neuronal concentrations of Fe have been reported for ALS, so the chosen experimental concentration of 1 mM Fe was based on the reported concentrations in the other neurodegenerative diseases, such as Alzheimer's disease.⁹¹ Upon Fe(III) binding, the appearance of electrochemical signal was expected, as the Fe(III) on the surface was reduced to Fe(II). However, when the Fe(III)-TDP-43-Au film was

measured, there were no peaks observed (Fig. 3.2A). This indicates that either 1) there was no Fe(III) bound to the TDP-43-Au surface, 2) the peaks were not visible in the potential range, or 3) Fe(III) bound to protein but was insulated and buried reducing its the electrochemical signal. In the absence of Fe(III)-related signal it was difficult to determine if Fe(III) bound to the protein. If Fe(III) bound to protein, then the protein film should be more conductive. To test for film conductivity, the films was subsequently tested in a solution containing a redox probe. This allowed us to measure conductivity through a redox probe. The redox signal was expected, and its magnitude was highly dependent on the film conductivity. If the signal of the redox probe was high, then the film conductivity was high as well. Hence, the Fe(III)-TDP-43-Au film was placed in a cell with the redox probe $[\text{Fe}(\text{CN})_6]^{3-/4-}$ redox probe to investigate film conductivity after Fe(III) exposure.¹¹⁸ Comparing the TDP-43-Au film to the Fe(III)-TDP-43-Au film, there was a change in the peak current density and separation (Fig. 3.2B), indicating that Fe(III) may have been bound to the surface and causing the change. The increased in $[\text{Fe}(\text{CN})_6]^{3-/4-}$ signal was indicative of a more conductive film, while a signal decrease would have indicated the formation of passivation (non-conductive) film. A shift in the oxidation (0.428 to 0.340 V) and reduction peak potentials (-0.00366 to 0.0573 V) was observed for the TDP-43-Au, and Fe(III) exposed film, respectively (Fig. 3.2B). Additionally, there was a change in current signals associated with the oxidation (63.81 and 70.56 μA), and reduction peaks (-72.90 and -88.19 μA) observed for the TDP-43-Au, and Fe(III) exposed film, respectively (Fig. 3.2B). Hence, a more conductive protein film was seen when TDP-43 was exposed to Fe (III) compared to metal-free TDP-43 protein film, suggesting that there were changes to the surface, caused by Fe(III) coordination and binding to the TDP-43-Au film.

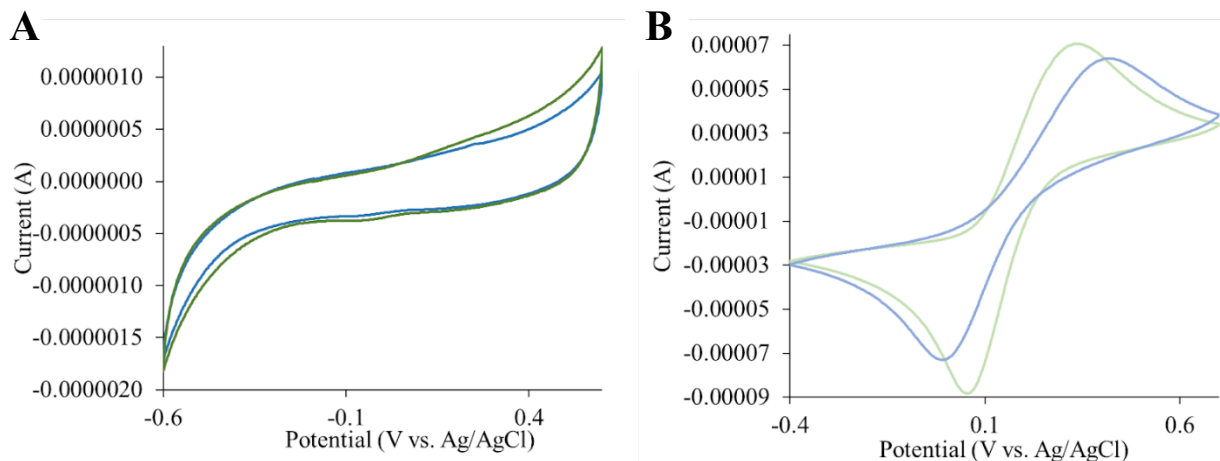


Figure 3.2. A) TDP-43-Au film exposed to 1 mM Fe (III) solution (green) and phosphate buffer (blue) in a phosphate buffer electrochemical cell. B) TDP-43-Au film exposed to 1 mM Fe (III) solution (green) and phosphate buffer (blue) in $[\text{Fe}(\text{CN})_6]^{3-/4}$ redox probe.

So far, I have determined that Fe(III) binding to the TDP-43-Au surface resulted in the conductive film due to Fe(III)-TDP-43 interactions (Fig. 3.2). Next, the impact of Fe(III) on Cu(II)-TDP-43-Au binding was evaluated based on the difference in Cu(II) signal measured. Following the Fe(III)-TDP-43-Au formation, the subsequent exposure of this film to Cu(II) produced the characteristic Cu(II)/(I) redox couple indicative of Cu(II) ability to bind to such film (Fig. 3.3A), which suggested that although Fe(III) may interact with the TDP-43-Au surface, Cu(II) could still bind to the protein to a similar extent. Additionally, Fe(III) was initially exposed to TDP-43, followed by Cu(II) exposure ($I = 3.45 \pm 1.68 \mu\text{A}$), and no statistical difference was observed in the current compared to when Cu(II) was exposed to TDP-43 alone ($I = 3.29 \pm 0.28 \mu\text{A}$) (Fig. S37 & S38, Table S1), indicating that Fe(III) had no impact on Cu(II) binding when exposed prior. Likely, the resulting mixed film Cu(II)-Fe(III)-TDP-43-Au was formed. Data indicated that Fe(III) and Cu(II) may not have share similar binding sites. This was further

supported by the experiment when Cu(II)-TDP-43-Au film was exposed to Fe(III). Similar currents were observed for Fe(III)-Cu(II)-TDP-43-Au ($I = 3.88 \pm 0.79 \mu\text{A}$) and Cu(II)-TDP-43-Au ($I = 3.29 \pm 0.28 \mu\text{A}$) (Fig. S35 & S36), indicating that Fe(III) did not displace Cu(II).

However, the Cu(II/I) current for TDP-43-Au film exposed to a mixture of Cu(II) and Fe(III) at the same time was lower ($I = 1.61 \pm 0.91 \mu\text{A}$) than for Cu(II)-TDP-43-Au film ($I = 3.29 \pm 0.28 \mu\text{A}$) (Figure 3.3B). There may be two plausible reasons for this trend. Firstly, the partial Cu(II) binding may introduce conformational protein change and promote Fe(III) binding, resulting in a unique mixed metal protein film which may have a lower affinity for Cu(II). Secondly, the mixed metal film formed under these conditions may have adapted a specific conformation, leading to shielding and insulating of Cu(II) centers, resulting in the lower current.

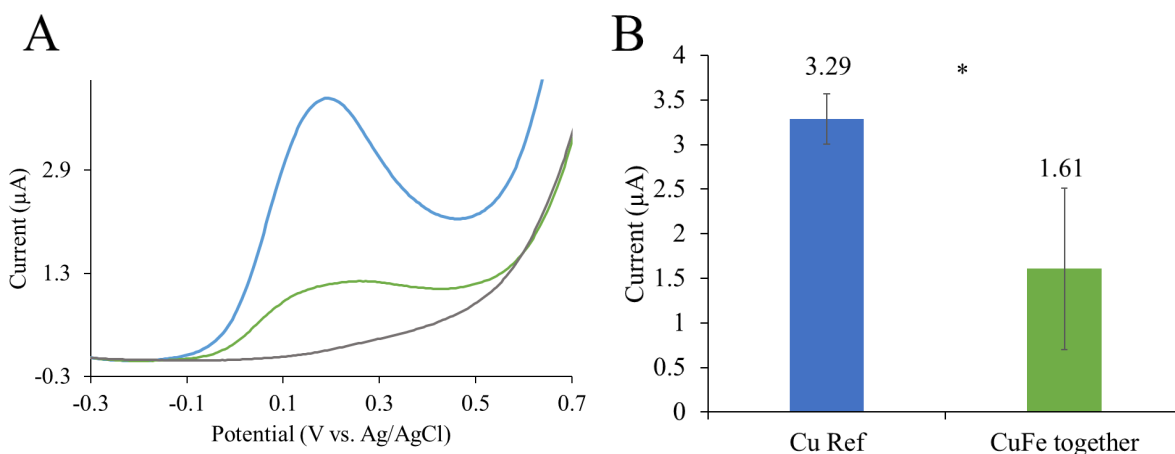



Figure 3.3. A) Representative SWV measurements of TDP-43-Au surface (grey), Cu(II)-TDP-43-Au surface (blue) and 350 μM Cu(II)-1 mM Fe(III) exposure surface (green), simultaneously; B) Plot of current for a mixture of 350 μM Cu(II)-1 mM Fe(III) exposure to TDP-43-Au, simultaneously, ($I = 1.60 \pm 0.91 \mu\text{A}$) (green) and 350 μM Cu(II)-TDP-43-Au signal ($I = 3.29 \pm 0.28 \mu\text{A}$) (blue). Statistical data performed for all data ($n=3$) (Table S9), statistical significance is indicated by ‘*’, non statistically significant data is indicated by ‘ns’.

Although Fe binding or other interactions with TDP-43 has not been explored, other neurodegenerative related proteins have reported Fe(III) binding to His residues. For example, Fe(II) was shown to bind to tau and promote aggregation, but Thr phosphorylation resulted in a loss of this interaction, indicating its importance to Fe(II) interactions with tau.¹¹⁸ Whereas, Fe(III) interactions with tau were unaffected by the phosphorylation of Thr residues,¹¹⁸ indicating the nature of the Fe(III) interaction with the protein is different than that which occurs between Fe(II) and tau. Additionally, in the microtubule binding domain of tau, Fe(III) binds strongly to His residues.¹³⁹ Smith et al. (1997) also determined that mutations in His residues abolished Fe(III) binding to neurofibrillary tangles.¹⁴⁰ Miura et al. (2001) identified a potential binding site for

Fe(III) in amyloid-beta between three His residues (His6, 13, and 14) and one Tyr residue (Tyr10).¹⁴¹ Tyr residues may also be a point for Fe(III) binding, as the phenolic oxygen can coordinate Fe(III) when it is deprotonated.¹⁴¹ Additionally, Fe(III) was shown to bind to the carboxylate groups of glutamate and aspartate side chains, in full-length amyloid- β .¹⁴¹ TDP-43 protein has several amino acid binding sites that may act as potential coordination points. Based on the literature evidence, Fe(III) exposure to the TDP-43 surface may have a different binding site compared to Cu(II) exposure. Indicating that the effect of Fe(III) on Cu(II)-TDP-43 binding was not due to competition of the binding site, but allosteric structural changes, inhibiting Cu(II) accessibility. Previous studies have looked at the effect of Fe(III) on Cu(II) coordination to the neurodegenerative related protein, tau. It was observed that Fe(III) exposure prevents Cu(II) interaction with the protein, suggesting that the tau-Fe(III) interaction prevented Cu(II) binding by blocking the accessibility through conformational changes.¹¹⁸ This change in structure after Fe(III) exposure was confirmed using CD.¹¹⁸ Thus, the reduction in signal seen after Fe(III) and Cu(II) are co-exposed to the TDP-43 surface may be a result of Fe(III) induce conformational changes, blocking some Cu(II) binding. However, further methods, such as CD, should be used to confirm these structural changes upon Fe(III) exposure.

3.4 Conclusions

Various metal ions play important biological roles, and a deeper understanding of their interplay in relation to proteins is needed. In this chapter, the interactions of Fe(III) with TDP-43 film was investigated by electrochemical methods. Exposure of the Fe(III) to TDP-43 resulted in the production of a more conductive film which was indicative of Fe(III) binding.

The second aspect of this chapter was to determine if Fe(III) competes or displaces Cu(II) ions from TDP-43 films. Co-exposing TDP-43 to 350 μM Cu(II) and 1 mM Fe(III) resulted in a statistically significant decrease in current signal of $1.60 \pm 0.91 \mu\text{A}$, compared to the Cu(II)-TDP-43-Au surface, $3.29 \pm 0.28 \mu\text{A}$. However, Cu(II) exposure followed by Fe(III) exposure, and Fe(III) exposure followed by Cu(II) exposure, did not produce statistical significant changes in the signal. The lack of changes observed for the Cu(II) signal in the cases where the metal ions were exposed following one another suggested that the Fe(III)-TDP-43 interaction caused a conformational protein change to the protein, which reduced Cu(II) binding or insulated Cu(II) centers.

Overall, the data showed that metal ions influenced each other and their binding to TDP-43, which is of biological significance. Additional structural studies are required to determine the amount of metal ion binding to TDP-43, and binding sites, by other methods, such as mass spectrometry. Additionally, methods such as circular dichroism should be conducted to gain insight into the nature of Fe(III) interactions, and confirm whether the hypothesis of the impacts of Fe(III) on Cu(II) is accurate as our work may have involved conformation changes.

Chapter 4 : Conclusions and Future Work

4.1 Conclusions

TDP-43, the major biomarker protein in ALS, has been shown to be linked to other neurodegenerative diseases, such as frontotemporal lobar degeneration and Alzheimer's disease. However, the protein still lacks full characterization and its role in ALS is not fully understood. Of the studies that have been conducted on TDP-43, most are targeted toward investigating specific domains, such as the CTD and RRM1/2. Studies investigating metal ion binding to TDP-43 are also rare. Only one metal ion, Zn(II), was shown to bind to TDP-43; still, further studies are required to determine how Zn(II) interacts with full-length TDP-43, as these studies looked at the RRM1/2 domains. Minimal studies have been conducted that look at metal interactions with TDP-43. From our knowledge, Koski et al. (2021)⁵⁷ is the only review of current literature on the topic, and there have been few studies investigating these interactions since the review was published.

Additionally, in the Koski et al (2021) review⁵⁷, it is highlighted that only Zn(II) metal ions has been reported to bind to TDP-43, whereas the others, such as mercury, lead, iron, and copper, are just shown to have a link between aggregation and pathogenesis of the protein, but no actual binding site has been identified. The findings from Chapter 2 expanded the current knowledge on metal ion interactions with full length TDP-43 and contribute to a broader understanding of the full-length protein *in vitro*. In Chapter 3, I investigated the influence of other metal ions on Cu(II)-TDP-43 interactions, which contribute to understanding how this interaction is influenced in biological settings.

4.1.1. Cu(II) Binding to TDP-43

Chapter 2 investigated the interaction between Cu(II) and TDP-43. The biological roles of Cu(II) are well understood, specifically within neurons. For example, Cu(II) is an important cofactor in numerous enzymes within the nervous system, such as copper/zinc superoxide dismutase, and is required for proper development. However, copper in excess is neurotoxic. Dysregulation of Cu can lead to increased oxidative stress. There has been a clear relationship between ROS and redox-active Cu(II). Since elevated Cu(II) has been reported in ALS patients, it was of interest to determine if the metal ion interacted with TDP-43 to provide a fundamental understanding of a possible mechanism in ALS pathogenesis.

In Chapter 2, our goal was to establish Cu(II) binding to full-length TDP-43 *in vitro*, using surface electrochemistry. To our knowledge, this study was the first to investigate Cu(II) binding to TDP-43. Our method of establishing the Cu(II) binding to TDP-43 can be broken down into two objectives. 1) Verification of surface modifications and TDP-43 immobilization to the Au surface. 2) Investigating the Cu(II) interactions with TDP-43 using surface electrochemistry.

Our surface characterization was completed using methods such as ellipsometry, contact angle, x-ray photoelectron spectroscopy (XPS), and electrochemistry. Electrochemical impedance spectroscopy (EIS) and cyclic voltammetry (CV) were used to monitor each step in surface modification, to allow for TDP-43 immobilization and subsequent Cu(II) exposure. For EIS measurements, successful modifications were characterized by changes in the R_{ct} . Additionally, CV measurements indicated successful surface modifications by changes in the peak separation and current intensity. Changes to the CV peaks and EIS R_{ct} indicated change to the electrode

surface due to reduced or increased availability of the redox probe to reach the Au surface. Various steps in modification were analyzed using ellipsometry, contact angle, and XPS. Ellipsometry revealed that the thickness of the TDP-43-Au film was 3.1 ± 0.3 nm. The contact angle measurements indicated that the final film is also more hydrophilic ($51.5 \pm 2.0^\circ$) compared to the bare Au ($67.1 \pm 1.1^\circ$). XPS confirmed the presence of a protein on the surface based on the peak binding energies and ratio of C, N, and O elements. Cu(II) binding to the protein surface was verified using XPS, based on the appearance of the two Cu 2p peaks at 933 and 952 eV, thus verifying that Cu(II) is bound to the TDP-43-Au surface fabricated.

For my second objective, I explored the Cu(II)-TDP-43 binding further. The direct binding of Cu(II) ions to the TDP-43-Au film was detected using electrochemistry. The coordination of Cu(II) ions to immobilized TDP-43-Au induced an electrochemical signal at approximately 0.18 V versus Ag/AgCl. The Cu(II)-related signal had a linear relationship with Cu(II) concentration, with an R^2 value of 0.91. I also determined that Cu(II)-TDP-43 binding was influenced by pH, so the binding of Cu(II) occurred favourably at physiological pH. A reduction in Cu(II) signal was observed at lower pH (pH = 3), which suggested that the protein structure may become disrupted, due to the protonation of residues in the RRM, such as Asp and His. These results indicated that elevated Cu(II) concentrations may lead to Cu(II) coordination with full-length TDP-43 in biological conditions.

4.1.2. The Influence of Zn(II) Cu(II)-TDP-43 Binding

Chapters 2 and 3 was built on the knowledge of the Cu(II)-TDP-43 binding and investigated the effect of other biologically relevant metal ions on this binding interaction. Chapter

2 focused on the impact of Zn(II) on Cu(II)-TDP-43 interactions. The biological roles of Zn are well understood, specifically within the brain. For example, Zn(II) contributes to normal cognitive and emotional functioning and has important roles in cell division, RNA and DNA synthesis, and protein synthesis. However, when Zn is in excess, it becomes neurotoxic. Additionally, the oxidative stress observed in neurodegenerative disorders, causes the release of Zn, which may impact TDP-43 and its aggregation.

In Chapter 2, our goal was to monitor the influence that Zn(II) had on Cu(II) binding to full-length TDP-43 *in vitro*, using surface electrochemistry. Our method of establishing the effect of Zn(II) on Cu(II) binding to TDP-43 can be broken down into two objectives. 1) Investigation of the metal ion effect on Cu(II)-TDP-43 binding through competitive and displacive studies. 2) Verifying metal ion binding and changes in elemental composition using XPS.

The effect of the Zn(II) on Cu(II) binding to TDP-43 was investigated by exposing the TDP-43-Au surface to the metal ions in different order, as well as together. These metal-exposed TDP-43-Au surfaces were then measured by electrochemistry and analyzed using the surface characterization method of XPS. The initial findings showed that while no changes in electrochemical signals were observed with Zn(II), thus the impact of Zn(II) exposure on Cu(II)-TDP-43 binding was monitored through the Cu(II) signal. Following this, I wanted to determine if Zn(II) could compete or displace Cu(II) ions from TDP-43 films. Zn(II) exposure to TDP-43, followed by Cu(II) exposure, resulted in a statistically significant increase in current signal, compared to the Cu(II)-TDP-43-Au surface, suggesting that Zn(II) caused a change to the protein surface rather than increased Cu(II) binding. From XPS studies, the Cu 2p was also observed when Cu(II)-TDP-43-Au film was exposed to the Zn(II), which indicated a lack of Cu(II) displacement. This was also observed in the electrochemical measurements.

Overall, data from Chapter 2 indicate that Zn(II) influenced Cu(II)-TDP-43 interactions, which is of biological significance. Additional structural studies are required to determine the amount of metal ion binding to TDP-43, and binding sites, by other methods, such as mass spectrometry.

4.1.3. The Influence of Fe(III) on Cu(II)-TDP-43 Binding

Similar to Chapter 2, Chapter 3 was built on the knowledge of the Cu(II)-TDP-43 binding and investigated the effect of other biologically relevant metal ions on this binding interaction, specifically Fe(III). Similar to Zn and Cu, the biological roles of Fe are well understood, specifically within the brain. Specifically, Fe is involved in DNA synthesis, as well as oxygen transport and respiration, myelin synthesis, and neurotransmitter synthesis and metabolism. However, excess Fe can be neurotoxic. Oversaturation of iron storage molecules leads to the formation of iron pools, which can lead to oxidative damage and cell death. Oxidative stress, which is often observed in neurodegenerative disorders, may cause TDP-43 aggregation.

In Chapter 3, our goal was to monitor the influence of Fe(III) on Cu(II) binding to full-length TDP-43 *in vitro*, using surface electrochemistry. Our method of establishing the effect of the impact Fe(III) has on Cu(II) binding to TDP-43 can be broken down into two objectives. 1) Investigation of the electrochemical response of Fe(III)-TDP-43 binding. 2) Investigation of the impact of Fe(III) on Cu(II)-TDP-43 binding through competitive and displacive studies.

The effect of Fe(III) on Cu(II) binding to TDP-43 was investigated by exposing the TDP-43-Au surface to Fe(III) and Cu(II) in different orders, as well as together. These metal-exposed

TDP-43-Au surfaces were then measured by electrochemistry. Initial findings showed Fe(III) interactions with TDP-43 produced a more conductive film. This increase in conductivity indicated one of the following: Fe(III) coordination and binding to the TDP-43-Au film, or Fe(III) exposure-induced changes, increasing conductivity. Following this, I wanted to determine if Fe(III) could compete or displace Cu(II) ions from TDP-43 films. Co-exposing TDP-43 to Cu(II) and Fe(III) resulted in a statistically significant decrease in the current signal, compared to the Cu(II)-TDP-43-Au surface, which indicated that Fe(III) interacts with TDP-43 and causes a change to the surface that reduces Cu(II) binding. Overall, data from Chapter 3 indicate that Fe(III) influenced Cu(II) binding to TDP-43, which is of biological significance. Additional structural studies are required to determine the structural impacts of metal ion binding to TDP-43, by other methods, such as circular dichroism.

4.2. Future Research Directions

This thesis explored the bioelectrochemistry of metal ion interactions with TDP-43 by exposing immobilized TDP-43 to Cu(II), Zn(II), and Fe(III). The surfaces were verified using ellipsometry, contact angle, and XPS. For the future of this research, the binding site of these various metals, if any, should be explored. Changes to the TDP-43 structure post metal ion binding should also be investigated. Additionally, other disease state variations of TDP-43 should be utilized to determine if this metal ion binding only occurs with full-length TDP-43.

4.2.1. Exploring Binding Sites of Metal Ions

Although the results of this thesis indicated that Cu(II) binds to TDP-43, a better understanding of this interaction could be obtained by determining the binding sites of Cu(II). The sequence of TDP-43 has been reported; however, deducing a reliable three-dimensional folded structure of a protein based on the amino acid sequence is difficult unless the sequence is very similar to that of a protein with a known structure. The primary technique used to discover the three-dimensional structure of a protein at an atomic resolution is x-ray crystallography.

X-rays directed at a sample of pure protein result in a small fraction of the x-rays being scattered by the atoms in the sample. If the sample contains a well-ordered crystal, the scattered waves will appear as diffraction spots when the x-rays are detected. Then the measured diffraction pattern, along with the amino acid sequence, can be used to produce an atomic model.¹⁴² The limiting factor to this experiment would be the generation of a suitable protein crystal for TDP-43. Characterization of metal binding sites in proteins using this method has an additional complication. Preparing metal-containing protein samples is difficult and usually irreproducible due to issues arising from changes in pH, incorporation of unexpected metals, and or the oxidation/reduction of the targeted metal.¹⁴³ Handling et al. (2018) have developed a protocol for producing sufficient metal-containing protein crystals for analyzing the structure of a metalloprotein using x-ray crystallography.¹⁴³ However, the protocol is time-consuming, with the protocol taking up to 190 days to complete, most of which is dedicated to crystal growing. However, this method would facilitate a better understanding of Cu(II) coordination to TDP-43 and identify specific binding sites.

However, before determining the binding sites, Cu(II) coordination should be verified using other methods. Additionally, the Zn(II) and Fe(III) interactions with TDP-43 and Cu(II)-TDP-43 should also be verified to determine if these metal ions bind in addition to Cu(II) or influence Cu(II) binding in another way. Mass spectroscopy (MS) could be used to verify metal coordination to TDP-43. This method can directly detect metal ion binding and the binding stoichiometry. Native MS would evaluate the mass changes corresponding to adding metal ions to the protein.¹⁴⁴ MS can be conducted on the Cu(II) exposed TDP-43 to verify the Cu(II) binding. Additionally, our Zn(II)-TDP-43 binding verification through XPS was unclear, due to the absence of the two expected Zn 2p peaks, thus MS could provide further verification as to whether Zn(II) is binding.

4.2.2. TDP-43 Structure Post Metal Ion Binding

After verifying Cu(II) binding to TDP-43, and determining the nature in which Fe(III) or Zn(II) are interacting with TDP-43, further investigation of the effect of these interactions on the structure of TDP-43 should be determined. Additionally, it would provide more information as to the nature in which Zn(II) exposure to TDP-43 prior to Cu(II) increases the Cu(II) binding, observed in the Chapter 2 displacement studies. Similarly, insight into why Cu(II) binding is reduced when Fe(III) and Cu(II) are exposed at the same time could be provided by investigating the structure of TDP-43 before and after the metal exposure. A technique which can be utilized to study changes in the structure is circular dichroism (CD).

Circular dichroism (CD) is a technique that facilitates an examination of protein structure. The data obtained from CD depends on the content of α -helix, β -sheet, turns, and random coil.⁹⁷

Thus, changes in these contents before and after metal ion exposure can be used to indicate whether the metal ion exposure resulted in changes to the structure. However, the metals make it difficult to clearly state the structure changes.⁹⁷ Isothermal titration calorimetry (ITC) may provide a better methodology to determine if changes to the structure occur.

ITC is a method used to determine the thermodynamic parameters of an interaction. For data collection, heat-sensing devices detect the difference between the measurement and control cell, produce a signal, and provide a dissociation constant. The constant obtained from the measurement can provide some information about whether the structure is more stable before or after metal ion binding. Data obtained from these studies could provide insight into how these metal interactions affect the structure of TDP-43. If the data indicated that changes in the structure occur after metal ion interactions, it would be of further interest to determine if these changes in the structure lead to TDP-43 aggregation.

4.2.3. Metal Ion Binding to Aggregated TDP-43

Currently, this thesis provides a basis that Cu(II), and perhaps Zn(II) and Fe(III), bind to full-length TDP-43 normal biological conditions. However, investigating these interactions under disease-state conditions would also be beneficial in understanding ALS. By examining this interaction in these different conditions, we could gain insight into whether these interactions occur as ALS progresses, or if it only occurs in the earlier stages, when TDP-43 is not aggregated.

Surface electrochemical methods can be used to analyze this interaction, similar to the methods utilized throughout this thesis. Phosphorylated TDP-43 (pTDP-43) will readily aggregate

in the cytoplasm of neuron.¹⁴⁵ Thus, by immobilizing pTDP-43 to the surface instead of the full-length TDP-43 used in these studies, we could have a better understanding of how Cu(II) interacts with the protein in ALS.

4.2.4. Metal Ion Binding to ALS-Linked TDP-43 Mutations

In addition to using pTDP-43, the interaction between metals and specific ALS-linked TDP-43 mutations should be studied. A similar surface electrochemistry method may be utilized to determine the impact of the common missense mutations on the Cu(II)-TDP-43 interactions. A common missense mutation in familial ALS patients is A382T in the TARDBP gene.¹⁴⁶ A382T has been linked to TDP-43 accumulation in the cytoplasm and negatively impacts the functions of the protein. A382T, along with other common missense mutations to TDP-43 associated with ALS, may affect the binding sites of the metal ions to TDP-43 and can either cause an increase in Cu(II) binding or a reduction. Thus, further surface electrochemical studies can be conducted to investigate the impact of common mutations associated with the disease on Cu(II) and metal ion coordination. Similar to the suggested pTDP-43 studies, this study would provide a better understanding of how Cu(II) interacts with the protein in ALS.

Overall, these studies indicate that Cu(II) binds to TDP-43 suggesting that metal ions can interact with TDP-43, and may have an impact on its pathogenesis linked to ALS. However, methods such as x-ray crystallography, mass spectroscopy, circular dichroism, and isothermal titration calorimetry, can be used to verify the interactions, and provide more information about the impact of metal ion binding to the structure of TDP-43. Additional studies should also be conducted to determine if disease-related states of TDP-43 also interact with Cu(II), so more insight can be gathered in the context of ALS. These methods and additional studies will be useful to provide a deeper understanding of this metal ion interaction, which in term will provide a better understanding of TDP-43, and perhaps its pathogenesis in ALS. The electrochemical detection of metal-binding to TDP-43 acts as a fundamental understanding of the interaction between the two and can provide more insight into ALS.

References

1. Dugger, B. N., and Dickson, D. W. (2017) Pathology of neurodegenerative diseases. *Cold Spring Harbor Perspec. in Bio.* 9.
2. Hollander, J., and Lawler, C. (2021, July 16) Neurodegenerative Diseases. *Nat. Inst. of Envir. Health Sci.* U.S. Department of Health and Human Services.
3. Mitchell, J. D., and Borasio, G. D. (2007) Amyotrophic lateral sclerosis. *The Lancet* 369, 2031–2041.
4. Blizzard, C. A., Southam, K. A., Dawkins, E., Lewis, K. E., King, A. E., Clark, J. A., and Dickson, T. C. (2015) Identifying the primary site of pathogenesis in amyotrophic lateral sclerosis – vulnerability of lower motor neurons to proximal excitotoxicity. *Dis. Mod. & Mech.* 8, 215–224.
5. Lu, H., Dong Le, W., Xie, Y.-Y., and Wang, X.-P. (2016) Current Therapy of Drugs in Amyotrophic Lateral Sclerosis. *Curr. Neuropharmacol.* 14, 314–321
6. Afroz, T., Hock, E. M., Ernst, P., Foglieni, C., Jambeau, M., Gilhespy, L. A. B., Laferriere, F., Maniecka, Z., Plückthun, A., Mittl, P., Paganetti, P., Allain, F. H. T., and Polymenidou, M. (2017) Functional and dynamic polymerization of the ALS-linked protein TDP-43 antagonizes its pathologic aggregation. *Nat. Commun.* 8, 1–14.
7. Zarei, S., Carr, K., Reiley, L., Diaz, K., Guerra, O., Altamirano, P. F., Pagani, W., Lodin, D., Orozco, G., and China, A. (2015) A comprehensive review of amyotrophic lateral sclerosis. *Surg. Neurol. Int.* 6.
8. Wijesekera, L. C., and Leigh, P. N. (2009) Amyotrophic lateral sclerosis. *Orphanet J. Rare Dis.* 4, 1–22.

9. Breen, S., Williams, S. J., Outram, M., Kobe, B., and Solomon, P. S. (2017) Emerging Insights into the Functions of Pathogenesis-Related Protein 1. *Trends Plant Sci.* 10, 671-879.
10. Kovacs, G. G. (2019) Molecular pathology of neurodegenerative diseases : principles and practice. *J. of Clin. Path.* 43, 725–735.
11. Sun, Y., and Chakrabarty, A. (2017) Phase to Phase with TDP-43. *Biochem.* 56, 809–823.
12. Jo, M., Lee, S., Jeon, Y.-M., Kim, S., Kwon, Y., and Kim, H.-J. (2020) The role of TDP-43 propagation in neurodegenerative diseases: Integrating insights from clinical and experimental studies. *Exper. & Mol. Med.* 52, 1652–1662.
13. Khalfallah, Y., Kuta, R., Grasmuck, C., Prat, A., Durham, H. D., and Vande Velde, C. (2018) TDP-43 regulation of stress granule dynamics in neurodegenerative disease-relevant cell types. *Sci. Reps.* 8.
14. Dejesus-hernandez, M., Mackenzie, I. R., Boeve, B. F., Boxer, A. L., Baker, M., Rutherford, N. J., Nicholson, A. M., Finch, N. A., Gilmer, F., Adamson, J., Kouri, N., Wojtas, A., Sengdy, P., Hsiung, G. R., Karydas, A., Seeley, W. W., Josephs, K. A., Geschwind, D. H., Wszolek, Z. K., Feldman, H., Petersen, R., Miller, B. L., Dickson, D., Boylan, K., Graff-Radford, N., and Rademakers, R. (2011) Expanded GGGGCC hexanucleotide repeat in non-coding region of C9ORF72 causes chromosome 9p-linked frontotemporal dementia and amyotrophic lateral sclerosis. *Neuron* 72, 245–256.
15. Mompeán, M., Romano, V., Pantoja-Uceda, D., Stuani, C., Baralle, F. E., Buratti, E., and Laurents, D. V. (2016) The TDP-43 N-terminal domain structure at high resolution. *The FEBS J.* 283, 1242–1260.

16. Kuo, P. H., Doudeva, L. G., Wang, Y. T., Shen, C. K. & Yuan, H. S. (2009) Structural insights into TDP-43 in nucleic-acid binding and domain interactions. *Nucleic Acids Res.* 37, 1799–1808.
17. Lukavsky, P. J., Daujotyte, D., Tollervey, J. R., Ule, J., Stuani, C., Buratti, E., Baralle, F. E., Damberger, F. F., and Allain, F. H.-T. (2013) Molecular basis of UG-rich RNA recognition by the human splicing factor TDP-43. *Nat. Struct. & Mol. Bio.* 20, 1443–1449.
18. Ayala, Y. M., Zago, P., D'Ambrogio, A., Xu, Y.-F., Petrucelli, L., Buratti, E., and Baralle, F. E. (2008) Structural determinants of the cellular localization and shuttling of TDP-43. *J. Cell Sci.* 121, 3778–3785.
19. Mackness, B. C., Tran, M. T., McClain, S. P., Matthews, C. R., and Zitzewitz, J. A. (2014) Folding of the RNA recognition motif (RRM) domains of the amyotrophic lateral sclerosis (als)-linked protein TDP-43 reveals an intermediate state. *J. Bio. Chem.* 289, 8264–8276.
20. Xu, Z.-S. (2012) Does a loss of TDP-43 function cause neurodegeneration? *Mol. Neurodegen.* 7, 27.
21. Donde, A., Sun, M., Ling, J. P., Braunstein, K. E., Pang, B., Wen, X., Cheng, X., Chen, L., and Wong, P. C. (2019) Splicing repression is a major function of TDP-43 in motor neurons. *Acta Neuropath.* 138, 813–826.
22. Buratti, E., and Baralle, F. E. (2010) The multiple roles of TDP-43 in pre-mrna processing and gene expression regulation. *RNA Biology* 7, 420–429.
23. Chen, H.-J., and Mitchell, J. C. (2021) Mechanisms of TDP-43 proteinopathy onset and propagation. *Int. J. Mol. Sci.* 22, 6004.

24. Freibaum, B. D., Chitta, R. K., High, A. A., and Taylor, J. P. (2010) Global analysis of TDP-43 interacting proteins reveals strong association with RNA splicing and translation machinery. *J. Proteome Res.* 9, 1104–1120.
25. François-Moutal, L., Perez-Miller, S., Scott, D. D., Miranda, V. G., Mollasalehi, N., and Khanna, M. (2019) Structural insights into TDP-43 and effects of post-translational modifications. *Frontiers in Mol. Neurosci.* 12.
26. Aulas, A., Stabile, S. & Vande Velde, C. (2012) Endogenous TDP-43, but not FUS, contributes to stress granule assembly via G3BP. *Mol Neurodegen.* 7, 1.
27. Xu, Y.-F., Gendron, T. F., Zhang, Y.-J., Lin, W.-L., D'Alton, S., Sheng, H., Casey, M. C., Tong, J., Knight, J., Yu, X., Rademakers, R., Boylan, K., Hutton, M., McGowan, E., Dickson, D. W., Lewis, J., and Petrucelli, L. (2010) Wild-type human TDP-43 expression causes TDP-43 phosphorylation, mitochondrial aggregation, motor deficits, and early mortality in transgenic mice. *J. Neurosci.* 30, 10851–10859.
28. Igaz, L. M., Kwong, L. K., Lee, E. B., Chen-Plotkin, A., Swanson, E., Unger, T., Malunda, J., Xu, Y., Winton, M. J., Trojanowski, J. Q., and Lee, V. M.-Y. (2011) Dysregulation of the ALS-associated gene TDP-43 leads to neuronal death and degeneration in mice. *J. Clin. Invest.* 121, 726–738.
29. Neumann, M., Kwong, L. K., Lee, E. B., Kremmer, E., Flatley, A., Xu, Y., Forman, M. S., Troost, D., Kretschmar, H. A., Trojanowski, J. Q., and Lee, V. M.-Y. (2009) Phosphorylation of S409/410 of TDP-43 is a consistent feature in all sporadic and familial forms of TDP-43 proteinopathies. *Acta Neuropath.* 117, 137–149.
30. Tsuji, H., Arai, T., Kametani, F., Nonaka, T., Yamashita, M., Suzukake, M., Hosokawa, M., Yoshida, M., Hatsuta, H., Takao, M., Saito, Y., Murayama, S., Akiyama, H.,

- Hasegawa, M., Mann, D. M., and Tamaoka, A. (2012) Molecular analysis and biochemical classification of TDP-43 proteinopathy. *Brain* 135, 3380–3391.
31. Hasegawa, M., Arai, T., Nonaka, T., Kametani, F., Yoshida, M., Hashizume, Y., Beach, T. G., Buratti, E., Baralle, F., Morita, M., Nakano, I., Oda, T., Tsuchiya, K., and Akiyama, H. (2008) Phosphorylated TDP-43 in frontotemporal lobar degeneration and amyotrophic lateral sclerosis. *Annals of Neuro.* 64, 60–70.
32. Barmada, S. J., Skibinski, G., Korb, E., Rao, E. J., Wu, J. Y., and Finkbeiner, S. (2010) Cytoplasmic mislocalization of TDP-43 is toxic to neurons and enhanced by a mutation associated with familial amyotrophic lateral sclerosis. *J. Neurosci.* 30, 639–649.
33. Suk, T.R., Rousseaux, M.W.C. (2020) The role of TDP-43 mislocalization in amyotrophic lateral sclerosis. *Mol Neurodegen.* 15, 45.
34. Conicella, A. E., Dignon, G. L., Zerze, G. H., Schmidt, H. B., D’Ordine, A. M., Kim, Y. C., Rohatgi, R., Ayala, Y. M., Mittal, J., and Fawzi, N. L. (2020) TDP-43 α -helical structure tunes liquid–liquid phase separation and function. *Proceedings of the Nat. Acad. of Sci.* 117, 5883–5894.
35. Johnson, B. S., Snead, D., Lee, J. J., McCaffery, J. M., Shorter, J., and Gitler, A. D. (2009) TDP-43 is intrinsically aggregation-prone, and amyotrophic lateral sclerosis-linked mutations accelerate aggregation and increase toxicity. *J. Bio. Chem.* 284, 20329–20339.
36. Conicella, A. E., Zerze, G. H., Mittal, J., and Fawzi, N. L. (2016) ALS mutations disrupt phase separation mediated by α -helical structure in the TDP-43 low-complexity C-terminal domain. *Structure* 24, 1537–1549.

37. Rajendran, L., Honsho, M., Zahn, T. R., Keller, P., Geiger, K. D., Verkade, P., and Simons, K. (2006) Alzheimer's disease β -amyloid peptides are released in association with exosomes. *Proceedings of the Nat. Acad. of Sci.* *103*, 11172–11177.
38. Emmanouilidou, E., Melachroinou, K., Roumeliotis, T., Garbis, S. D., Ntzouni, M., Margaritis, L. H., Stefanis, L., and Vekrellis, K. (2010) Cell-produced α -synuclein is secreted in a calcium-dependent manner by exosomes and impacts neuronal survival. *The J. of Neurosci.* *30*, 6838–6851.
39. Asai, H., Ikezu, S., Tsunoda, S., Medalla, M., Luebke, J., Haydar, T., Wolozin, B., Butovsky, O., Kügler, S., and Ikezu, T. (2015) Depletion of microglia and inhibition of exosome synthesis halt tau propagation. *Nat. Neurosci.* *18*, 1584–1593.
40. Ling SC, Polymenidou M, Cleveland DW. (2013) Converging mechanisms in ALS and FTD: disrupted RNA and protein homeostasis. *Neuron* *79*, 416-38.
41. Buratti E. (2015) Functional Significance of TDP-43 Mutations in Disease. *Adv Genet.* *91*, 1-53.
42. Sun, Y., Cruz, A. M., Hadley, K. C., Galant, N. J., Law, R., Vernon, R. M., Morris, V. K., Robertson, J., and Chakrabarty, A. (2018) Physiologically Important Electrolytes as Regulators of TDP-43 Aggregation and Droplet-Phase Behavior. *Biochem.* *58*, 590–607.
43. Babinchak, W. M., Haider, R., Dumm, B. K., Sarkar, P., Surewicz, K., Choi, J. K., and Surewicz, W. K. (2019) The role of liquid-liquid phase separation in aggregation of the TDP-43 low-complexity domain. *J. Biol. Chem.* *294*, 6306–6317.
44. Lin, Y., Zhou, X., Kato, M., Liu, D., Ghaemmaghami, S., Tu, B. P., and McKnight, S. L. (2020) Redox-mediated regulation of an evolutionarily conserved cross- β structure formed

- by the TDP43 low complexity domain. *Proceedings of the National Acad. of Scie.* 117, 28727–28734.
45. Hussain, H., Djurin, T., Rodriguez, J., Daneelien, L., Sundi, S., Fadel, A., and Saadoon, Z. (2022) Transactivation response DNA-binding protein of 43 (TDP-43) and glial cell roles in neurological disorders. *Cureus*.
46. Dewey, C. M., Cenik, B., Sephton, C. F., Dries, D. R., Mayer, P., Good, S. K., Johnson, B. A., Herz, J., and Yu, G. (2011) TDP-43 is directed to stress granules by sorbitol, a novel physiological osmotic and oxidative stressor. *Mol. and Cell. Bio.* 31, 1098–1108.
47. Colombrita, C., Zennaro, E., Fallini, C., Weber, M., Sommacal, A., Buratti, E., Silani, V., and Ratti, A. (2009) TDP-43 is recruited to stress granules in conditions of oxidative insult. *J. of Neurochem.* 111, 1051–1061.
48. Barmada, S. J., Serio, A., Arjun, A., Bilican, B., Daub, A., Ando, D. M., Tsvetkov, A., Pleiss, M., Li, X., Peisach, D., Shaw, C., Chandran, S., and Finkbeiner, S. (2014) Autophagy induction enhances TDP43 turnover and survival in neuronal ALS models. *Nat. Chem. Bio.* 10, 677–685.
49. McDonald, K. K., Aulas, A., Destroismaisons, L., Pickles, S., Beleac, E., Camu, W., Rouleau, G. A., and Vande Velde, C. (2011) Tar DNA-binding protein 43 (TDP-43) regulates stress granule dynamics via differential regulation of G3BP and TIA-1. *Human Mol. Gen.* 20, 1400–1410.
50. Campos-Melo D, Hawley ZCE, Droppelmann CA, Strong MJ. (2021) The Integral Role of RNA in Stress Granule Formation and Function. *Front Cell Dev Biol.* 9.

51. Udan-Johns, M., Bengoechea, R., Bell, S., Shao, J., Diamond, M. I., True, H. L., Weihl, C. C., and Baloh, R. H. (2013) Prion-like nuclear aggregation of TDP-43 during heat shock is regulated by HSP40/70 Chaperones. *Human Mol. Gen.* 23, 157–170.
52. Miller, J., McLachlan, A. D., and Klug, A. (1985) Repetitive zinc-binding domains in the protein transcription factor IIIA from xenopus oocytes. *The EMBO J.* 4, 1609–1614.
53. Lee, M. S., Gippert, G. P., Soman, K. V., Case, D. A., and Wright, P. E. (1989) Three-dimensional solution structure of a single zinc finger DNA-binding domain. *Sci.* 245, 635–637.
54. Meloni, G., Cramer, A., Fritz, G., Davies, P., Brown, D. R., Kroneck, P. M., and Vašák, M. (2012) The catalytic redox activity of prion protein-cu^{II} is controlled by metal exchange with the zinc-thiolate clusters of zinc7metallothionein-3. *ChemBioChem* 13, 1261–1265.
55. Bolognin, S., Messori, L. & Zatta, P. (2009) Metal Ion Physiopathology in Neurodegenerative Disorders. *Neuromol Med* 11, 223–238.
56. Mitra J, Vasquez V, Hegde PM, Boldogh I, Mitra S, Kent TA, Rao KS, Hegde ML. (2014) Revisiting Metal Toxicity in Neurodegenerative Diseases and Stroke: Therapeutic Potential. *Neurol Res Ther.* 1, 107.
57. Koski, L., Ronnevi, C., Berntsson, E., Wärmländer, S. K., & Roos, P. M. (2021). Metals in ALS TDP-43 pathology. *International Journal of Mol. Sci.*, 22, 12193.
58. Othman, S. B., and Yabe, T. (2015) Use of hydrogen peroxide and peroxy radicals to induce oxidative stress in neuronal cells. *Reviews in Agricultural Sci.* 3, 40–45.
59. Patten, D. A., Germain, M., Kelly, M. A., and Slack, R. S. (2010) Reactive oxygen species: Stuck in the middle of neurodegeneration. *J. of Alzheimer's Disease* 20.

60. Bar-Sela, S., Reingold, S., and Richter, E. D. (2001) Amyotrophic lateral sclerosis in a battery-factory worker exposed to Cadmium. *Internat. J. of Occup. and Envir. Health* 7, 109–112.
61. Bachmeyer, C., Bagur, E., Lenglet, T., Maier-Redelsperger, M., and Lecomte, I. (2012) Lead poisoning mimicking amyotrophic lateral sclerosis: An adverse effect of rituals. *The Amer. J. of Med.* 125.
62. Oh, S.-S., Kim, E. A., Lee, S.-W., Kim, M.-K., and Kang, S.-K. (2007) A case of amyotrophic lateral sclerosis in electronic parts manufacturing worker exposed to lead. *NeuroTox.* 28, 324–327.
63. Peters, T. L., Kamel, F., Lundholm, C., Feychting, M., Weibull, C. E., Sandler, D. P., Wiebert, P., Sparén, P., Ye, W., and Fang, F. (2016) Occupational exposures and the risk of amyotrophic lateral sclerosis. *Occup. and Envir. Med.* 74, 87–92.
64. Hamilton, A. Lead Poisoning in Potteries, Tile Works, and Porcelain Enameled Sanitary Ware Factories; Bureau of Labor: Washington, DC, USA, 1912.
65. OSHA. Safety and Health Topics Lead; United States Department of Labor: Washington, DC, USA, 2021.
66. Fang, F., Kwee, L. C., Allen, K. D., Umbach, D. M., Ye, W., Watson, M., Keller, J., Oddone, E. Z., Sandler, D. P., Schmidt, S., and Kamel, F. (2010) Association between blood lead and the risk of amyotrophic lateral sclerosis. *American J. of Epidem.* 171, 1126–1133.
67. Garzillo, E. M., Lamberti, M., Genovese, G., Pedata, P., Feola, D., Sannolo, N., Daniele, L., Trojsi, F., Monsurro, M. R., and Miraglia, N. (2014) Blood lead, manganese, and

- aluminum levels in a regional Italian cohort of ALS patients. *J. of Occup. & Envir. Med.* 56, 1062–1066.
68. Roos, P. M., Vesterberg, O., Syversen, T., Flaten, T. P., and Nordberg, M. (2012) Metal concentrations in cerebrospinal fluid and blood plasma from patients with amyotrophic lateral sclerosis. *Biol. Trace Element Res.* 151, 159–170.
69. Vinceti, M., Solovyev, N., Mandrioli, J., Crespi, C. M., Bonvicini, F., Arcolin, E., Georgouloupoulou, E., and Michalke, B. (2013) Cerebrospinal fluid of newly diagnosed amyotrophic lateral sclerosis patients exhibits abnormal levels of selenium species including elevated selenite. *NeuroTox.* 38, 25–32.
70. Sheykhansari, S., Kozielski, K., Bill, J., Sitti, M., Gemmati, D., Zamboni, P., and Singh, A. V. (2018) Redox metals homeostasis in multiple sclerosis and amyotrophic lateral sclerosis: A Review. *Cell Death & Disease* 9.
71. Konoha, K., Sadakane, Y., and Kawahara, M. (2006) Zinc neurotoxicity and its role in Neurodegenerative Diseases. *J. of Health Sci.* 52, 1–8.
72. Li, Z., Liu, Y., Wei, R., Yong, V. W., and Xue, M. (2022) The important role of zinc in neurological diseases. *Biomol.* 13, 28.
73. Garnier, C., Devred, F., Byrne, D., Puppo, R., Roman, A. Y., Malesinski, S., Golovin, A. V., Lebrun, R., Ninkina, N. N., and Tsvetkov, P. O. (2017) Zinc binding to RNA recognition motif of TDP-43 induces the formation of amyloid-like aggregates. *Sci. Reps.* 7.
74. Pace, N. J. & Weerapana, E. (2014) Zinc-binding cysteines: diverse functions and structural motifs. *Biomol.* 4, 419–434.

75. Maret, W. (2005) Zinc coordination environments in proteins determine zinc functions. *J Trace Elem Med Biol* 19, 7–12.
76. Golovin, A. V., Devred, F., Yatoui, D., Roman, A. Y., Zalevsky, A. O., Puppo, R., Lebrun, R., Guerlesquin, F., and Tsvetkov, P. O. (2020) Zinc binds to RRM2 peptide of TDP-43. *Internat. J. of Mol. Sci.* 21, 9080.
77. Bernhoft R.A. (2011) Mercury toxicity and treatment: a review of the literature. *J Environ Public Health.* 2012, 460508.
78. Berlin, M., Zalups, R., and Fowler, B. (2007) Mercury. *Handbook on the Tox. of Metals* 675–729.
79. Adams, C. R. (1983) Mercury intoxication simulating amyotrophic lateral sclerosis. *JAMA: The J. of the American Med. Ass.* 250, 642–643.
80. Barber, T.E. (1978) Inorganic mercury intoxication reminiscent of amyotrophic lateral sclerosis. *J. Occup. Med.* 20, 667–669.
81. Mangelsdorf, I., Walach, H., and Mutter, J. (2017) Healing of amyotrophic lateral sclerosis: A case report. *Complementary Med. Res.* 24, 175–181.
82. Pamphlett, R., and Kum Jew, S. (2011) Inorganic Mercury within motor neurons does not cause the TDP-43 changes seen in sporadic ALS. *Tox. Letters* 201, 58–61.
83. Ash, P. E., Dhawan, U., Boudeau, S., Lei, S., Carlomagno, Y., Knobel, M., Al Mohanna, L. F., Boomhower, S. R., Newland, M. C., Sherr, D. H., and Wolozin, B. (2018) Heavy metal neurotoxicants induce ALS-linked TDP-43 pathology. *Tox. Sci.* 167, 105–115.
84. Flora, G., Gupta, D., and Tiwari, A. (2012) Toxicity of lead: A review with recent updates. *Interdis. Tox.* 5, 47–58.

85. Wani, A. L., Ara, A., and Usmani, J. A. (2015) Lead toxicity: A Review. *Interdis. Tox.* 8, 55–64.
86. Miller, C. J., Rose, A. L., and Waite, T. D. (2016) Importance of iron complexation for Fenton-mediated hydroxyl radical production at circumneutral pH. *Frontiers in Marine Sci.* 3.
87. Caragounis, A., Price, K. A., Soon, C. P. W., Filiz, G., Masters, C. L., Li, Q.-X., Crouch, P. J., and White, A. R. (2010) Zinc induces depletion and aggregation of endogenous TDP-43. *Free Radical Bio. and Med.* 48, 1152–1161.
88. Mitani, T. T., Beck, G., Kido, K., Yamashita, R., Yonenobu, Y., Ogawa, T., Saeki, C., Okuno, T., Nagano, S., Morii, E., Hasegawa, M., Saito, Y., Murayama, S., and Mochizuki, H. (2021) Amyotrophic lateral sclerosis with speech apraxia, predominant upper motor neuron signs, and prominent iron accumulation in the frontal operculum and precentral gyrus. *Neuropath.* 41, 324–331.
89. (2000) Copper in drinking water. National Academy Press Washington, D.C.
90. Desai, V., and Kaler, S. G. (2008) Role of copper in human neurological disorders. *The American J. of Clin. Nutrition* 88.
91. Faller, P., and Hureau, C. (2009) Bioinorganic chemistry of copper and zinc ions coordinated to amyloid- β peptide. *Dalton Trans.* 1080–1094.
92. Pham, A. N., Xing, G., Miller, C. J., and Waite, T. D. (2013) Fenton-like copper redox chemistry revisited: Hydrogen peroxide and superoxide mediation of copper-catalyzed oxidant production. *J. of Catalysis* 301, 54–64.
93. Zubčić, K., Hof, P. R., Šimić, G., and Jazvinščak Jembrek, M. (2020) The role of copper in tau-related pathology in Alzheimer's disease. *Frontiers in Mol. Neurosci.* 13.

94. Parker, S. J., Meyerowitz, J., James, J. L., Liddell, J. R., Nonaka, T., Hasegawa, M., Kanninen, K. M., Lim, S. C., Paterson, B. M., Donnelly, P. S., Crouch, P. J., and White, A. R. (2012) Inhibition of TDP-43 accumulation by Bis(thiosemicarbazonato)-copper complexes. *PLoS ONE* 7.
95. Boyd, J. D., Lee-Armandt, J. P., Feiler, M. S., Zaarur, N., Liu, M., Kraemer, B., Concannon, J. B., Ebata, A., Wolozin, B., and Glicksman, M. A. (2014) A high-content screen identifies novel compounds that inhibit stress-induced TDP-43 cellular aggregation and associated cytotoxicity. *SLAS Discovery* 19, 44–56.
96. Kelly, S. M., Jess, T. J., & Price, N. C. (2005). How to study proteins by circular dichroism. *Biochimica Et Biophysica Acta (BBA) - Proteins and Proteomics*, 1751, 119–139.
97. Faller, P., Hureau, C., Dorlet, P., Hellwig, P., Coppel, Y., Collin, F., & Alies, B. (2012). Methods and techniques to study the bioinorganic chemistry of metal–peptide complexes linked to neurodegenerative diseases. *Coordination Chem. Rev.*, 256, 2381–2396.
98. Tsvetkov, P. O., Kulikova, A. A., Golovin, A. V., Tkachev, Y. V., Archakov, A. I., Kozin, S. A., and Makarov, A. A. (2010) Minimal zn^{2+} binding site of amyloid- β . *Biophys. J.* 99.
99. Dai, Y., Wang, C., Chiu, L.-Y., Abbasi, K., Tolbert, B. S., Sauv e, G., Yen, Y., and Liu, C.-C. (2018) Application of bioconjugation chemistry on biosensor fabrication for detection of tar-DNA binding protein 43. *Biosens. and Bioelect.* 117, 60–67.
100. Serafin, V., Razzino, C. A., Gamella, M., Pedrero, M., Povedano, E., Montero-Calle, A., Barderas, R., Calero, M., Lobo, A. O., Y a ez-Sede o, P., Campuzano, S., and Pingarr on, J. M. (2020) Disposable immunoplatforms for the simultaneous determination of biomarkers for neurodegenerative disorders using poly(amidoamine) Dendrimer/gold nanoparticle nanocomposite. *Anal. and Bioanal. Chem.* 413, 799–811.

101. Jiang, D., Men, L., Wang, J., Zhang, Y., Chickenyen, S., Wang, Y., and Zhou, F. (2007) Redox reactions of copper complexes formed with different β -amyloid peptides and their neuropathological relevance. *Biochem.* *46*, 9270–9282.
102. Peng, Y., Wang, C., Xu, H. H., Liu, Y.-N., and Zhou, F. (2010) Binding of α -synuclein with Fe(III) and with Fe(II) and biological implications of the resultant complexes. *J. of Inorganic Biochem.* *104*, 365–370.
103. Martic, S., Rains, M. K., and Kraatz, H.-B. (2013) Probing copper/tau protein interactions electrochemically. *Anal. Biochem.* *442*, 130–137.
104. Golec, C., Esteves-Villanueva, J. O., and Martic, S. (2021) Electrochemical characterization of Cu(II) complexes of brain-related tau peptides. *Canadian J. of Chem.* *99*, 628–636.
105. Li, S. P., and Kerman, K. (2019) Electrochemical detection of interaction between copper(II) and peptides related to pathological α -synuclein mutants. *Anal. Chem.* *91*, 3818–3826.
106. Davies, P., Wang, X., Sarell, C. J., Drewett, A., Marken, F., Viles, J. H., and Brown, D. R. (2010) The synucleins are a family of redox-active copper binding proteins. *Biochem.* *50*, 37–47.
107. Brzyska, M., Trzesniewska, K., Wieckowska, A., Szczepankiewicz, A., and Elbaum, D. (2009) Electrochemical and conformational consequences of copper (Cu(I) and Cu(II)) binding to β -amyloid(1-40). *ChemBioChem* *10*, 1045–1055.
108. Guilloreau, L., Combalbert, S., Sournia-Saquet, A., Mazarguil, H., and Faller, P. (2007) Redox chemistry of copper–amyloid- β : The generation of hydroxyl radical in the

- presence of ascorbate is linked to redox-potentials and aggregation state. *ChemBioChem* 8, 1317–1325.
109. Rasia, R. M., Bertocini, C. W., Marsh, D., Hoyer, W., Cherny, D., Zweckstetter, M., Griesinger, C., Jovin, T. M., and Fernández, C. O. (2005) Structural characterization of copper(ii) binding to α -synuclein: Insights into the bioinorganic chemistry of parkinson's disease. *Proceedings the Nati. Acad. Sci.* 102, 4294–4299.
110. Tōugu, V., Karafin, A., and Palumaa, P. (2008) Binding of zinc(ii) and copper(ii) to the full-length alzheimer's amyloid- β peptide. *J. Neurochem.* 104, 1249–1259.
111. Zhou, L.-X., Du, J.-T., Zeng, Z.-Y., Wu, W.-H., Zhao, Y.-F., Kanazawa, K., Ishizuka, Y., Nemoto, T., Nakanishi, H., and Li, Y.-M. (2007) Copper (II) modulates in vitro aggregation of a tau peptide. *Peptides* 28, 2229–2234.
112. Jobling, M. F., Huang, X., Stewart, L. R., Barnham, K. J., Curtain, C., Volitakis, I., Perugini, M., White, A. R., Cherny, R. A., Masters, C. L., Barrow, C. J., Collins, S. J., Bush, A. I., and Cappai, R. (2001) Copper and zinc binding modulates the aggregation and neurotoxic properties of the prion peptide PRP106–126. *Biochem.* 40, 8073–8084.
113. Kim, A., Lim, S., and Kim, Y. (2018) Metal ion effects on AB and Tau Aggregation. *Inter. J. Mol. Sci.* 19, 128.
114. Deas, E., Cremades, N., Angelova, P. R., Ludtmann, M. H. R., Yao, Z., Chen, S., Horrocks, M. H., Banushi, B., Little, D., Devine, M. J., Gissen, P., Klenerman, D., Dobson, C. M., Wood, N. W., Gandhi, S., and Abramov, A. Y. (2016) Alpha-synuclein oligomers interact with metal ions to induce oxidative stress and neuronal death in parkinson's disease. *Antioxi. & Redox Sig.* 24, 376–391.

115. Dang, T. N., Lim, N. K., Grubman, A., Li, Q.-X., Volitakis, I., White, A. R., and Crouch, P. J. (2014) Increased metal content in the TDP-43^{315t} transgenic mouse model of frontotemporal lobar degeneration and amyotrophic lateral sclerosis. *Frontiers in Aging Neurosci.* 6.
116. Chang, C.-ke, Chiang, M.-hui, Toh, E. K.-W., Chang, C.-F., and Huang, T.-huang. (2013) Molecular mechanism of oxidation-induced TDP-43 RRM1 aggregation and loss of function. *FEBS Letters* 587, 575–582.
117. Azzam, R. M. A. (1982) Division-of-amplitude photopolarimeter (DOAP) for the simultaneous measurement of all four stokes parameters of light. *Optica Acta: Inte. J. Optics* 29, 685–689.
118. Ahmadi, S., Ebralidze, I. I., She, Z., and Kraatz, H.-B. (2017) Electrochemical studies of tau protein-iron interactions—potential implications for alzheimer’s disease. *Electrochimica Acta* 236, 384–393.
119. Bandarenka, A. S. (2013) Exploring the interfaces between metal electrodes and aqueous electrolytes with electrochemical impedance spectroscopy. *The Anal.* 138, 5540.
120. Wang, M., Wang, L., Wang, G., Ji, X., Bai, Y., Li, T., Gong, S., and Li, J. (2004) Application of impedance spectroscopy for monitoring colloid au-enhanced antibody immobilization and antibody–antigen reactions. *Biosens. and Bioelec.* 19, 575–582.
121. Asav, E., and Sezgentürk, M. K. (2014) A novel impedimetric disposable immunosensor for rapid detection of a potential cancer biomarker. *Int. J. Biol. Macromole.* 66, 273–280.

122. Onda, T., Shibuichi, S., Satoh, N., and Tsujii, K. (1996) Super-water-repellent fractal surfaces. *Langmuir* 12, 2125–2127.
123. Castner, D. G., Hinds, K., and Grainger, D. W. (1996) X-ray photoelectron spectroscopy Sulfur 2P study of organic thiol and disulfide binding interactions with gold surfaces. *Langmuir* 12, 5083–5086.
124. Furutani, M., Nakayama, K., Okuma, K., and Arimitsu, K. (2019) Photoadhesive of acrylates containing cross-links of Dipyridyl disulfide. *J. Photopolymer Sci. and Tech.* 32, 619–622.
125. Cao, R., Díaz, A., Cao, R., Otero, A., Cea, R., Rodríguez-Argüelles, M. C., and Serra, C. (2007) Building layer-by-layer a bis(dithiocarbamate)copper(ii) complex on $\text{Au}\{111\}$ surfaces. *J. Amer. Chem. S.* 129, 6927–6930.
126. Del Bello, F., Pellei, M., Bagnarelli, L., Santini, C., Giorgioni, G., Piergentili, A., Quaglia, W., Battocchio, C., Iucci, G., Schiesaro, I., Meneghini, C., Venditti, I., Ramanan, N., De Franco, M., Sgarbossa, P., Marzano, C., and Gandin, V. (2022) Cu(I) and Cu(II) complexes based on lonidamine-conjugated ligands designed to promote synergistic antitumor effects. *Inorg. Chem.* 61, 4919–4937.
127. Ivanova, T. M., Maslakov, K. I., Sidorov, A. A., Kiskin, M. A., Linko, R. V., Savilov, S. V., Lunin, V. V., and Eremenko, I. L. (2020) XPS detection of unusual Cu(II) to Cu(I) transition on the surface of complexes with redox-active ligands. *J. Electron Spec. and Related Phenom.* 238, 146878.
128. Hornbeck, P. V., Zhang, B., Murray, B., Kornhauser, J. M., Latham, V., and Skrzypek, E. (2014) PhosphoSitePlus, 2014: Mutations, PTMS and recalibrations. *Nucleic Acids Res.* 43.

129. Patni, D., and Jha, S. K. (2021) Protonation–deprotonation switch controls the amyloid-like misfolding of nucleic-acid-binding domains of TDP-43. *J. Phys. Chem. B* 125, 8383–8394.
130. Bitanhirwe, B. K. Y., and Cunningham, M. G. (2009) Zinc: The brain's dark horse. *Synapse* 63, 1029–1049.
131. Osredkar, J., and Sustar, N. (2011) Copper and zinc, biological role and significance of copper/zinc imbalance. *J. Clin. Tox. s3*.
132. Curtain, C. C., Ali, F., Volitakis, I., Cherny, R. A., Norton, R. S., Beyreuther, K., Barrow, C. J., Masters, C. L., Bush, A. I., and Barnham, K. J. (2001) Alzheimer's disease amyloid- β binds copper and zinc to generate an allosterically ordered membrane-penetrating structure containing superoxide dismutase-like subunits. *J. of Biol. Chem.* 276, 20466–20473.
133. Gerstel, P., Hoffmann, R. C., Lebowski, P., Jeurgens, L. P., Bill, J., and Aldinger, F. (2005) Mineralization from aqueous solutions of zinc salts directed by amino acids and peptides. *Chem. Mat.* 18, 179–186.
134. Abbaspour, N., Hurrell, R., and Kelishadi, R. (2014) Review on iron and its importance for human health. *J. of Res. in Medi. Sci.* 19, 164-174.
135. Ward, R. J., Zucca, F. A., Duyn, J. H., Crichton, R. R., and Zecca, L. (2014) The role of iron in Brain Ageing and Neurodegenerative Disorders. *The Lancet Neuro.* 13, 1045–1060.
136. Nadjar, Y., Gordon, P., Corcia, P., Bensimon, G., Pieroni, L., Meininger, V., and Salachas, F. (2012) Elevated serum ferritin is associated with reduced survival in amyotrophic lateral sclerosis. *PLoS ONE* 7.

137. Veyrat-Durebex, C., Corcia, P., Mucha, A., Benzimra, S., Mallet, C., Gendrot, C., Moreau, C., Devos, D., Piver, E., Pagès, J.-C., Maillot, F., Andres, C. R., Vourc'h, P., and Blasco, H. (2014) Iron metabolism disturbance in a French cohort of ALS patients. *BioMed Res. Internat.* 2014, 1–6.
138. Baker, H. M., Anderson, B. F., and Baker, E. N. (2003) Dealing with iron: Common structural principles in proteins that transport iron and heme. *Proceedings of the Nat. Acad. of Sci.* 100, 3579–3583.
139. Nair, N. G., Perry, G., Smith, M. A., and Reddy, V. P. (2010) NMR studies of zinc, copper, and iron binding to histidine, the principal metal ion complexing site of amyloid- β peptide. *J. of Alzheimer's Disease* 20, 57–66.
140. Smith, M. A., Harris, P. L., Sayre, L. M., and Perry, G. (1997) Iron accumulation in alzheimer disease is a source of redox-generated free radicals. *Proceedings of the Nat. Acad. of Sci.s* 94, 9866–9868.
141. Miura, T., Suzuki, K., and Takeuchi, H. (2001) Binding of iron(iii) to the single tyrosine residue of amyloid β -peptide probed by Raman spectroscopy. *J. of Mol. Structure* 598, 79–84.
142. Wilson, J. H., and Hunt, T. (2002) Molecular biology of the cell, 4th edition: A problems approach. Garland ScienceNew York.
143. Handing, K. B., Niedzialkowska, E., Shabalin, I. G., Kuhn, M. L., Zheng, H., and Minor, W. (2018) Characterizing metal-binding sites in proteins with X-ray crystallography. *Nature Protocols* 13, 1062–1090.
144. Lin, Y., and Gross, M. L. (2022) Mass spectrometry-based structural proteomics for metal ion/protein binding studies. *Biomol.* 12, 135.

145. Riva, N., Gentile, F., Cerri, F., Gallia, F., Podini, P., Dina, G., Falzone, Y. M., Fazio, R., Lunetta, C., Calvo, A., Logroscino, G., Lauria, G., Corbo, M., Iannaccone, S., Chiò, A., Lazzerini, A., Nobile-Orazio, E., Filippi, M., and Quattrini, A. (2022) Phosphorylated TDP-43 aggregates in peripheral motor nerves of patients with amyotrophic lateral sclerosis. *Brain* 145, 276–284.
146. Giannini, M., Bayona-Feliu, A., Sproviero, D., Barroso, S. I., Cereda, C., and Aguilera, A. (2020) TDP-43 mutations link amyotrophic lateral sclerosis with R-loop homeostasis and R loop-mediated DNA damage. *PLOS Gen.* 16.

Appendices

Appendix 1. Other Significant Research Contributions

1. Martić, S., **Tabobondung, M.**, Gao, S., and Lewis, T. (2022) Emerging electrochemical tools for microplastics remediation and sensing. *Frontiers in Sensors*. 3, 23.

This review explored the current electrochemical based studies related to detection of microplastics. Although there are some fundamental studies which demonstrate the ability to monitor and remediate microplastic pollutants, more studies to address and remove the harmful pollutant from the environment are required. The electrochemical studies highlighted in the minireview demonstrate the power behind this method, and how they can be used for environmental sensing and removal of the pollutants.

My contributions to this project included additional experiments on every gelsolin peptide in the absence of inhibitors to satisfy the journal reviewer's revisions and suggestions. Here, the peptides (both mutants and non-mutants) were aged over the course of 7 days and ThT fluorescence, TEM, and turbidity results were used to characterize the peptide using additional methods not reported in the original manuscript. Additionally, select peptides were chosen for sonication experiments to determine if the aggregates could be broken down using sound waves. Finally, theoretical calculations on the pI, net charges, and hydrophobicity of each peptide were conducted using ThermoFisher's online Peptide Analyzing Tool. Writing of the manuscript and the Supplementary Information were also part of my contributions to the publication.

2. UNDER REVISION: Wallace W., **Tabobondung M.**, Espoto J., and Martic S. (2023) Antibody Based electrochemical Sensor for Detection of the Full-Length Phosphorylated TDP-43 Protein Biomarker of Amyotrophic Lateral Sclerosis. *Journal of The Electrochemical Society*. Manuscript ID: JES-109020.R1

This study explored the design and development of an electrochemical immunosensor. The fabricated immunosensor was designed to detection Transactive response DNA binding protein (TDP-43), a biomarker associated with amyotrophic lateral sclerosis (ALS). The diagnosis relies on the onset of symptoms. Hence, novel methods are needed for the early detection of TDP-43. Specifically, the sensor designed was tested to detection full-length phosphorylated TDP-43 (pTDP-43) using electrochemical impedance spectroscopy (EIS). The TDP-43 antibodies (Abs) on gold (Au) surfaces (Ab-Au) were employed as recognition probes for the protein detection. Detection of the protein was based on changes to the R_{ct} , which was calculated from the EIS measurements.

My contributions to this project included additional experiments on the surface characterization of the fabricated sensor. These surface characterization methods included contact angle, ellipsometry, x-ray photoelectron spectroscopy, electrochemical impedance spectroscopy, and cyclic voltammetry. Writing of the manuscript and the Supplementary Information were also part of my contributions to the publication.

3. SUBMITTED: Mitti M., Dingman Peterson F., Camilus N., **Tabobondung M.**, Golec C., Macairan J-R., and Naccache R. (2023) Guanosine vs. Cu(II): Quenching of dual-fluorescent carbon dots. *Physical Chemistry Chemical Physics*. Manuscript ID: CP-ART-03-2023-001001.

My contributions to this project included additional experiments on the detection of guanosine using carbon dots in an electrochemical setting. Here, a classy carbon electrode was placed in a three-electrode cell, containing a Ag/AgCl reference and platinum wire counter electrode. The solution in the cell contained the carbon dots used in the rest of the studies throughout the manuscript. Electrochemical methods such as cyclic voltammetry was used for the detection. Providing this data in the Supplementary Information were also part of my contributions to the publication.

Appendix 2. Supplementary information (Chapter 2)

SUPPORTING INFORMATION

Electrochemical and surface analysis of Cu(II) and Zn(II) metal ions and TDP-43 protein interactions

Meaghan Tabobondung¹, Chloe Connelly³, Josephine Esposto¹, Dr. Iraklii Ebralidze⁴, and Dr. Colin G. Wu, ³Dr. Sanela Martić^{1,2*}

¹*Environmental and Life Sciences, Trent University, Peterborough, Ontario K9L 0G2, Canada*

²*Department of Forensic Science, Trent University, Peterborough, Ontario K9L 0G2, Canada*

³*Department of Chemistry, Oakland University, Rochester, Michigan 48309, USA*

⁴*Faculty of Science, University of Ontario Institute of Technology, Oshawa, Ontario L1H 7K4, Canada*

*Corresponding Author E-mail: sanelamartic@trentu.ca

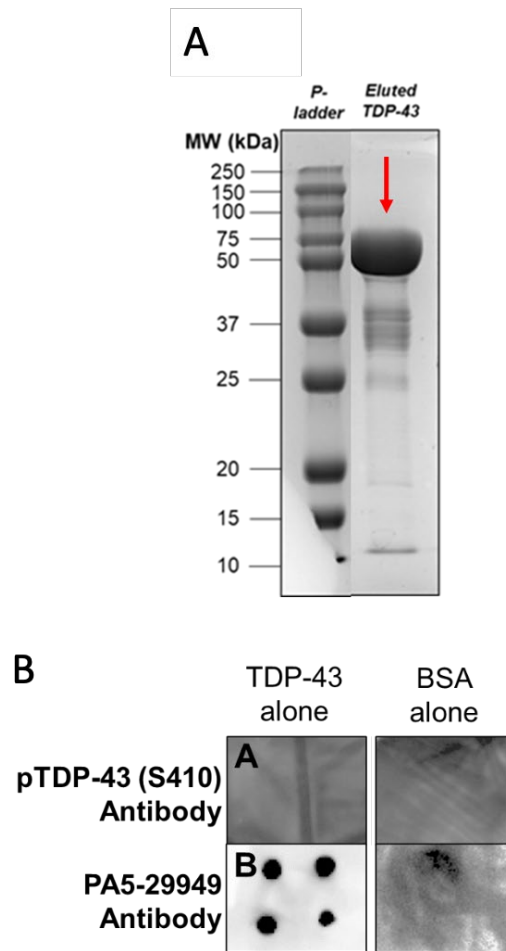


Figure S1. (A) SDS-PAGE of MBP-tagged, full-length TDP-43 protein. The single band at approximately 75-80 kDa (red arrow) indicates the protein is monomeric (~43 kDa), since the weight of the MBP-tag is ~42.5 kDa. The molecular weight marker (MW) was the Precision Plus Dual Colour from Bio-Rad; (B) Dot blots of TDP-43 stained with A) anti-pTDP-43 (pS410) antibody or B) PA5-29949 (residues 1-289) antibody ($[TDP-43]_{final} = 0.52 \mu M$).

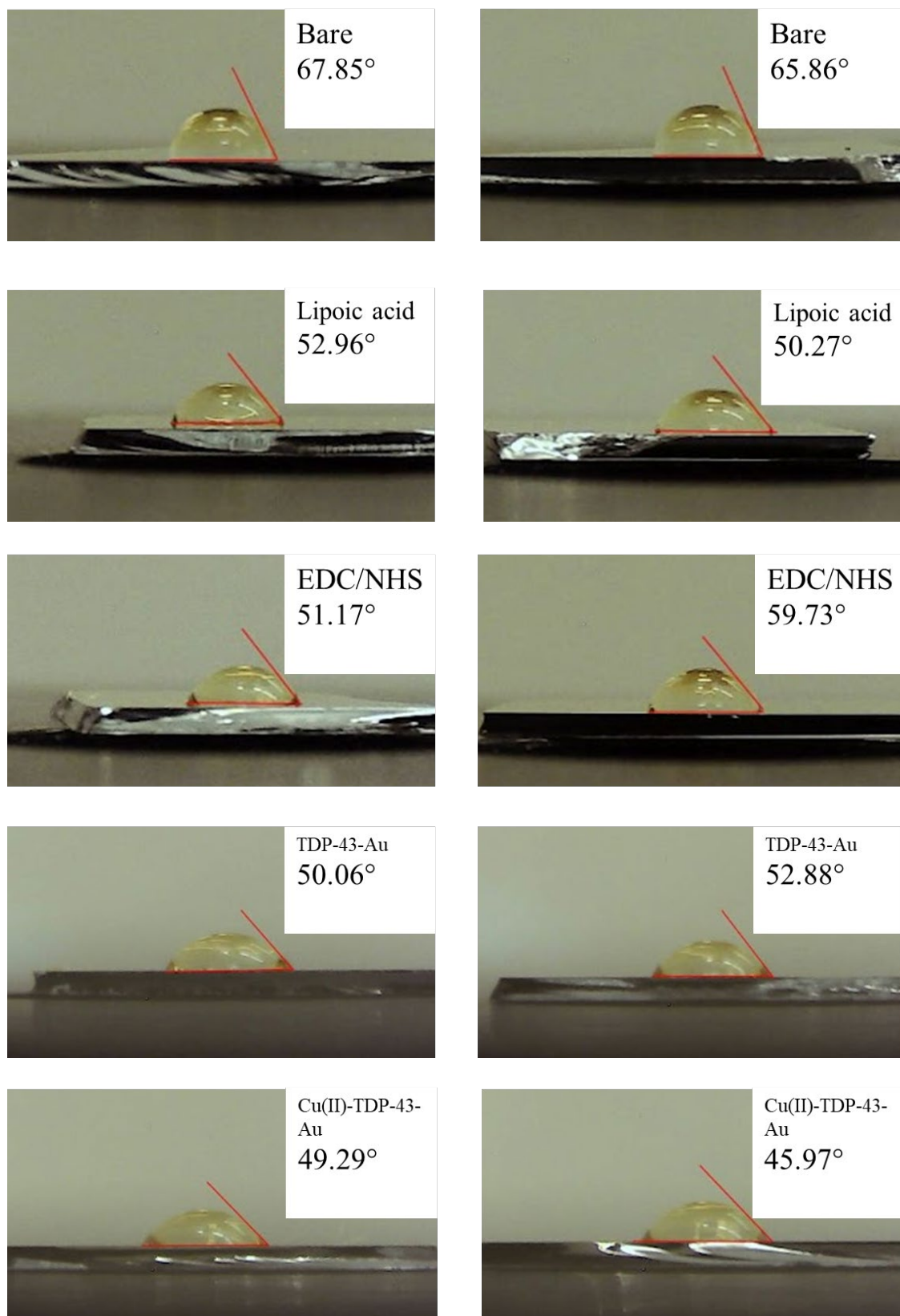


Figure S2: Contact angle (q) of various surface modification steps.

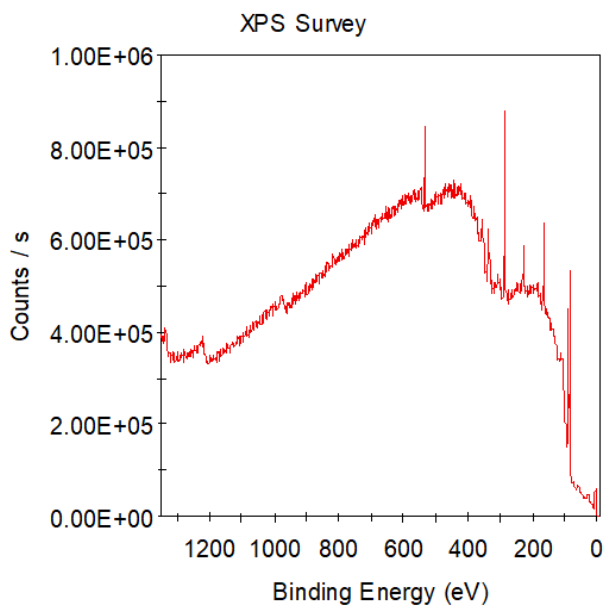


Figure S3: XPS spectra of lipioic acid monolayer

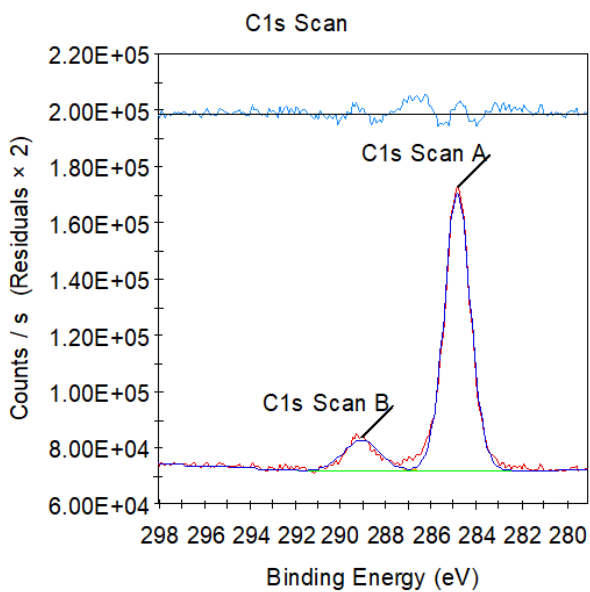


Figure S3: XPS C1s spectra of lipioic acid monolayer

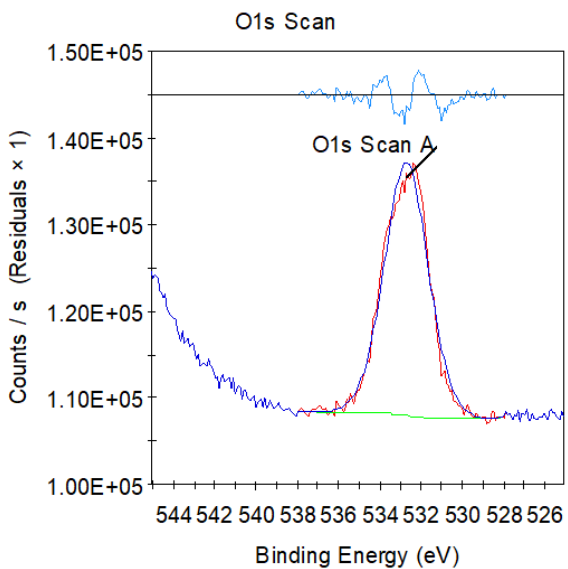


Figure S4: XPS O1s spectra of lipoic acid monolayer

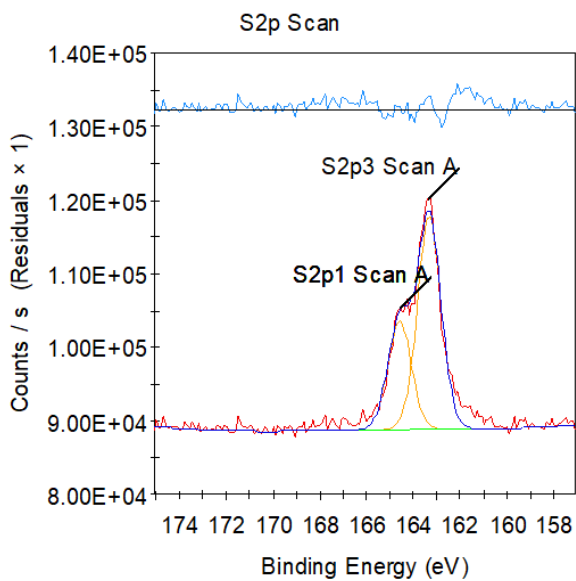


Figure S5: XPS S2p spectra of lipoic acid monolayer

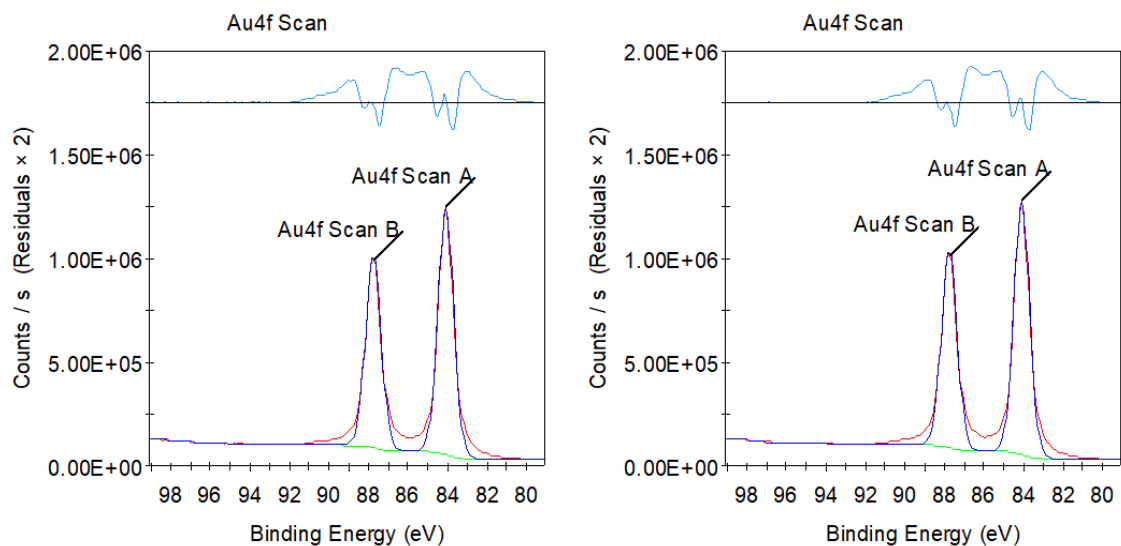


Figure S6: XPS Au 4f spectra of TDP-43-Au (N=2).

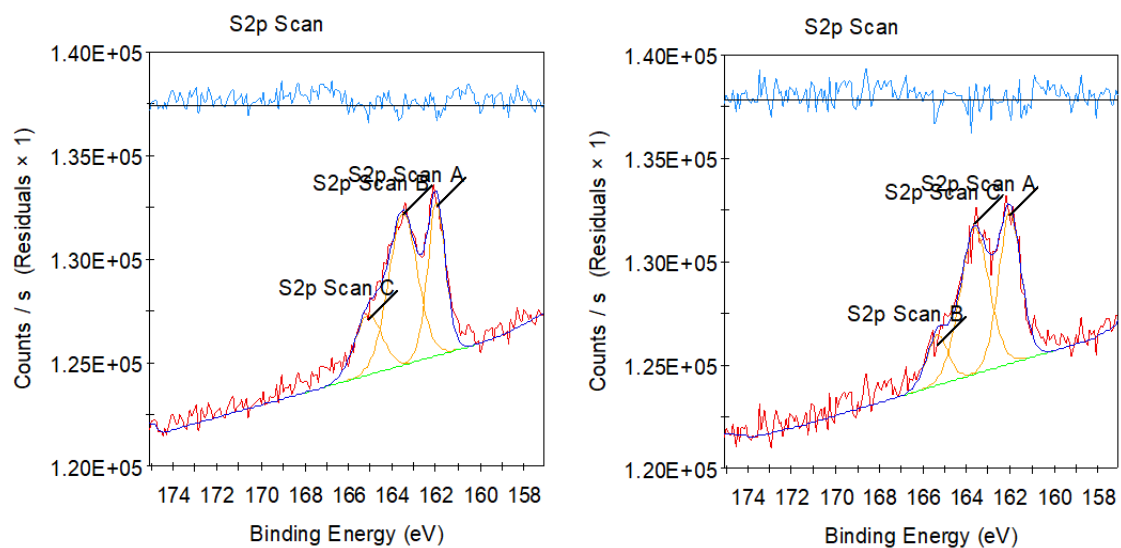


Figure S7: XPS S 2p spectra of TDP-43-Au (N=2).

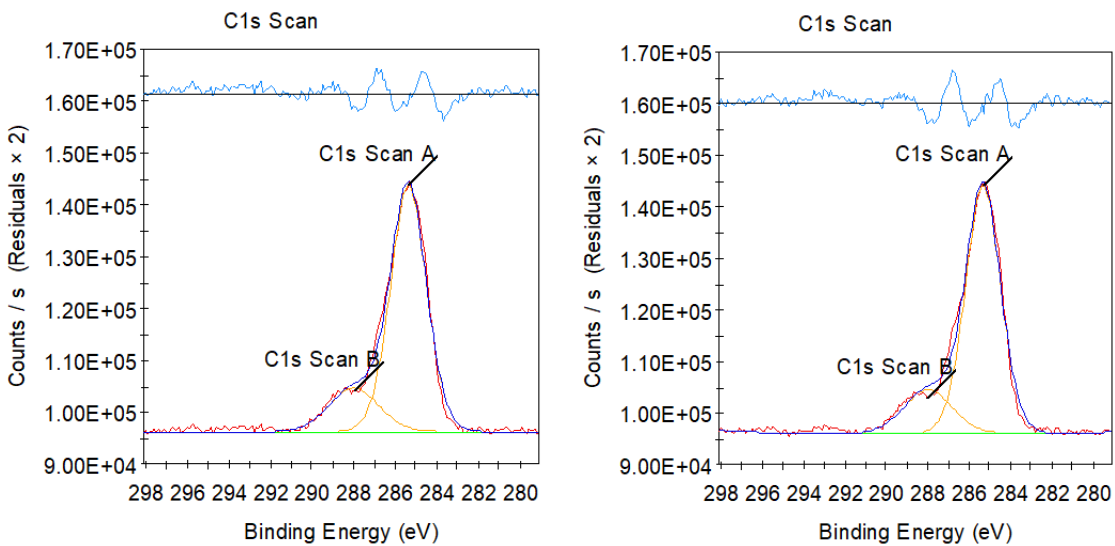


Figure S8: XPS C1s spectra of TDP-43-Au (N=2).

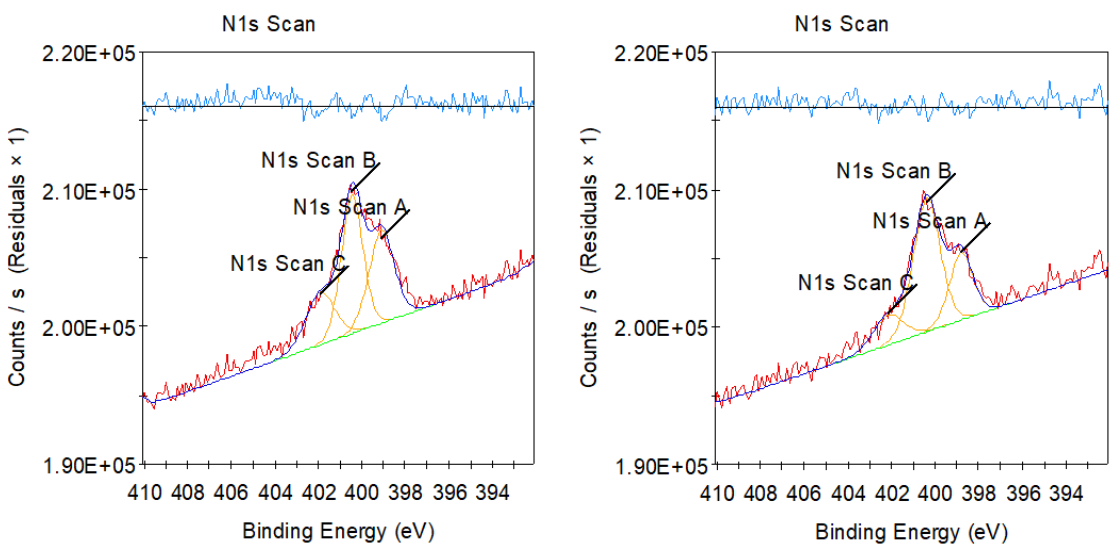


Figure S9: XPS N1s spectra of TDP-43-Au (N=2).

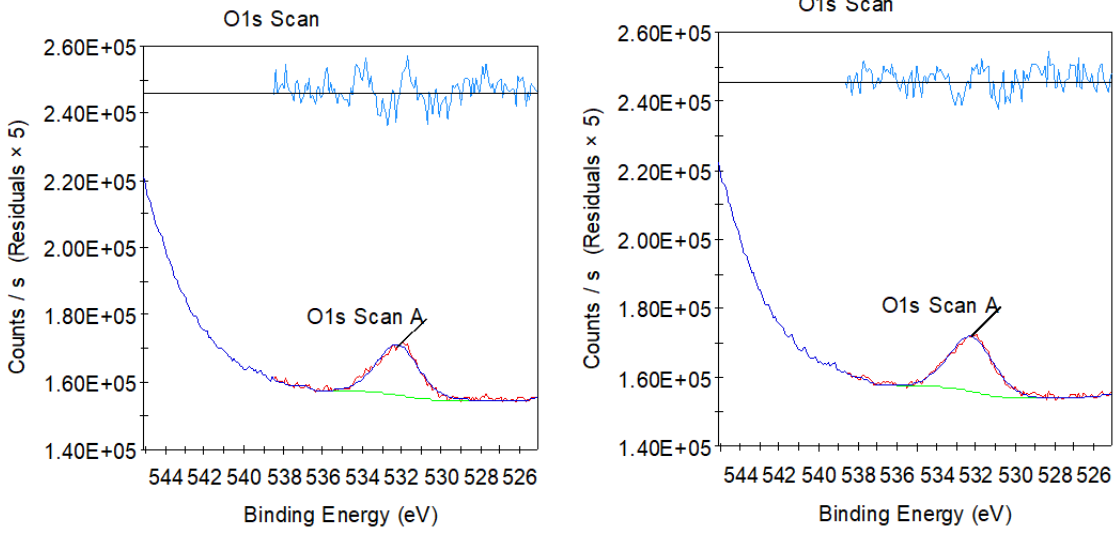


Figure S10: XPS O1s spectra of TDP-43-Au (N=2).

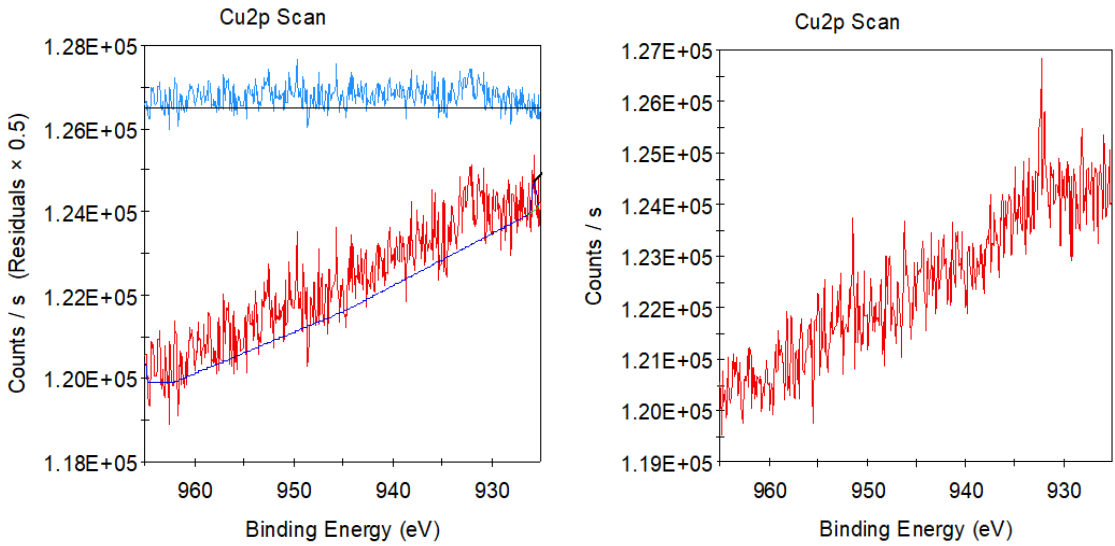
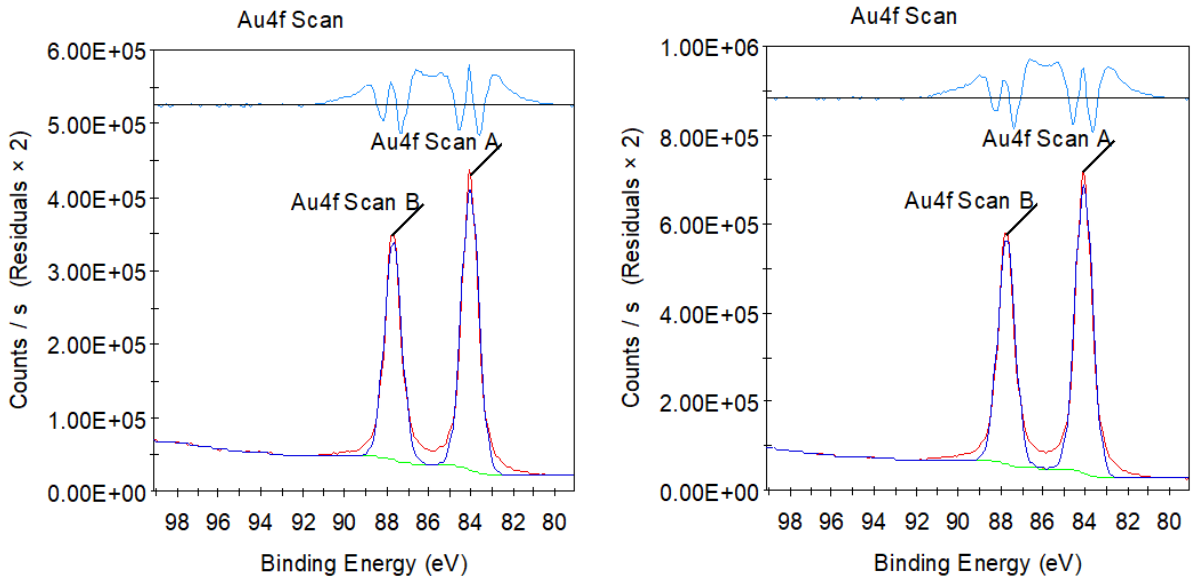


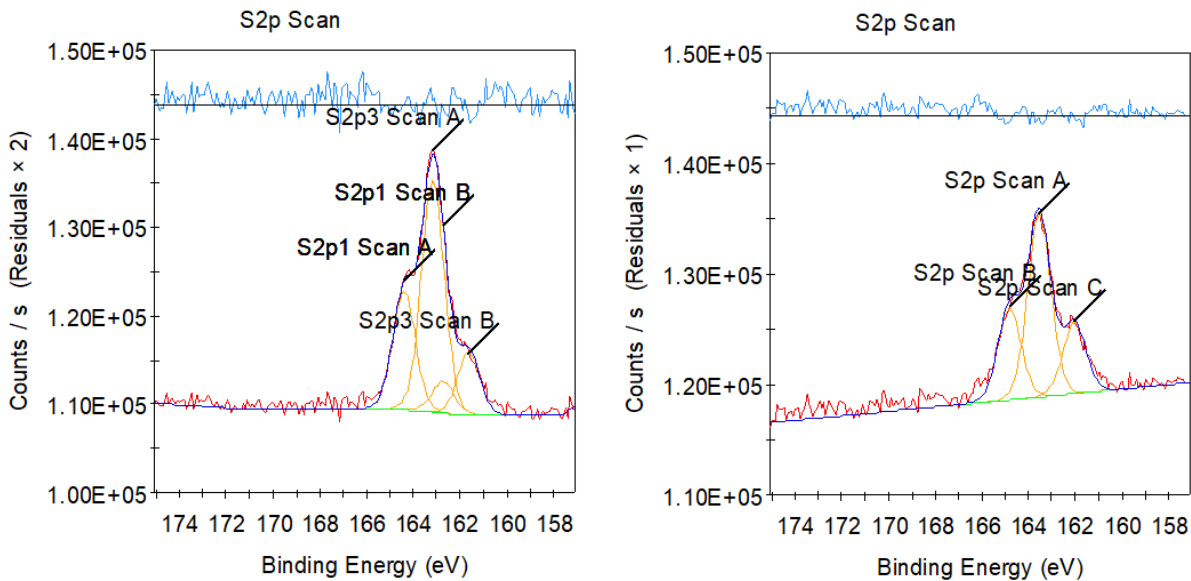
Figure S11: XPS Cu 2p spectra of TDP-43-Au film (N=2).

Figure S12: XPS spectra of TDP-43-Au film (N=2).

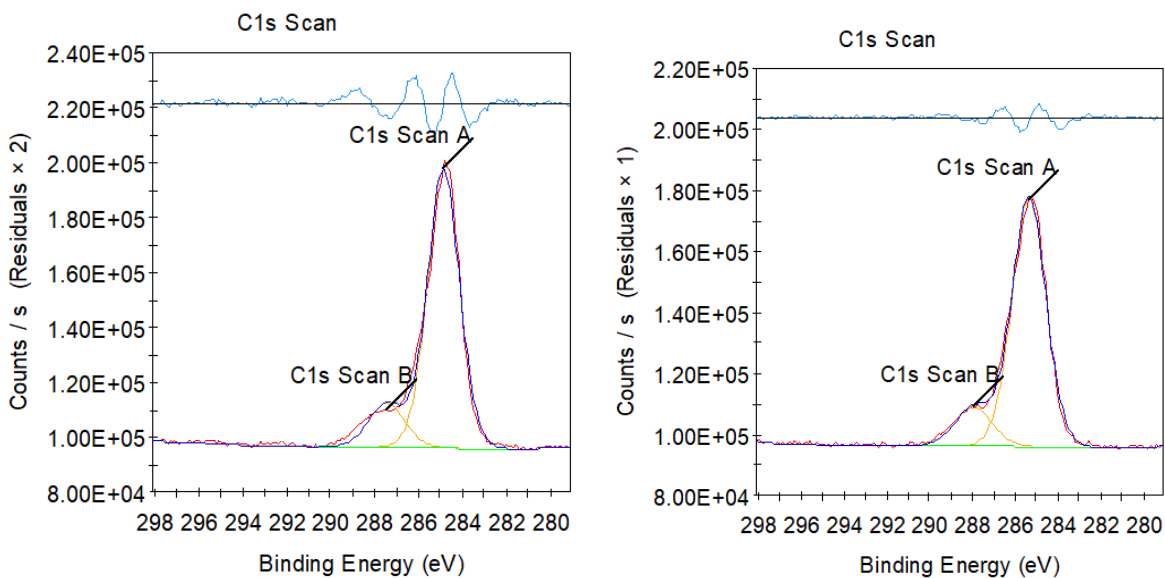
Figure S13: XPS spectra of Cu(II)-TDP-43-Au film (N=2).



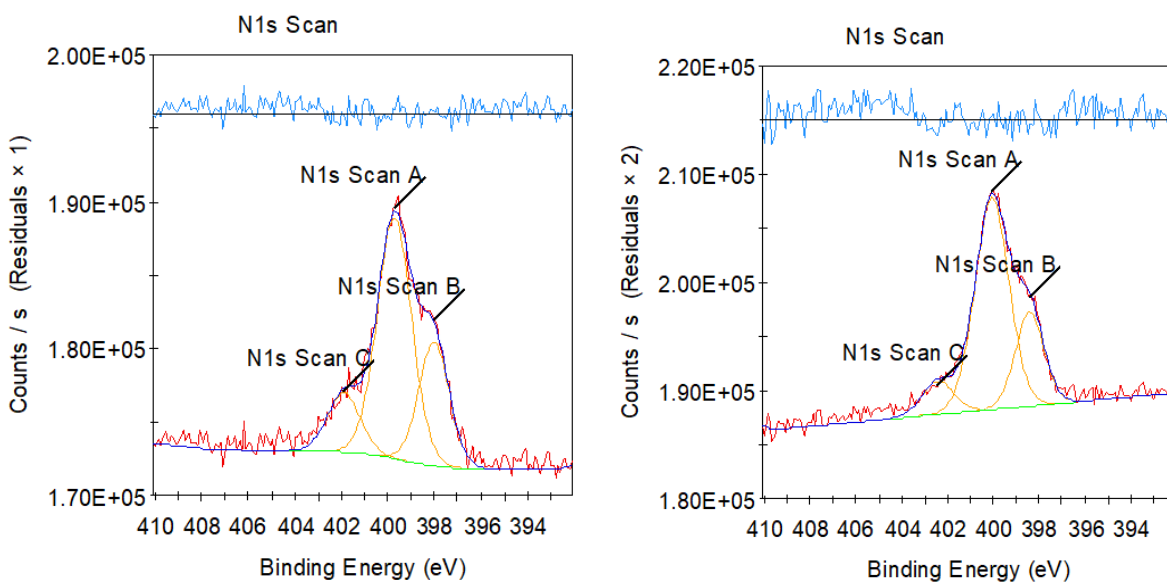
Figures S14. XPS Au 4f spectra of Cu(II)-TDP-43-Au film (N=2).



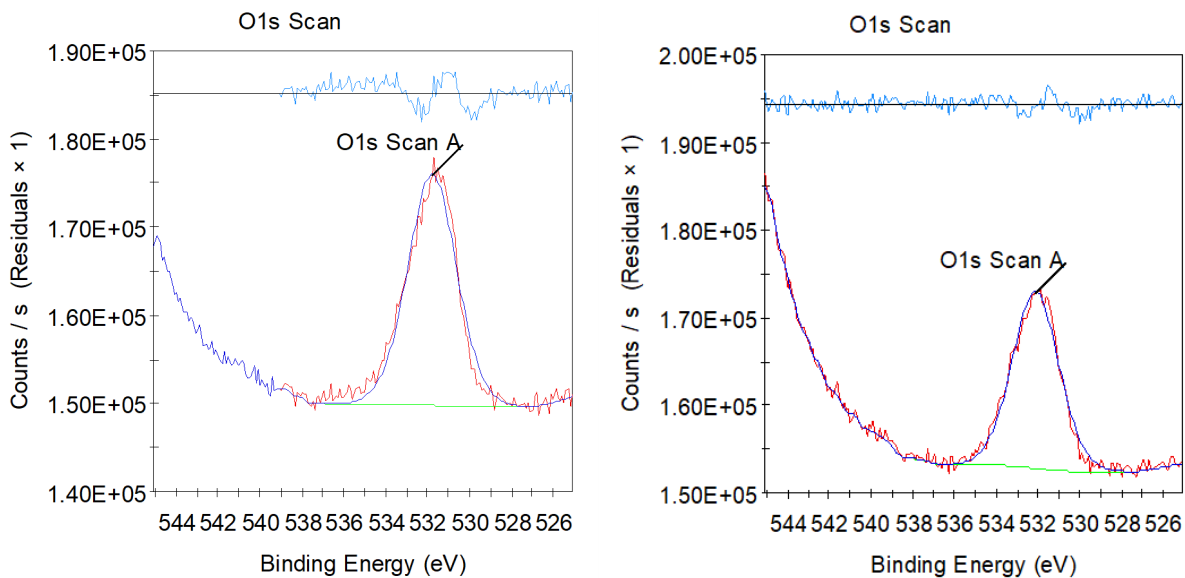
Figures S15. XPS S 2p spectra of Cu(II)-TDP-43-Au film (N=2).



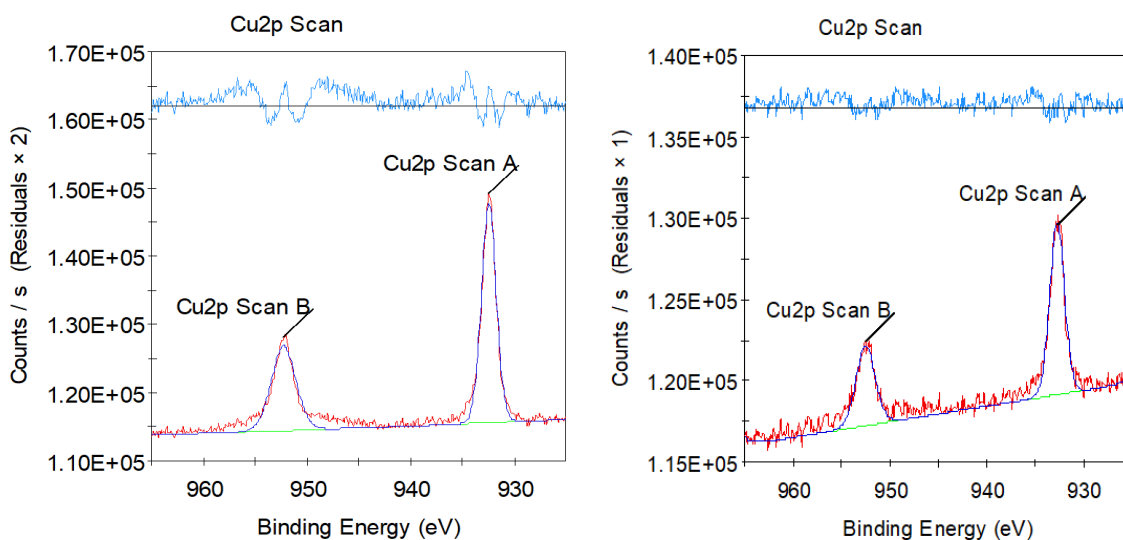
Figures S16. XPS C 1s spectra of Cu(II)-TDP-43-Au film (N=2).



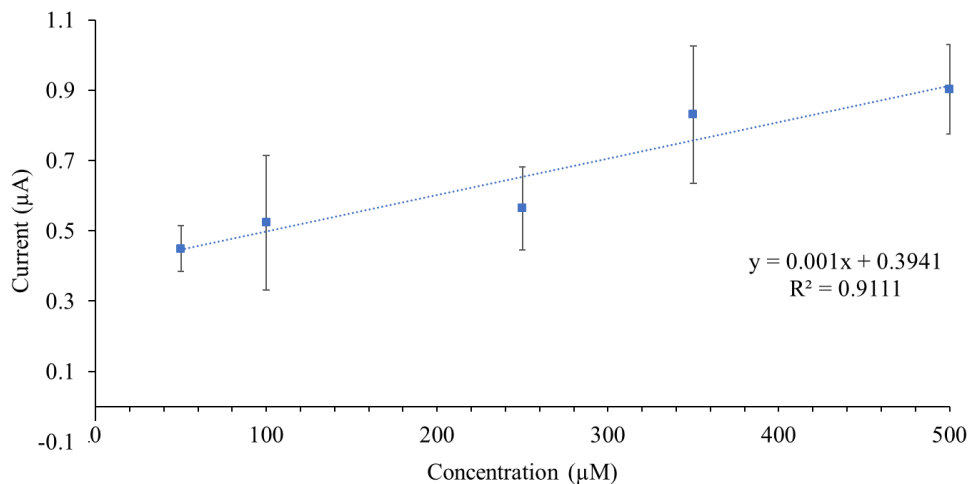
Figures S17. XPS N 1s spectra of Cu(II)-TDP-43-Au film (N=2).



Figures S18. XPS O 1s spectra of Cu(II)-TDP-43-Au film (N=2).



Figures S19. XPS Cu 2p spectra of Cu(II)-TDP-43-Au film (N=2).



Figures S20. Calibration curve of electrochemical peak signal for various concentrations of Cu(II) exposed to TDP-43 (n=3).

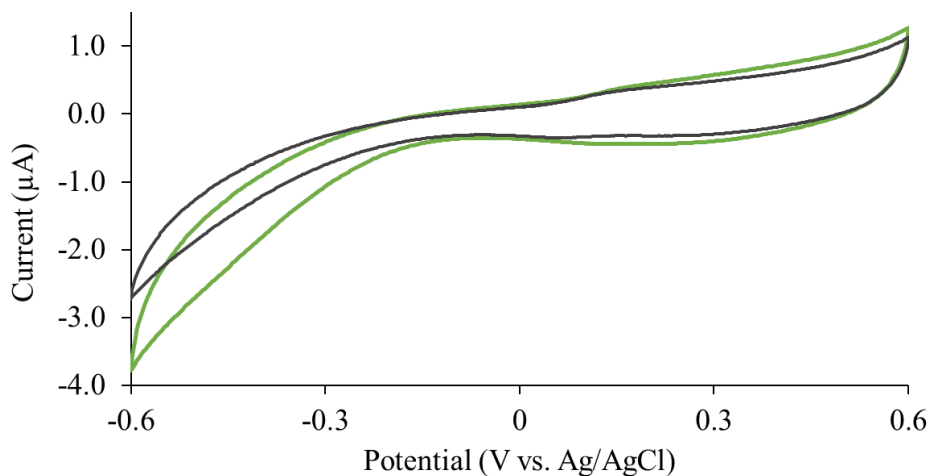


Figure S21: CV of TDP-43-Au film before (black line) and after (green line) 2 mM Zn(II) binding.

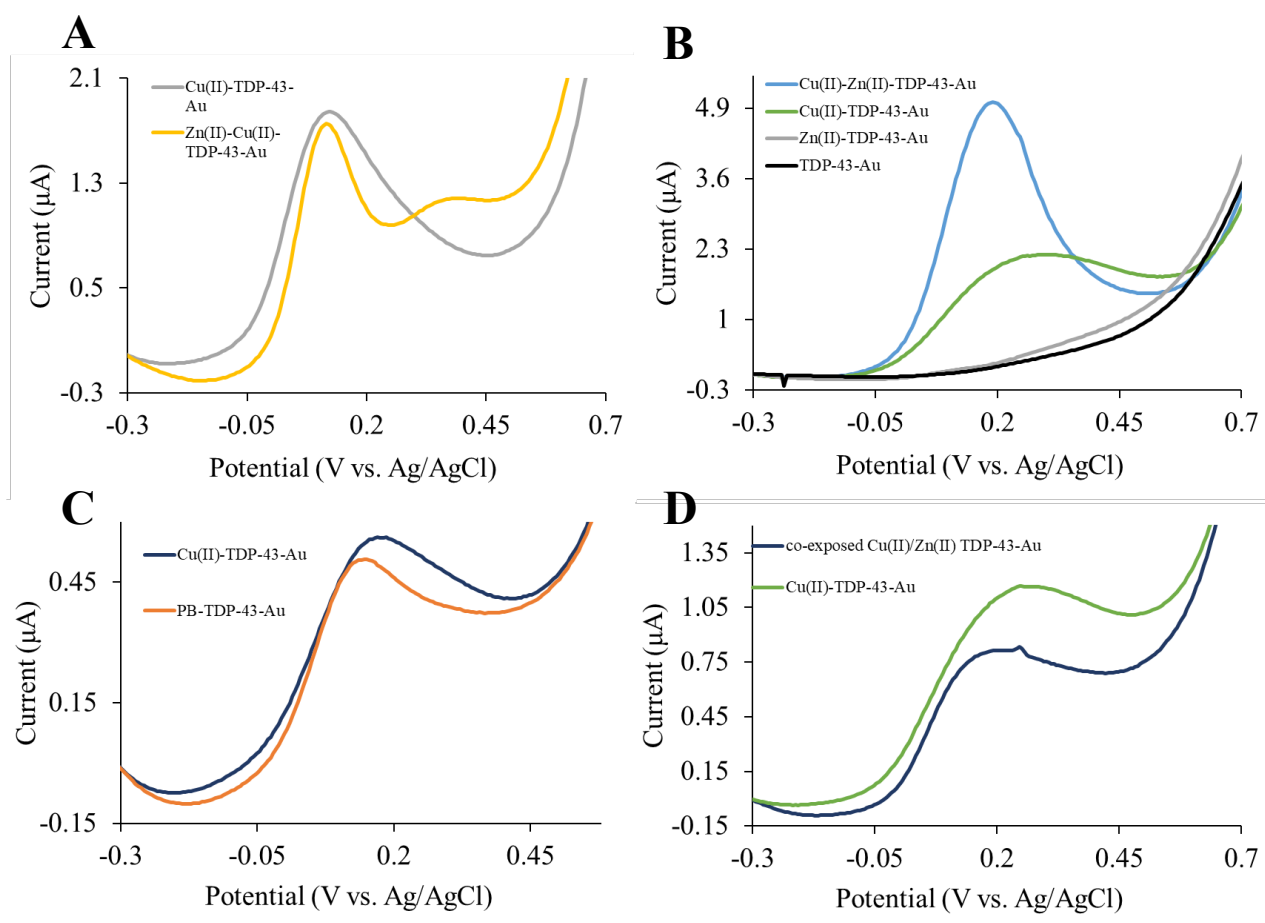


Figure S22: A) Representative SWV measurements of 350 μM Cu(II)-TDP-43-Au (grey) and 2 mM Zn(II) exposure to Cu(II)-TDP-43-Au (yellow). B) Representative SWV measurements of 350 μM Cu(II)-TDP-43-Au (blue) and 350 μM Cu(II) exposure to Zn(II)-TDP-43-Au (green). C) Representative SWV measurements of 350 μM Cu(II)-TDP-43-Au (blue) and PB incubation to Cu(II)-TDP-43-Au (orange). D) Representative SWV measurements of 350 μM Cu(II)-TDP-43-Au (green) and simultaneous 2 mM Zn(II) 350 μM Cu(II) exposure to TDP-43-Au (blue).

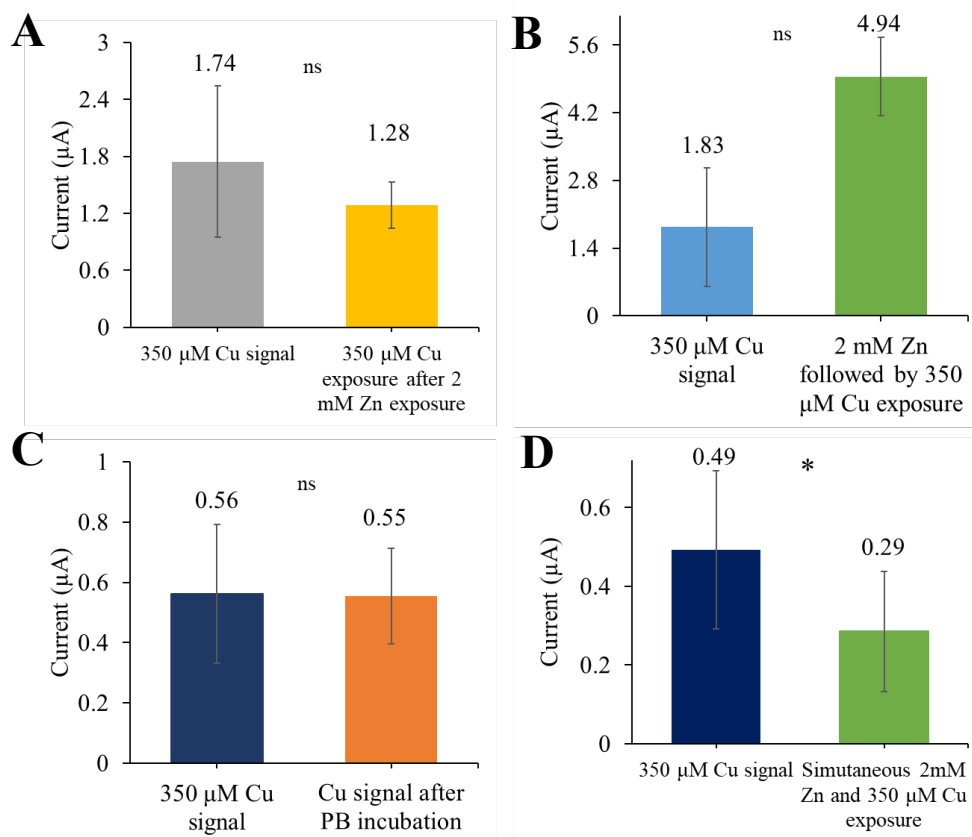
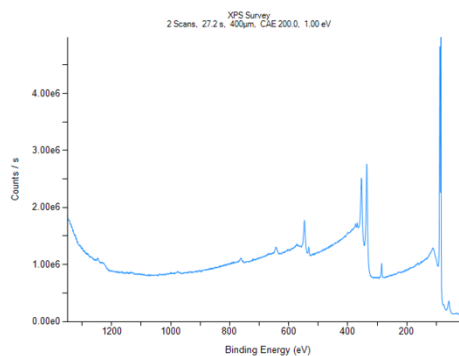
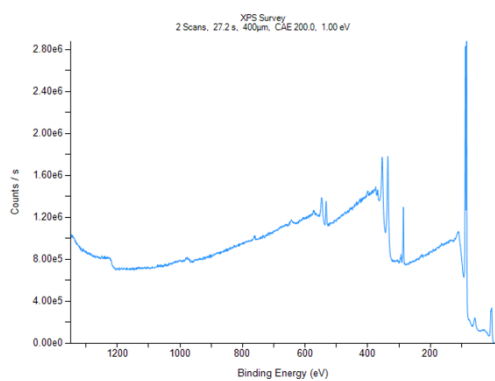
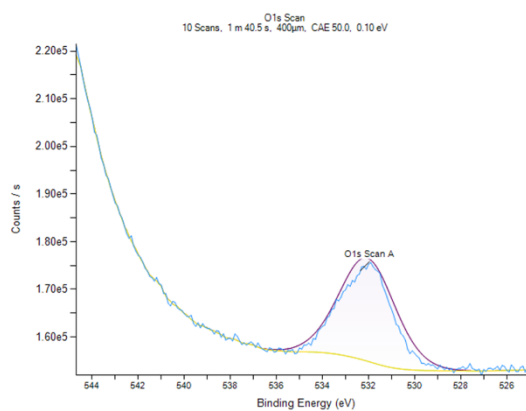
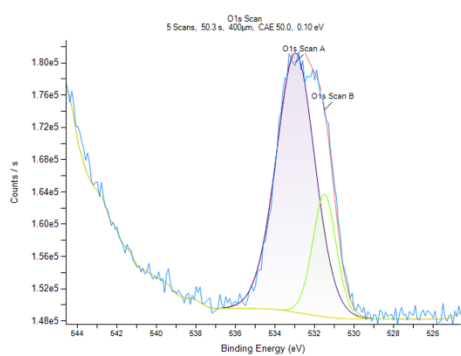


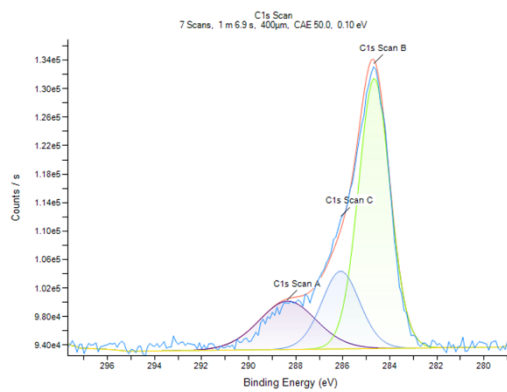
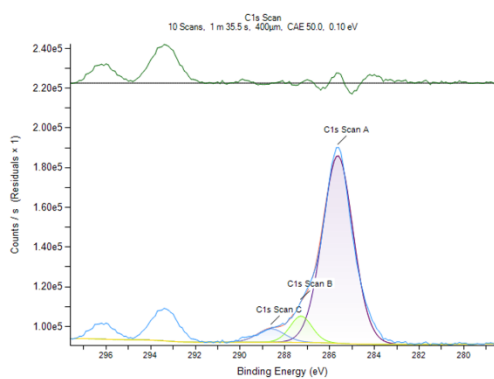
Figure S23: A) Plot of current for 350 µM Cu(II)-TDP-43-Au (grey) ($I = 1.74 \pm 0.80 \mu\text{A}$) and 2 mM Zn(II) exposure to Cu(II)-TDP-43-Au (yellow) ($I = 1.28 \pm 0.24 \mu\text{A}$). B) Plot of current for 350 µM Cu(II)-TDP-43-Au (blue) ($I = 1.83 \pm 1.22 \mu\text{A}$) and 350 µM Cu(II) exposure to Zn(II)-TDP-43-Au (green) ($I = 4.94 \pm 0.81 \mu\text{A}$). C) Plot of current for 350 µM Cu(II)-TDP-43-Au (blue) ($I = 0.56 \pm 0.23 \mu\text{A}$) and PB incubation to Cu(II)-TDP-43-Au (orange) ($I = 0.55 \pm 0.16 \mu\text{A}$). D) Plot of current for 350 µM Cu(II)-TDP-43-Au (green) ($I = 0.49 \pm 0.15 \mu\text{A}$) and simultaneous 2 mM Zn(II) 350 µM Cu(II) exposure to TDP-43-Au (blue) ($I = 0.29 \pm 0.20 \mu\text{A}$). Statistical test results in Table S9.



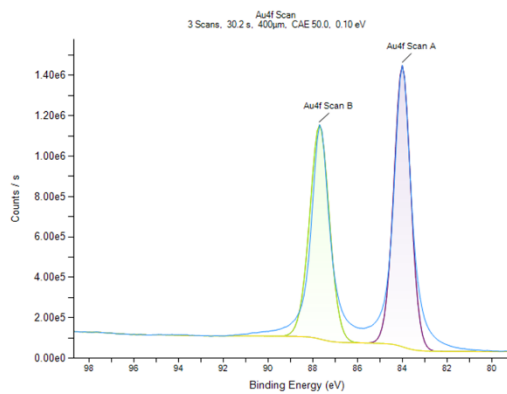
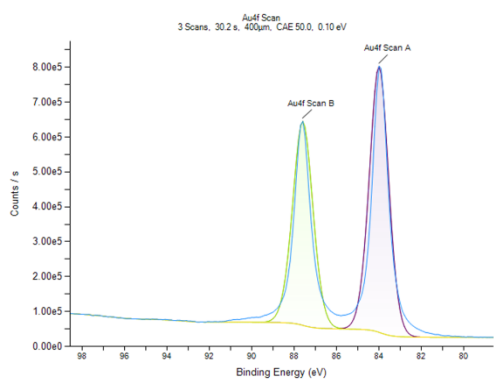
Figures S24. XPS spectra of Zn(II)-TDP-43-Au film (N=2)



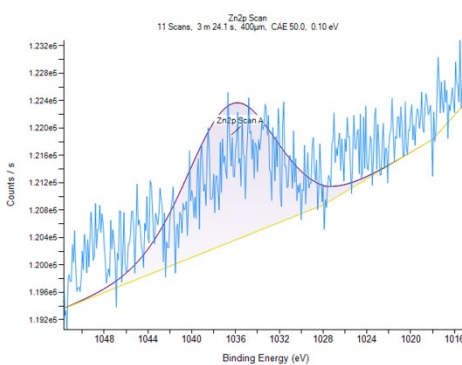
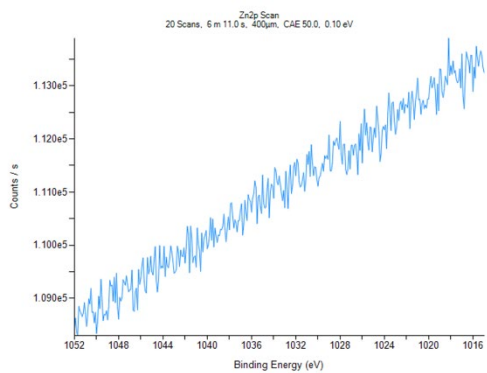
Figures S25. XPS O 1s spectra of Zn(II)-TDP-43-Au film (N=2)



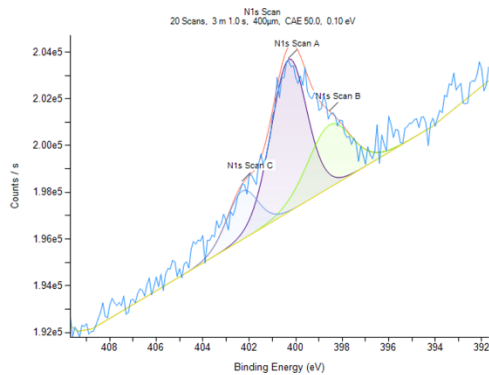
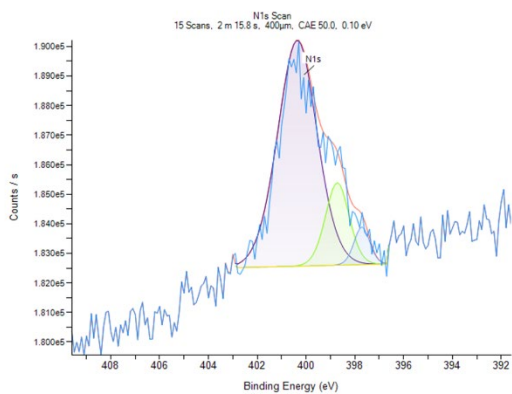
Figures S26. XPS C 1s spectra of Zn(II)-TDP-43-Au film (N=2)



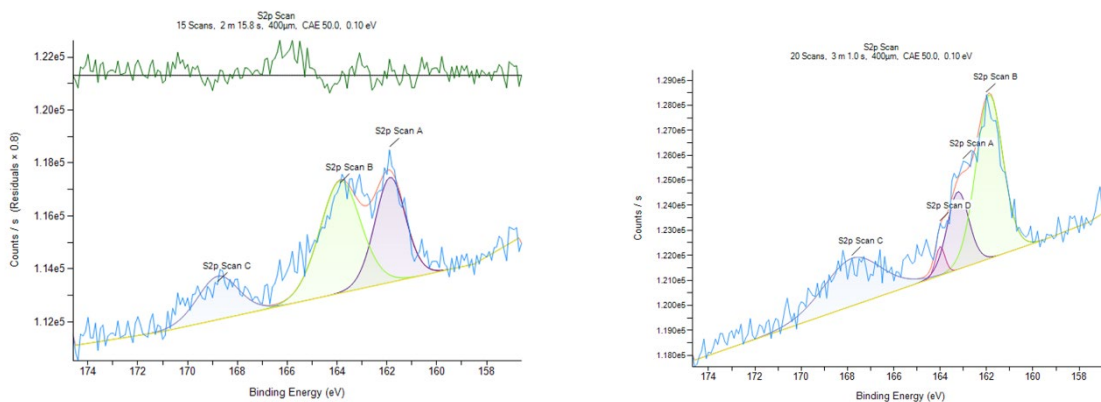
Figures S27. XPS Au4f spectra of Zn(II)-TDP-43-Au film (N=2)



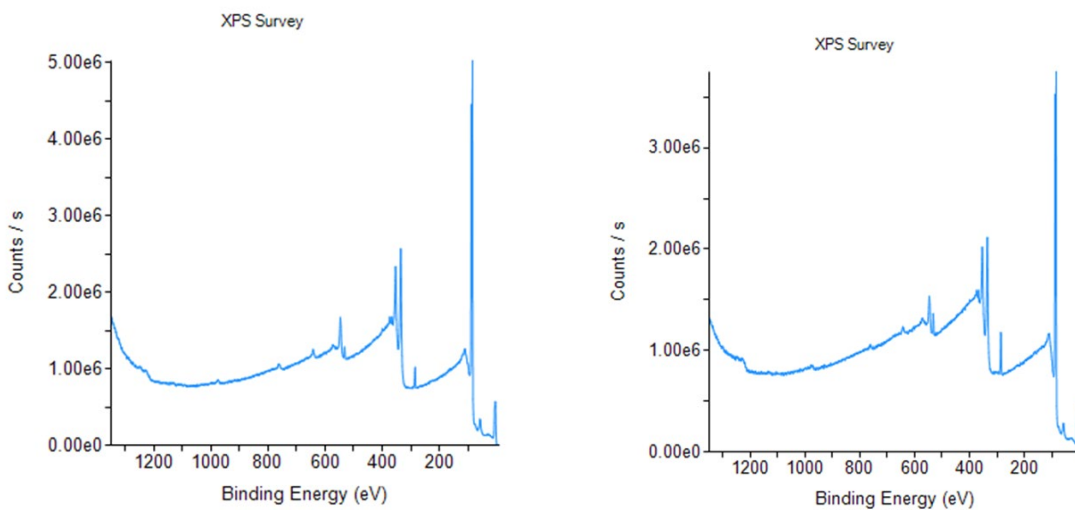
Figures S28. XPS Zn 2p spectra of Zn(II)-TDP-43-Au film (N=2)



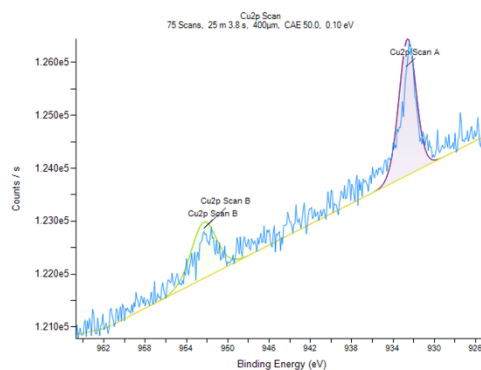
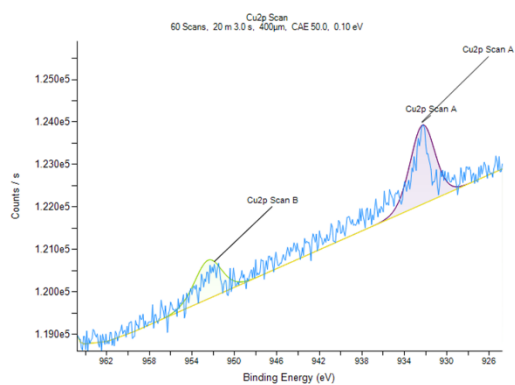
Figures S29. XPS N 1s spectra of Zn(II)-TDP-43-Au film (N=2)



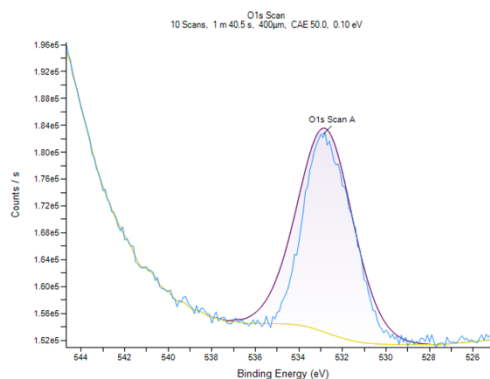
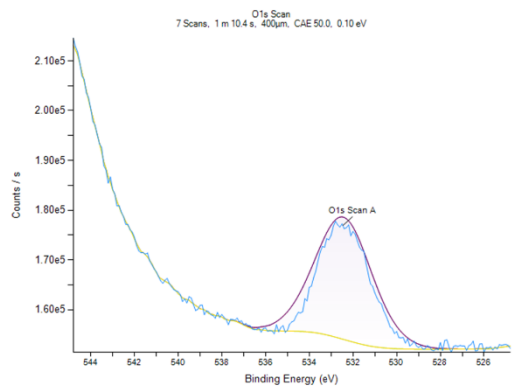
Figures S30. XPS S 1s spectra of Zn(II)-TDP-43-Au film (N=2)



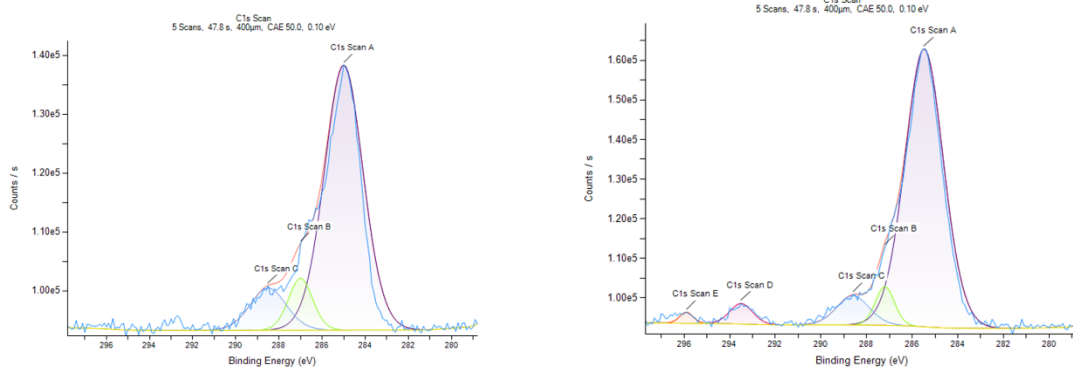
Figures S31. XPS spectra of Zn(II) exposed Cu(II)-TDP-43-Au film (N=2)



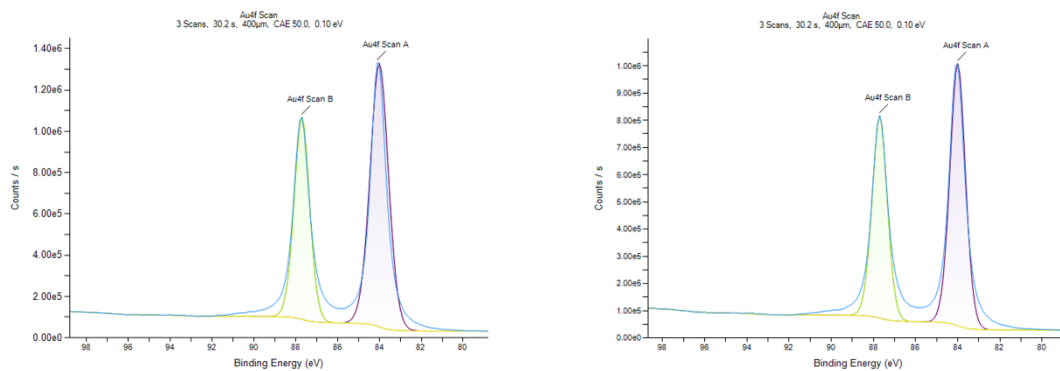
Figures S32. XPS Cu 2p spectra of Zn(II) exposed Cu(II)-TDP-43-Au film (N=2)



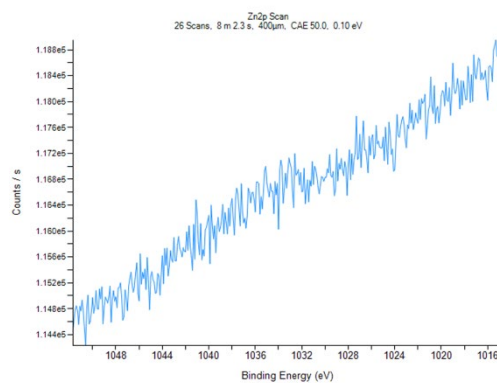
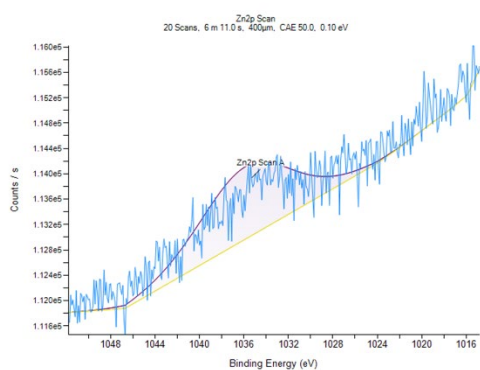
Figures S33. XPS O 1s spectra of Zn(II) exposed Cu(II)-TDP-43-Au film (N=2)



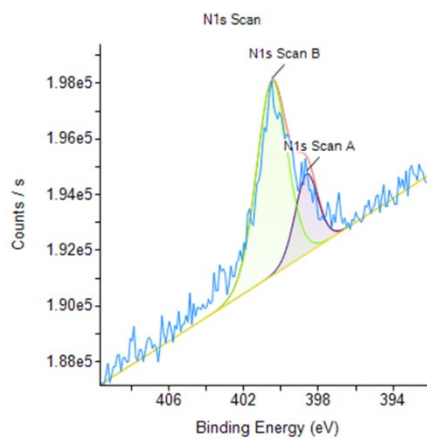
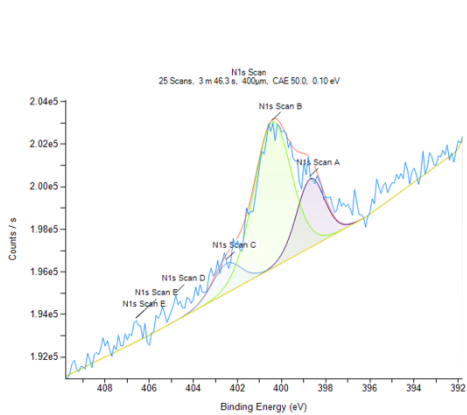
Figures S34. XPS C1s spectra of Zn(II) exposed Cu(II)-TDP-43-Au film (N=2)



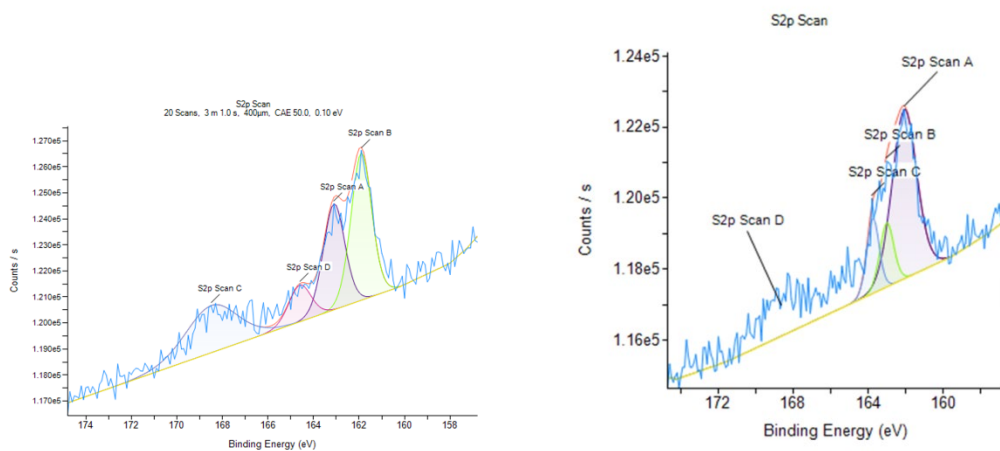
Figures S35. XPS Au4f spectra of Zn(II) exposed Cu(II)-TDP-43-Au film (N=2)



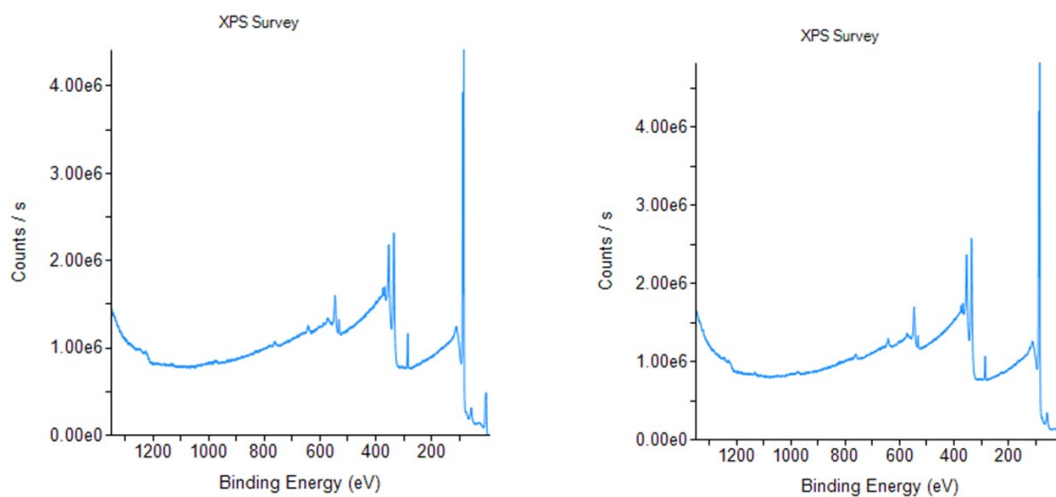
Figures S36. XPS Zn 2p spectra of Zn(II) exposed Cu(II)-TDP-43-Au film (N=2)



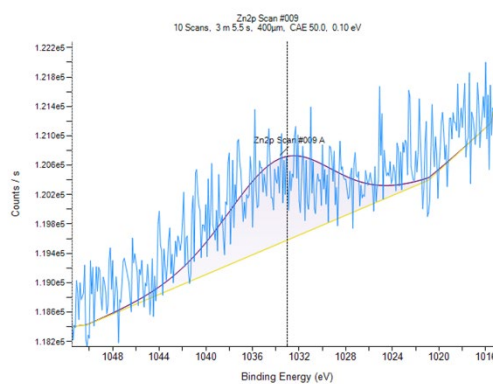
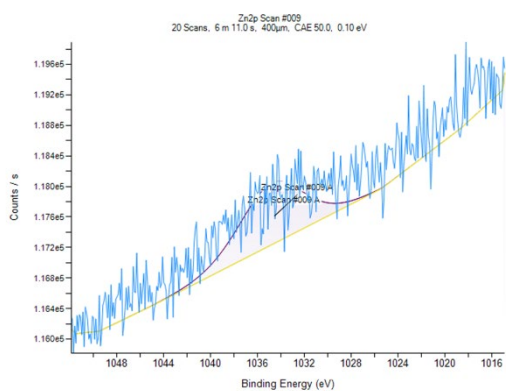
Figures S37. XPS N 1s spectra of Zn(II) exposed Cu(II)-TDP-43-Au film (N=2)



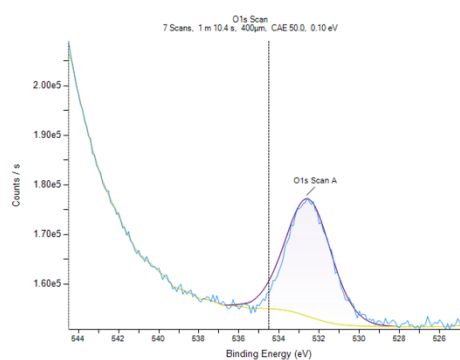
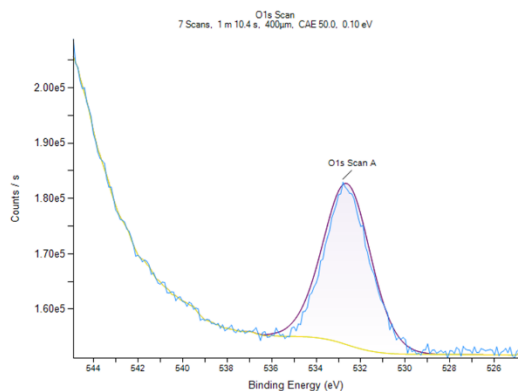
Figures S38. XPS S2p spectra of Zn(II) exposed Cu(II)-TDP-43-Au film (N=2)



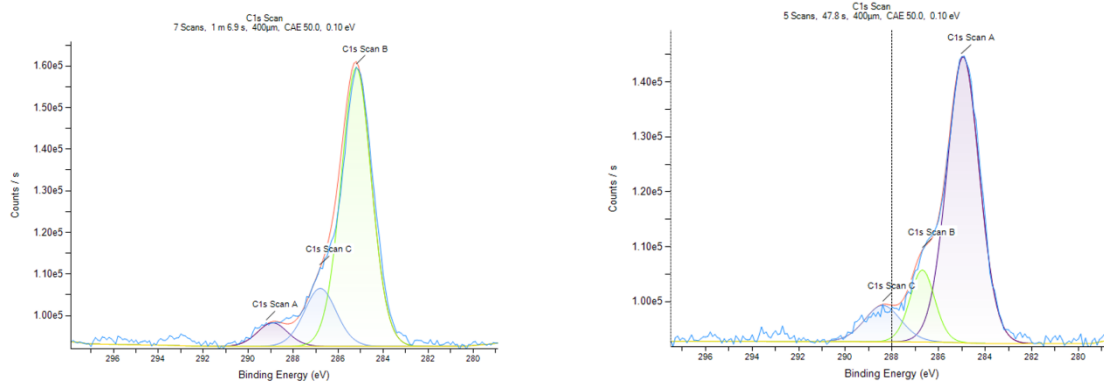
Figures S39. XPS spectra of Cu(II) exposed Zn(II)-TDP-43-Au film (N=2)



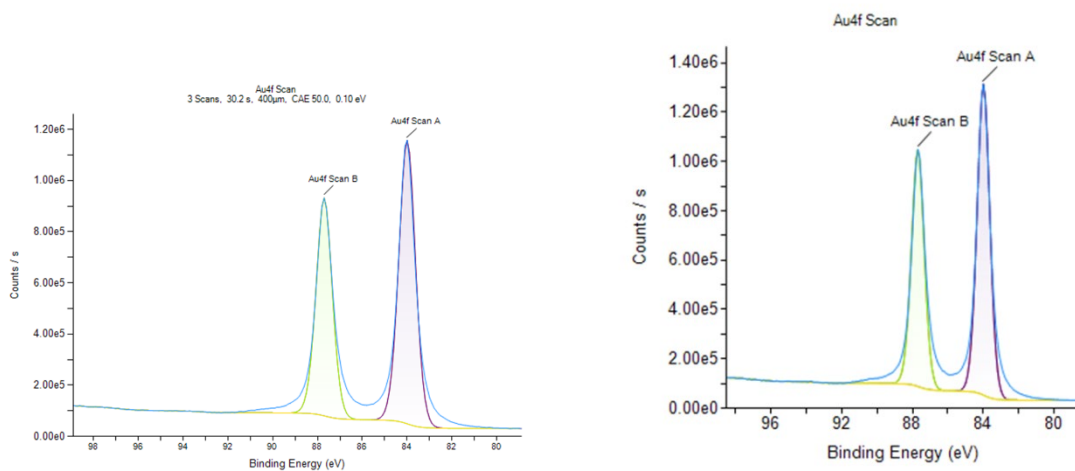
Figures S40. XPS Zn_{2p} spectra of Cu(II) exposed Zn(II)-TDP-43-Au film (N=2)



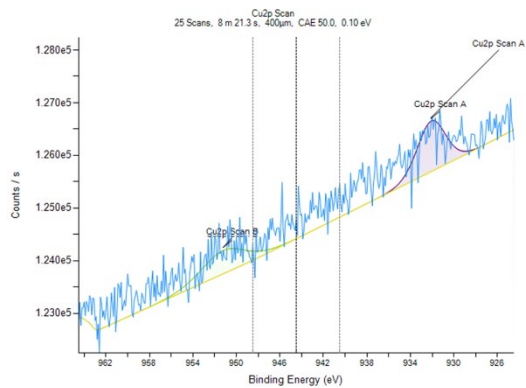
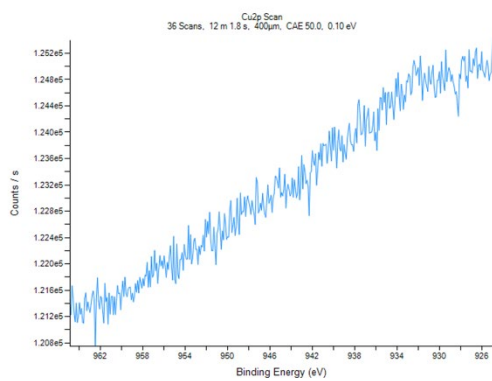
Figures S41. XPS O_{1s} spectra of Cu(II) exposed Zn(II)-TDP-43-Au film (N=2)



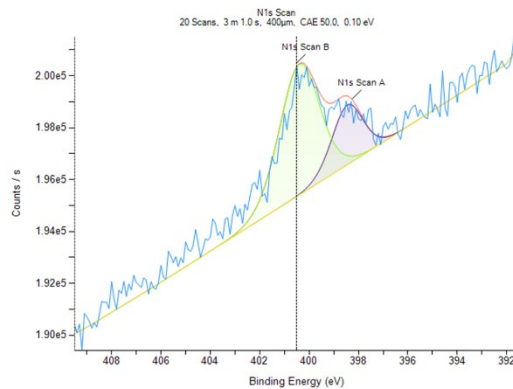
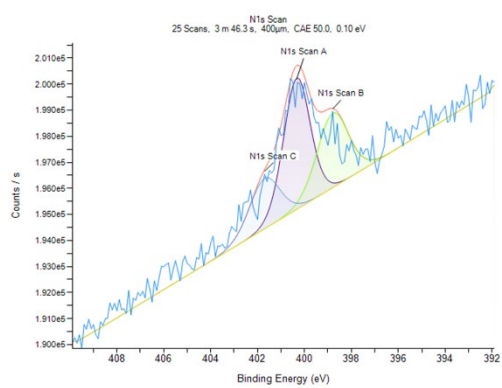
Figures S42. XPS C1s spectra of Cu(II) exposed Zn(II)-TDP-43-Au film (N=2)



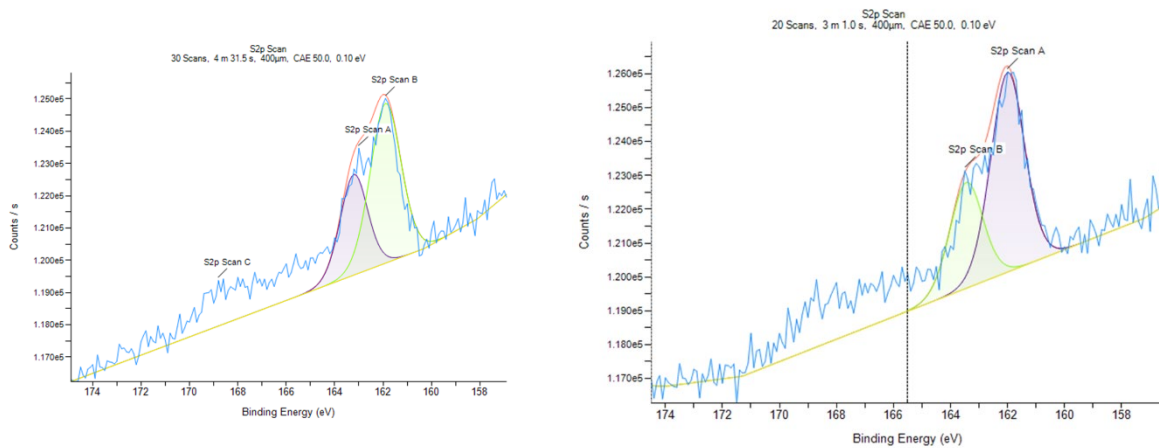
Figures S43. XPS Au4f spectra of Cu(II) exposed Zn(II)-TDP-43-Au film (N=2)



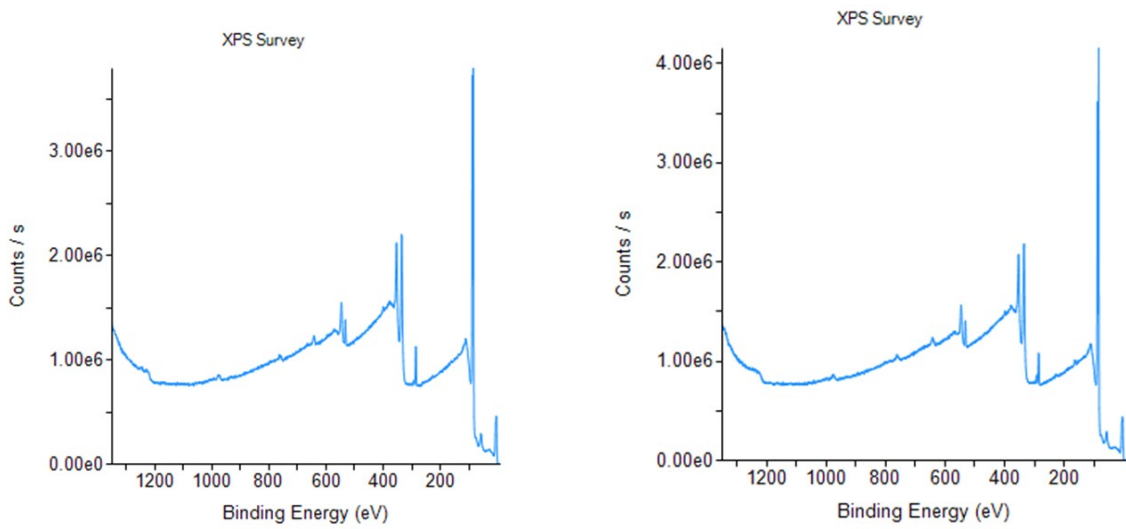
Figures S44. XPS Cu 2p spectra of Cu(II) exposed Zn(II)-TDP-43-Au film (N=2)



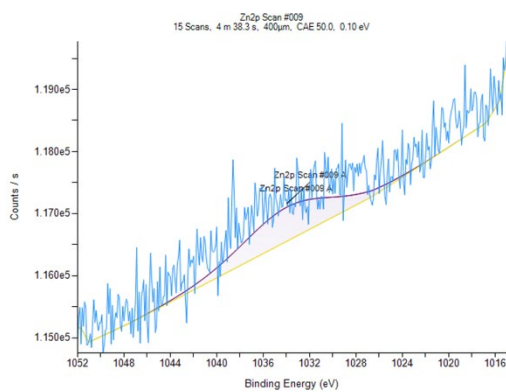
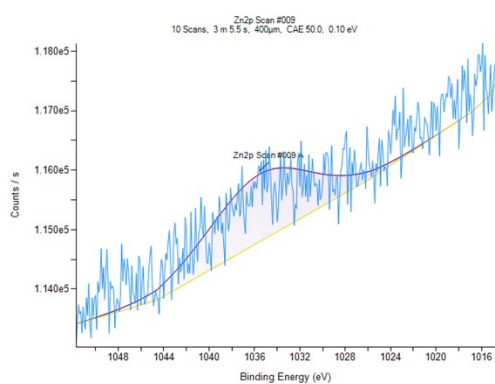
Figures S45. XPS N1s spectra of Cu(II) exposed Zn(II)-TDP-43-Au film (N=2)



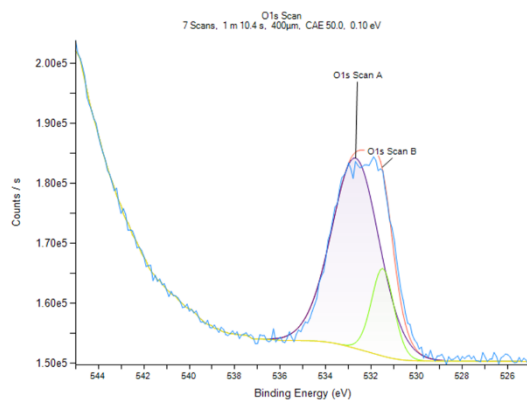
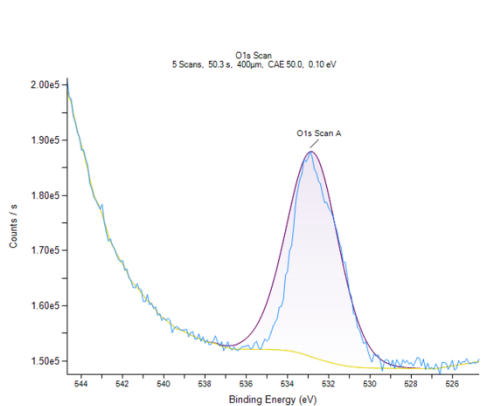
Figures S46. XPS S2p spectra of Cu(II) exposed Zn(II)-TDP-43-Au film (N=2)



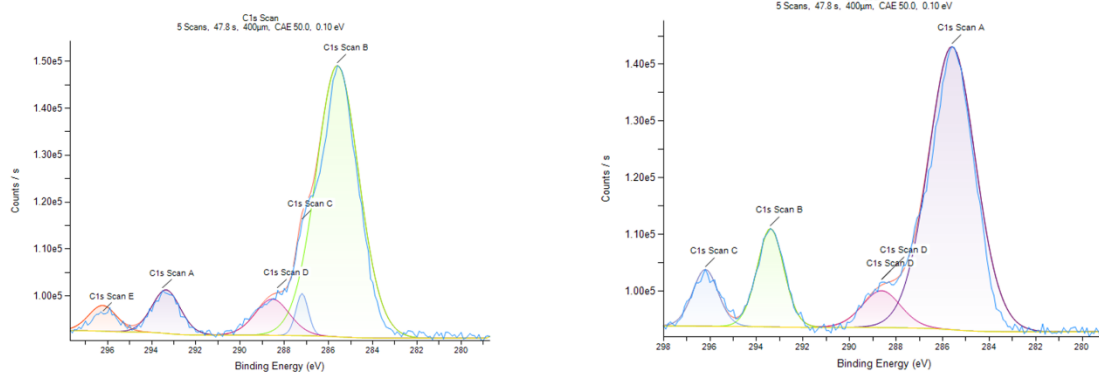
Figures S47. XPS spectra of simultaneous Cu(II) and Zn(II) exposure to TDP-43-Au film (N=2)



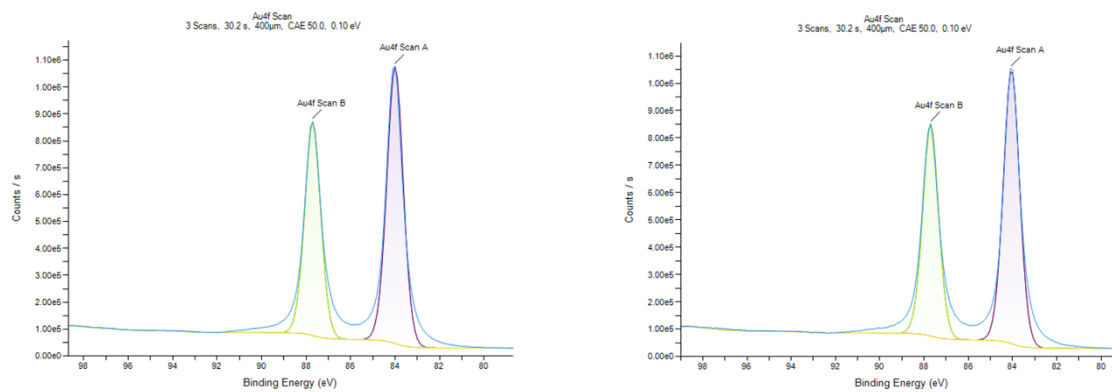
Figures S48. XPS Zn_{2p} spectra of simultaneous Cu(II) and Zn(II) exposure to TDP-43-Au film (N=2)



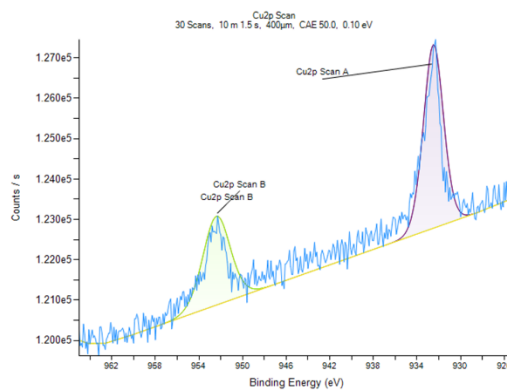
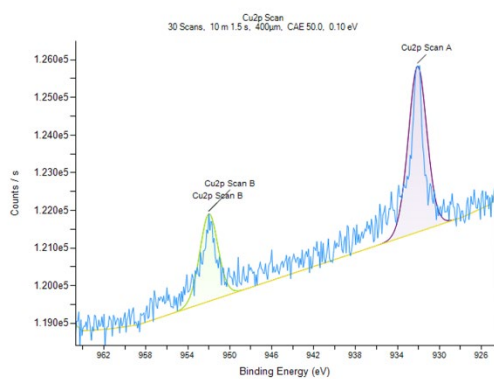
Figures S49. XPS O_{1s} spectra of simultaneous Cu(II) and Zn(II) exposure to TDP-43-Au film (N=2)



Figures S50. XPS C1s spectra of simultaneous Cu(II) and Zn(II) exposure to TDP-43-Au film (N=2)

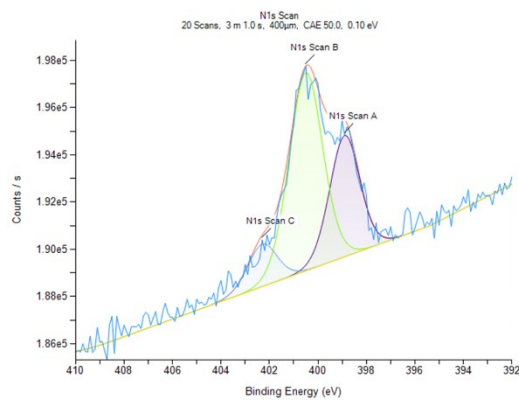
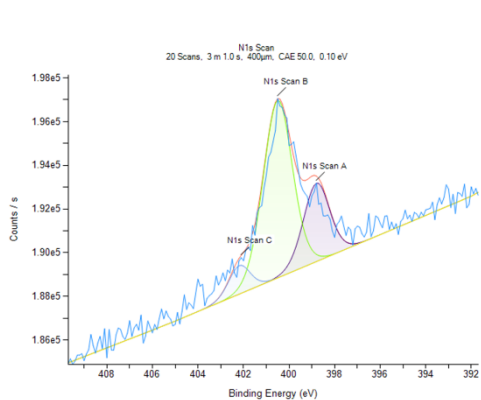


Figures S51. XPS Au4f spectra of simultaneous Cu(II) and Zn(II) exposure to TDP-43-Au film (N=2)



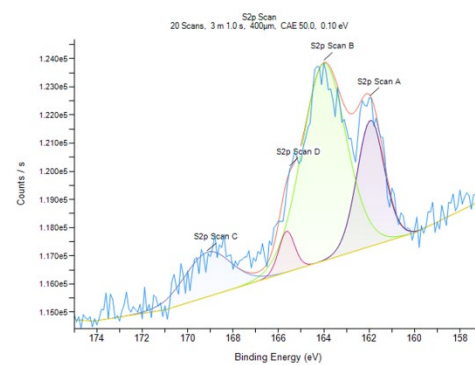
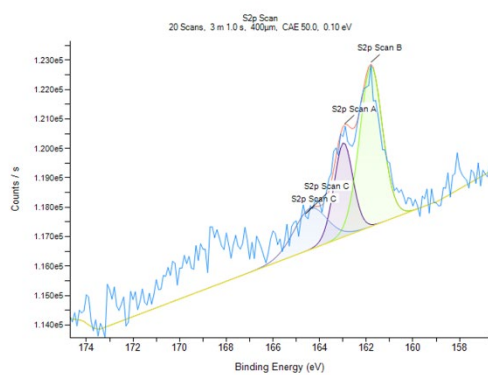
Figures S52. XPS Cu 2p spectra of simultaneous Cu(II) and Zn(II) exposure to TDP-43-Au film

(N=2)



Figures S53. XPS N1s spectra of simultaneous Cu(II) and Zn(II) exposure to TDP-43-Au film

(N=2)



Figures S54. XPS S2p spectra of simultaneous Cu(II) and Zn(II) exposure to TDP-43-Au film

(N=2)

Table S1. The peak potentials and peak separation for various surface modification steps in $[\text{Fe}(\text{CN})_6]^{3-/4}$.

Surface modification steps	E _{pc} (V)	E _{pa} (V)	ΔE (V)
Bare	0.245361	0.079346	0.166016
Lipoic acid	0.255127	0.062256	0.192871
EDC/NHS	0.299072	0.096436	0.185577
TDP-43	0.26001	0.096436	0.163574
1-butylamine	0.41626	-0.01587	0.432129
hexanethiol	0.313721	0.047607	0.266113

Table S2. The peak potentials and peak separation for various surface modification steps in $[\text{Fe}(\text{CN})_6]^{3-/4}$.

Surface modification steps	I _{pc} (mA)	I _{pa} (mA)
Bare	0.095306	-0.08838
Lipoic acid	0.08374	-0.07672
EDC/NHS	0.082672	-0.10291
TDP-43	0.082947	-0.09802
1-butylamine	0.064606	-0.07584
hexanethiol	0.079254	-0.09

Table S3. Circuit fit parameters for various stepwise surface characterization steps.

Parameters	Au	Lip	EDC/NHS	TDP-43	1BA	Hex	Units
R_s	2.81E+02	3.22E+02	2.43E+02	2.76E+02	3.44E+02	2.31E+02	Ohm
R_{ct}	1.49E+02	1.87E+03	4.78E+02	2.02E+02	2.81E+04	1.09E+03	Ohm
W	1.04E-03	1.54E-03	1.35E-03	1.40E-03		2.05E-03	$s^{(1/2)}/\text{Ohm}$
CPE	3.45E-06	5.07E-06	1.95E-06	1.10E-05	2.61E-05	6.50E-06	s^N/Ohm
N	8.79E-01	8.76E-01	8.57E-01	7.31E-01	9.03E-01	9.61E-01	

Table S4: Thickness of various surface modification steps determined using ellipsometry.

Surface modification step	Sample 1 (nm)	Sample 2 (nm)	Average (nm)	SD (\pm)
Bare Au	0	0.3	0.15	0.212
Lip-Au	3.41	2.57	2.99	0.5939
TDP-43-Au	2.82	3.29	3.055	0.3323
Cu(II)-TDP-43-Au	3.95	3.62	3.785	0.2333

Table S5: Contact angle (q) of various surface modification steps.

Surface modification step	Sample 1 ($^\circ$)	Sample 2 ($^\circ$)	Average ($^\circ$)	SD (\pm)
Bare	67.85	66.27	67.06	1.117229
Lipoic acid	52.96	50.27	51.615	1.902117
EDC/NHS	49.73	51.17	50.45	1.018234
TDP-43	50.06	52.88	51.47	1.99
Cu(II)	49.29	45.97	47.63	2.35

Table S6: X-ray photoelectron peak binding energy, CPS count, and spectroscopy atomic percentages for Lip-Au surface.

Name	Peak BE (eV)	Height CPS	Atomic %
C1s	284.83	98870.42	63.74
C=O	289.08	10971.73	9.85
O1s	532.7	29159.34	14.36
S2p _{3/2}	163.32	28937.83	12.05
S2p _{1/2}	164.59	14781.76	6.15

Table S7: X-ray photoelectron peak binding energy, CPS count, and spectroscopy atomic percentages for TDP-43-Au surface.

Name	Sample 1			Sample 2		
	Peak BE (eV)	Height CPS	Atomic %	Peak BE (eV)	Height CPS	Atomic %
Au4f _{7/2}	84.08	1185083.74	18.79	84.08	1220459.72	19.23
Au4f _{5/2}	87.75	920076.61	14.62	87.75	947259.87	14.96
S2p _{3/2}	163.52	7349.6	2.26	163.64	7065.99	2.16
	165.1	2922.91	0.84	165.34	2403.18	0.55
S2p _{1/2}	161.98	7373.97	1.42	162.03	7300.42	1.74
C1s	285.35	47558.05	39.13	285.31	48213.7	38.76
C=O	287.98	8476.42	9.6	287.98	8626.98	9.38
N1s	399.09	6780.71	2.38	398.81	4941.81	1.6
	400.44	10192.96	3.07	400.39	9747.61	3.65
	401.91	3835.86	1.54	402.14	2193.44	0.93
O1s	532.18	15113.3	6.34	532.22	16001.12	7.02

Table S8: X-ray photoelectron peak binding energy, CPS count, and spectroscopy atomic percentages for Cu(II)-TDP-43-Au surface.

Name	Sample 1			Sample 2		
	Peak BE (eV)	Height CPS	Atomic %	Peak BE (eV)	Height CPS	Atomic %
Au4f _{7/2}	84.03	382113.74	4.82	84.06	649753.59	8.88
Au4f _{5/2}	87.7	295338.1	3.74	87.73	503076.7	6.89
S2p _{3/2}	163.16	26113.29	6.75	163.54	16543.27	3.13
				164.82	8289.8	1.57
S2p _{1/2}	161.63	7044.45	1.77	162.04	6443.55	1.22
C1s	284.85	101467.22	53.22	285.34	82090.64	50.7
C=O	287.45	15901.68	9.4	287.94	12847.17	8.63
N1s	399.72	16422.7	5.58	400.07	19581.93	7.25
	398.02	8467.08	2.56	398.42	8665.06	2.71
	401.89	4073.7	1.32	402.42	3085.4	1.08
O1s	531.77	26193.49	9.04	532.11	20140.45	7.28
Cu2p _{3/2}	932.5	32127.48	1.09	932.74	10575.14	0.42
Cu2p _{1/2}	952.33	12438.67	0.72	952.58	4925.54	0.26

Table S9. Mean and standard deviation results for displacive and competitive Zn(II) and Cu(II) studies. T-test results were obtained by using an online statistical calculator GraphPad Prism 9 (<https://www.graphpad.com/quickcalcs/ttest1.cfm>).

	Average	SD	t-test results	Significance
350 μ M Cu exposure	0.56104	0.229922	t = 0.0405 df = 4	Not statistically significant (ns)
Phosphate buffer incubation and washing	0.554502	0.159195	standard error of difference = 0.161 P value = 0.9696	
350 μ M Cu exposure	1.744187	0.799227	t = 3.6701 df = 4	Statistically significant (*)
350 μ M Cu signal after 2 mM Zn exposure	1.283997	0.243907	standard error of difference = 0.847 P value = 0.0214	
350 μ M Cu signal	1.834354	1.221952	t = 0.9539 df = 4	Not statistically significant (ns)
2 mM Zn followed by 350 μ M Cu exposure	4.943983	0.812731	standard error of difference = 0.482 P value = 0.3942	
Simultaneous 2mM Zn and 350 μ M Cu exposure	0.285452	0.200377	t = 1.4221 df = 4	Not statistically significant (ns)
350 μ M Cu signal	0.492375	0.152843	standard error of difference = 0.146 P value = 0.2281	

Table S10: X-ray photoelectron spectroscopy peak binding energy and spectroscopy atomic percentages for Zn(II)-TDP-43-Au surface.

	Sample 1		Sample 2	
Name	Peak BE	Atomic %	Peak BE	Atomic %
S2p _{3/2}	163.88	1.42	163	0.49
			164	0.2
S2p _{1/2}	161.88	1	162	2.37
Contamination	168.79	0.55	167.8	1.13
C1s	285.64	53.46	284.67	24.29
	287.28	5.41	286.09	8.47
	288.62	3.46	288.35	7.95
N1s	400.05	3.83	400.3	3.11
	397.71		398.55	1.56
	398.72		402.3	0.57
O1s	532.96	10.71	532.37	10.5
	531.5	3.1		
Zn2p			1036.35	0.46
Au4f _{7/2}	84	9.75	84	20.59
Au4f _{5/2}	87.6	7.31	87.7	18.32

Table S11: X-ray photoelectron spectroscopy atomic percentages for Zn(II)-Cu(II)- TDP-43-Au surface, displacement.

	Sample 1		Sample 2	
Name	Peak BE (eV)	Atomic %	Peak BE (eV)	Atomic %
S2p _{3/2}	163.1	0.7	163.8	0.35
	164.6	0.18	163.8	0.35
S2p _{1/2}	161.9	1.07	162.07	0.78
Contamination	168.48	0.87	168.66	0.24
C1s	285	39.29	285.48	48.18
	287	2.39	287.2	3.35
	288.5	4.04	288.6	4.32
Contamination			293.5	2.13
			295.9	0.68
N1s	400.43	3.18	400.5	3
	398.7	1.12	398.64	0.37
	402.5	0.49		
Contamination	404.8	0.12		
	406.6	0.09		
O1s	532.44	16.51	532.89	14.75
Au4f _{7/2}	84.1	16.78	84	12.1
Au4f _{5/2}	87.7	12.91	87.7	9.15
Cu2p _{3/2}	932.31	0.05	932.74	0.25
Cu2p _{1/2}	951.9	0.02	952.33	0.04
Zn2p	1035.29	0.17		

Table S12: X-ray photoelectron spectroscopy atomic percentages for Cu(II)-Zn(II)- TDP-43-Au surface, displacement.

	Sample 1		Sample 2	
Name	Peak BE (eV)	Atomic %	Peak BE (eV)	Atomic %
S2p _{3/2}	163	0.76	163.5	0.47
S2p _{1/2}	161.9	1.11	162	1.52
C1s	285.2	43.76	285.01	36.15
	286.8	7.67	286.7	6.97
	289.2	3.72	288.4	5.15
Contamination	168.8	0.53		
N1s	400.33	1.5	400.5	2.41
	398.8	0.4	398.25	0.53
	401.7	0.79		
O1s	532.8	10.64	532.61	12.92
Au4f _{7/2}	84	16.59	84	16.59
Au4f _{5/2}	87.7	12.49	87.7	12.49
Cu2p _{3/2}			932.08	0.08
Cu2p _{1/2}			951.22	0.06
Zn2p	1034.54	0.05	1033.64	0.33

Table S13: X-ray photoelectron spectroscopy atomic percentages for co-mixed Cu(II) and Zn(II) with TDP-43-Au surface.

Name	Sample 1		Sample 2	
	Peak BE (eV)	Atomic %	Peak BE (eV)	Atomic %
S2p _{3/2}	162.9	0.45	163	0.3
	164.6	0.09	163.8	0.35
S2p _{1/2}	161.8	0.84	162.07	0.78
Contamination			168.66	0.24
C1s	285.6	41.97	285.6	41.97
	287.2	1.88	287.2	1.88
	288.3	2.82	288.3	2.82
Contamination	293.5	10.29	293.5	10.29
	296.2	0.49	296.2	0.49
N1s	402.1	0.18	400.5	3
	400.5	2.35	398.64	0.37
	398.8	0.99		
O1s	532.9	16.29	532.89	14.75
Au4f _{7/2}	84	11.93	84	12.1
Au4f _{5/2}	87.7	9	87.7	9.15
Cu2p _{3/2}	932.1	0.12	932.74	0.25
Cu2p _{1/2}	952	0.06	952.33	0.04
Zn2p	1035.54	0.25		

Appendix 3. Supplementary information (Chapter 3)

SUPPORTING INFORMATION

Electrochemical analysis of Fe(III) and Cu(II) interactions with TDP-43

Meaghan Tabobondung¹, Dr. Sanela Martić^{1,2}

¹*Environmental and Life Sciences, Trent University, Peterborough, Ontario K9L 0G2, Canada*

²*Department of Forensic Science, Trent University, Peterborough, Ontario K9L 0G2, Canada*

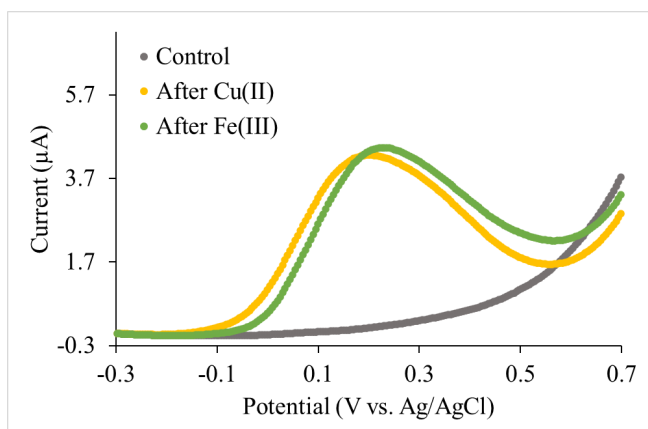


Figure S1.A) Representative SWV measurements of TDP-43-Au surface (grey), 350 μM Cu(II)-TDP-43-Au surface (yellow), and 1 mM Fe(III) exposure to 350 μM Cu(II)-TDP-43-Au surface (green).

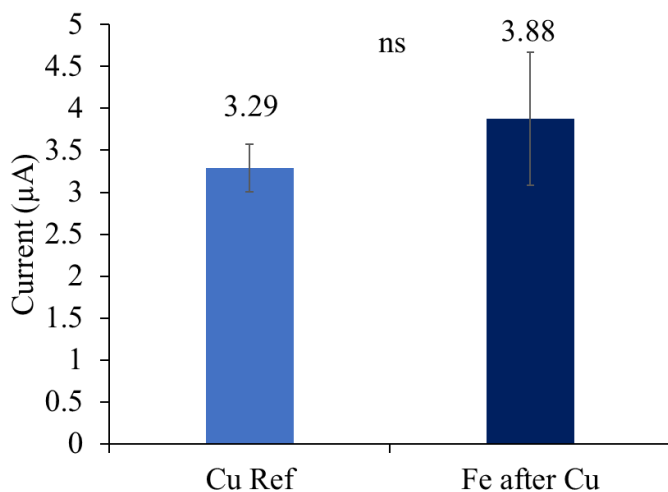


Figure S2. Plot of current for 350 μM Cu(II)-TDP-43-Au surface (light blue) ($3.29 \pm 0.28 \mu\text{A}$), and 1 mM Fe(III) exposure to 350 μM Cu(II)-TDP-43-Au surface (dark blue) ($1.61 \pm 0.91 \mu\text{A}$).

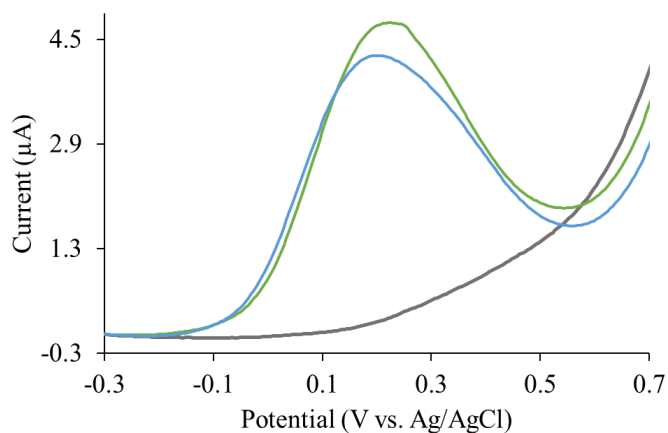


Figure S3. A) Representative SWV measurements of TDP-43-Au surface (grey), 350 μM Cu(II)-TDP-43-Au surface (blue), and 350 μM Cu(II) exposure to 1 mM Fe(III)-TDP-43-Au surface (green).

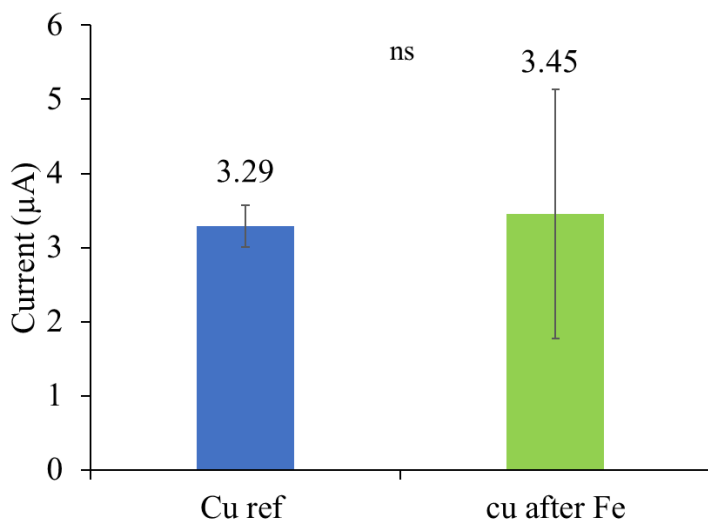


Figure S4. Plot of current for 350 μM Cu(II)-TDP-43-Au surface (blue) ($3.29 \pm 0.28 \mu\text{A}$), and 350 μM Cu(II) exposure to 1 mM Fe(III)-TDP-43-Au surface (dark blue) ($3.45 \pm 1.68 \mu\text{A}$).

Table S9. Mean and standard deviation results for displacive and competitive Fe(III) and Cu(II) studies. T-test results were obtained by using an online statistical calculator GraphPad Prism 9 (<https://www.graphpad.com/quickcalcs/ttest1.cfm>).

Sample	Average	SD	t-test results	Significance
350 μ M Cu exposure	3.28979	0.281372	t = 3.0742 df = 4 standard error of difference = 0.547 P value = 0.0371	Statistically significant (*)
Simultaneous 1 mM Fe and 350 μ M Cu exposure	1.607428	0.905156		
350 μ M Cu exposure	3.28979	0.281372	t = 1.2154 df = 4 standard error of difference = 0.485 P value = 0.2910	Not statistically significant (ns)
1 mM Fe exposure after 350 μ M Cu signal	3.879718	0.792212		
350 μ M Cu exposure	3.28979	0.281372	t = 0.1614 df = 4 standard error of difference = 0.984 P value = 0.8796	Not statistically significant (ns)
350 μ M Cu exposure after 1 mM Fe followed	3.448573	1.681031		